université de BORDEAUX

THÈSE PRÉSENTÉE
POUR OBTENIR LE GRADE DE

DOCTEUR DE

L'UNIVERSITÉ DE BORDEAUX

ÉCOLE DOCTORALE DES SCIENCES DE LA VIE ET DE LA SANTÉ

SPÉCIALITÉ : NEUROSCIENCES

Par Alena SPITSYN

Au-delà de la mémoire sociale : activité de la région CA2 de l'hippocampe lors de la navigation en direction d'une récompense.

Beyond social memories: hippocampal CA2 activity when navigating for rewards.

Sous la direction de : Dr. Lisa ROUX
Institut Interdisciplinaire de Neurosciences de Bordeaux

Soutenue le 11 juillet 2025

Membres du jury :

Mme. ROUX Lisa	Directrice de recherche, Université de Bordeaux	Directrice de thèse
Mme. OLIVA Azahara	Assistant professor, Cornell University, Ithaca	Rapportrice
Mme. TROUCHE Stéphanie	Chargée de recherche, IGF, Montpellier, UMR 5203, U1191	Rapportrice
M. GEORGES François	Directeur de recherche, Université de Bordeaux	Examinateur

Membres invités :

Mme. PISKOROWSKI Rebecca Ann	Directrice de recherche, IBPS, Paris	Invitée
M. STÖBER Tristan	Chargé de recherche, Ruhr University, Bochum	Invité

Au-delà de la mémoire sociale : activité de la région CA2 de l'hippocampe lors de la navigation en direction d'une récompense.

Résumé

La survie des animaux dépend de leur capacité à se souvenir des lieux d'intérêt, tels que des sources de nourriture ou la localisation d'un abri. L'hippocampe est central pour la mémoire spatiale, et l'activité des neurones hippocampaux appelés "cellules de lieux" forme une carte cognitive de l'environnement physique. De manière intéressante, il a été montré chez le rongeur que les cellules de lieux de la région CA1 de l'hippocampe deviennent plus actives au niveau des lieux d'intérêt suite à un apprentissage spatial. Cependant, les mécanismes qui sous-tendent ce remaniement de la carte cognitive sont encore peu compris. De plus, il reste à déterminer si la région CA2 de l'hippocampe, une zone encore peu étudiée, présente le même phénomène de réorganisation et/ou participe à celui-ci.

Le but de ce projet de thèse a été de caractériser l'activité de la région CA2 hippocampique lors d'une tâche de navigation en direction d'une récompense et pendant la consommation de celle-ci, afin d'explorer le rôle de CA2 dans la réorganisation des cellules de lieu.

Mots clés : **mémoire, hippocampe, récompense, navigation spatiale, électrophysiologie.**

Beyond social memories: hippocampal CA2 activity when navigating for rewards.

Abstract

Animals' survival largely depends on their ability to learn and remember how to navigate towards sites of interest such as food locations or home. The hippocampus is a key brain structure for spatial memory. Hippocampal place cells fire at discrete locations (their place fields) as subjects move through their environment, thereby providing a neural code for current location during locomotion. However, in the CA1 region of the hippocampus, this cognitive spatial map is not homogeneous: several studies indicate that place fields tend to accumulate next to salient cues such as rewards, a process called "goal-oriented remapping". The mechanisms underlying the establishment of this "biased" map are very little understood. Moreover, whether the often overlooked CA2 region of the hippocampus also presents such map goal-oriented bias and/or contributes to CA1 remapping is unknown.

The goal of this PhD project was to characterize the activity of the CA2 region during spatial navigation towards rewards and during reward consumption to test the hypothesis that it participates in biasing the hippocampal cognitive towards salient locations.

Keywords: memory, hippocampus, reward, spatial navigation, electrophysiology.



Thèse réalisée à

Institut Interdisciplinaire des Neurosciences (IINS)

CNRS UMR5297

Neurophysiology of Natural Behaviors

146, rue Léo Saignat, 33077 Bordeaux Cedex

CC BY

μεράκι

[may – rah – kee] · greek
(noun) when you do something with soul,
creativity or love;
putting a piece of yourself into what you do

Acknowledgements

I would like to thank all my jury members, Azahara Oliva, Stéphanie Trouche, Rebecca Piskorowski, Tristan Stöber and François Georges. Thank you for accepting to review my PhD work and take your precious time to do so. I admire your scientific work, it was a great motivation for me during this PhD and when we spoke about the potential jury composition, more than a year ago with Lisa, never would I imagine that all of you would accept and be available for this day. It is a great honour to be able to discuss my work with each one of you, I am deeply grateful for this opportunity and looking forward for the presentation in July.

I would like to thank the person that made this dream of mine come true, my PhD supervisor, thank you Lisa. Thank you for giving me the chance to join your team, five years ago now. From a medical student with zero background in *in vivo* neurosciences to now, sending my PhD work to the most brilliant researchers in the field, it has been a long way, only possible with your support. Your enthusiasm and trust gave me continuous motivation and inspiration throughout these five years of great scientific and life challenges. I believe I could not have made it without such an amazing supervisor who was present for the exciting recordings in CA2 and many failed experiments, up and downs and obviously for these last months of writing. I believe you helped me grow and become more independent, and for that trust and investment I will be forever grateful. I would like to thank you also for the amazing team you created and I am very proud working with you!

Even though this manuscript has administratively one author name, it has been a work and investment supported by many and I would like to give my acknowledgements to the amazing people who contributed immensely to this work.

First, I would like to thank ENS and FRM for funding my work and giving me this opportunity, and IINS and University of Bordeaux for hosting me. Unfortunately, not every girl in our world are given the right to study and the opportunity to succeed, therefore I am very grateful for having this right.

I was infinitely blessed with people that I met along this journey. A blessing for which I am beyond grateful, that helped me to go through these very tough years: physically and emotionally draining, intense professionally and personally, it was indeed a journey I will not forget.

I would like to than the amazing Roux team, alumni and current members!

Thank you, Evan, for our daily morning coffees, family stories and a lot of laughs. I'm very grateful for all your help during the past years, with coding, witnessing the wonder woman cells, helping with the spaghetti monster (aka the Clock maze), stats and of course human support.

Thank you, Giulio! Thank you for taking your precious time to help me with my infinite number of questions, "cause matlab is always right", for taking your time to explain me everything and develop my critical thinking. Without your enthusiasm, support and chocolate breaks, I could not have made through these long days.

Joe, thank you so much for your help with analysis these past two years and particularly months. Thank you for your patience and support, the amazing graphs and colours! I learned so much with your help, my skills in programming followed an exponential curve I believe.

Merci à Tim et nos night sessions de boulot sur nos manuscrits respectifs cette dernière semaine, je croise les doigts pour que tu rejoignes la team en tant que thésard !

J'aimerais remercier les Roux girls, Éline et Tessa, merci d'avoir été là ! nos discussions au bureau et en dehors, des plantes et tout le reste. Merci Éline pour ton incroyable talent et tous les concerts qui me faisaient me changer les idées et profiter d'une super ambiance ! Merci Tessa pour ton soutien quotidien, ma voisine de bureau ces derniers mois, et tous les conseils plantes. And of course, merci pour ta compagnie sur les roller coasters, aux fêtes foraines et au labo !

J'aimerais remercier les anciens membres du labo qui ont quand même était là pour la première moitié de cette thèse et mes débuts.

Merci à Edith qui m'a appris les manips de comportement social, merci de m'avoir accompagné lors de ces premières manips de comportement pour moi.

Merci à mes grands frères de labo, Geoffrey et Pascal, vos blagues, vos moqueries, zéro filtres et cent pour cent honnêteté, vos conseils. Grandir au labo c'est difficile et vous m'avez énormément manqué ces dernières années. Merci à la FENS et autres occasions pour nos réunions de temps en temps.

Merci à ma co-thésarde supérieure Camille ! la toute première thésarde du labo ! Ouvrir la marche est une tâche difficile et on te remercie pour ça ! merci pour tout ton soutien et tes conseils, merci pour l'accueil dans cette équipe et dans la ville ! je suis tellement contente qu'on reste en contact !

I would like also to thank Ashley, thank you for your kindness. You supported me as a big sister would do, I still remember crying in your office after my first implanted and failed surgery, for your kind words and hugs, thank you for being there for me.

I would like to thank the members of Piskorowski team. Thank you, Rebecca! I am so grateful to Vivien and you for giving me this internship opportunity, for learning slice electrophysiology and for transmitting me your passion of oddly curious region CA2! I am grateful for the knowledge you and him have transmitted to me. I miss him so much, even being called the Russian spy … but the passion he transmitted for CA2 and interneurons followed me through this PhD and I believe inspired and will inspire many others researchers.

Merci à Maithé, car tu donnes exemple, inspires et donnes du courage ! tu m'as appris que ce n'est jamais le bon moment pour rien dans la vie alors faut saisir l'occasion de tout quand la vie nous donne l'opportunité !

Merci à Maude et Eude, à Vérone ! à nos pauses cafés sur les escaliers au soleil, vous m'avez manqué à Bordeaux. Merci à Maud de continuer à prendre des nouvelles, j'espère qu'on se revoit bientôt !

J'aimerais remercier les « anciens », les adultes du cursus médecine-sciences, ceux qui montrent le chemin à travers cette vie de galère. Merci à Gaspard Gerschenfeld, je pense que cette aventure, de thèse et médecine, est devenue un projet sérieux après nos discussions pendant mon stage à l'ENS et après, sur la science, la médecine et la vie en générale, merci !

J'aimerais également remercier Vivien Szabo et Mathieu Tihy dont les parcours m'ont inspiré pour continuer dans cette voie.

Merci à Thomas Bienvenu, pour ton soutien et ton aide dans ce parcours pas évident !

J'aimerais remercier Gabrielle Girardeau, car un jour tu as pris la peine d'avoir un appel téléphonique avec une pauvre étudiante en médecine, perdue, qui voulait commencer à faire de l'electrophy, et, qui depuis a toujours eu un mot de conseil et de rassurance pour moi à chacune de nos rencontres.

J'aimerais remercier Hajer pour sa gentillesse, soutien et le management du PIV sans lesquel ces expériences de thèse n'auraient pas été possible.

I would like to thank my friends from the lab, the vibes and ski groups! Thank you for all the fun without which this PhD life would be kind of monotonous.

I would like particularly to thank the Mulle team members that, I believe, have adopted me in their hearts. Thanks Anael, Catherine, Julio and Ana! thank you for your daily support, kindness, our laughs, coffee breaks and our trips to Belgium.

Merci à Rémi, pour répondre toujours à l'appel à l'aide, pour m'avoir introduit aux incroyables bouquins Dune, les verres et diner à Oxford arms. Car l'institut n'a plus jamais été pareil depuis que tu es parti mais qu'on continue à garder contact !

Frank, merci, merci à nos discussions, à ton soutien et à ta compréhension de ma réalité, car je n'ai jamais eu besoin de t'expliquer pourquoi mais que tu as toujours été là pour discuter de comment.

I would like to thank Hannah and Tom for their kindness and for the chill diners in the garden with Frida.

I would like to thank Max, old grandpa, thank you for your wisdom and friendship, for putting the lights in my house and bringing simplicity concept in the life of overthinkers.

Merci à mes copains, Sylvain et Enzo, de ne pas m'avoir oublié après mon exile à Bordeaux. Merci de toujours d'avoir toujours accepté et pris le temps de prendre un verre avant mes trains ces quatre dernières années. Pour garder la tradition, vous revenez me voir le we du 14 juillet à Bordeaux, merci encore !!

Merci aux filles, Eve et Nadia, je vous aime merci d'avoir été là pour moi !

Merci Eve d'être venue me voir et prendre des nouvelles, nos we du 14 févier deviennent une tradition, le prochain à Milan !

Merci à Wiou, et nos rires infinis même après tant de temps ! la PACES unit pour toujours !

Merci à Déborah Grand, ma garante, ma marraine de cœur. Merci d'avoir été là pour moi dès mon arrivé en France, pour ton soutien, mes bouffé d'air chez toi à Bruxelles, nos déjeuners et pause-café. Si j'ai pu faire ma thèse.

I would like to thank my family who supported me for these infinite and crazy long years of study, not yet other! Спасибо мои дорогие за вашу поддержку все ети годы. Спасибо, мама и папа что помогайте и поддерживаете меня в моей длиной учебе. Спасибо маме за эту возможность. Хочу поблагодарить своего старшего брата Кирилла. Спасибо что всегда в меня верил и настоял на поступление в ENS, я бы не попробовала без твой поддержки. Спасибо мелким, Ксюше и Максиму, вы наша радость, вы самые классные умные, добрые и смешные, люблю вас очень сильно и скучаю.

Спасибо бабуля за рогалики, пирожки и наши прогулки.

I would like to thank my girlfriends, Ana, Dominique, Margaux, Konstantina, I am infinitely grateful for having you in my life. Brilliant, strong, wise, kind, gentle, funny, you are my wonder women. I could not possibly have gone through these past months without you, without your love and support. You bring inspiration and joy to my life every day!

Margaux, ma belle, si on n'est pas co-thésarde dans le même labo, on est sœurs de labo, de couloir, de we d'histo. Merci de partager ces années de thèse et struggle avec moi ! Le couloir toujours si vivant avec tes rires venant du bureau ! P.S. : Faudra que je te partage pleins de tips pour cette rédaction qui j'espère pourront rendre certaines parties de la tâche plus facile !

My sweet Portuguese: Ana, Domi, thank you for your love and immense support, for always listening, for reality check ups, for kicking my stupid ass. Thank you for believing in me when I could not, for loving me when I could not. Thank you for reminding me I am strong enough but I can always count on you. Never would I think that I would have Portuguese sisters. Obrigadissima, minhas queridas!

Ηλιακάδα μου, Konstantina, so grateful to have you in my life, coffee, sushi, books and good conversations will always bring us together, but I will always up show up for you and you know you can ALWAYS count on me. Σε ευχαριστώ από τα βάθη της καρδιάς μου.

Théo, merci d'avoir été là au cours de toutes ces années de labeur, qui aurait cru que deux étudiants en médecine qui se sont rencontré à Bordeaux lors d'un we, venant de deux villes différentes, qui prévoyaient de faire leur thèse sur deux continents différents, vont finir par se retrouver à Bordeaux ? merci d'avoir été mon moteur quand je n'avais plus de force, énergie ou motivation de continuer, si j'ai pu me lever tous les jours et continuer ce travail et cette life c'est grâce à toi ! Car je ne suis jamais trop ambitieuse ou trop avec toi, merci copain !

Bon on soutient le même jour, si ce n'est pas incroyable Tiphaine ? Les mots ne sont pas assez pour remercier de tout ce que tu as fait pour moi, pour ton soutient moral, pour tout le travail de conception et d'édition de figures, jusqu'au moindre détails (notre acharnement et perfectionnisme n'ont pas facilité la tâche). Pendant ces années de thèse t'as été mon life coach, malgré tes propres problèmes et soucis, l'année sans toi a été très édifice et je suis si heureuse que tu sois revenue.

(Un grand merci à Aurel sans qui je n'aurais pas pu déménager et aménager mon incroyable chez moi).

Table of contents

ACKNOWLEDGEMENTS **5**

TABLE OF FIGURES **13**

LIST OF ABBREVIATIONS **14**

CHAPTER 1: INTRODUCTION **17**

1. HIPPOCAMPUS AND MEMORY **17**
1.1. EARLY WORKS ON MEMORY FUNCTION 17
1.2. THE DIFFERENT TYPES OF MEMORY 17
1.3. THE HIPPOCAMPAL CIRCUIT 20
1.4. HIPPOCAMPAL LAYERS 21
1.5. HIPPOCAMPAL CELL DIVERSITY 23
2. THE HIPPOCAMPAL COGNITIVE MAP **25**
2.1. THE HIPPOCAMPAL COGNITIVE MAP AND ITS CELLULAR SUBSTRATES 25
2.2. MODULATION OF THE COGNITIVE MAP 29
2.3. PLACE CELLS CAN CAUSALLY DRIVE BEHAVIOUR 29
3. MODULATION OF THE HIPPOCAMPAL COGNITIVE MAP BY REWARDS **30**
3.1. GOAL OVER-REPRESENTATION 30
3.2. REMAPPING ONLY OCCURS IN PARTICULAR CONDITIONS: THE IMPORTANCE OF CONSCIOUS NAVIGATION 31
3.3. REWARD CELLS IN THE HIPPOCAMPUS 32
3.4. REWARD SIGNALS IN THE HIPPOCAMPUS 33
3.5. MANIPULATION OF DOPAMINERGIC INPUTS TO RESHAPE GOAL-DIRECTED BEHAVIOUR 38
4. CA2 IN THE HIPPOCAMPAL CIRCUITS **40**
4.1. A DISTINCT REGION OF THE HPC MORPHOLOGICALLY AND PHYSIOLOGICALLY 40
4.2. CA2: A "HIDDEN" HUB INSIDE OF THE HIPPOCAMPUS 43
4.3. INTERNEURONS OF CA2 47
4.4. MODULATION OF CA2 ACTIVITY AND SYNAPTIC PLASTICITY 48
4.5. CA2 ROLE IN SOCIAL MEMORY 50
4.6. CA2 BEYOND SOCIAL MEMORY 52
5. HYPOTHESES AND AIMS OF THE PHD PROJECT **55**

CHAPTER 2: MATERIAL AND METHODS **56**

1. ANIMALS **56**
2. BEHAVIORAL PARADIGM AND SETUP **56**
3. IMPLANTATION SURGERIES **58**
4. HISTOLOGY **60**
5. ELECTROPHYSIOLOGICAL RECORDINGS **63**
6. ELECTROPHYSIOLOGY DATA ANALYSIS **63**
7. QUANTIFICATION AND STATISTICAL ANALYSIS **69**

CHAPTER 3: RESULTS 70

1. LEARNING IN THE « CLOCK-MAZE » TASK 70
1.1. THE CLOCK-MAZE TASK 70
1.2. LEARNING IN THE CLOCK MAZE TASK 72
2. SPATIAL CODING IN THE CA1 AND CA2 REGIONS DURING CLOCK-MAZE TASK 75
2.1. PROPERTIES OF PYR IN CA1 AND CA2 REGIONS IN THE CLOCK-MAZE TASK. 75
2.2. PROPERTIES OF PUTATIVE INTERNEURONS IN CA1 AND CA2 REGIONS. 78
2.3. GLOBAL INCREASE IN PYR ACTIVITY DURING THE TASK 80
2.4. ACCUMULATION OF CA1 PLACE FIELDS NEAR THE LEARNED REWARD LOCATION 82
2.5. CA1 ACTIVITY AT THE PREVIOUS REWARD LOCATION. 84
2.6. ACCUMULATION OF CA2 PLACE FIELDS AROUND THE LEARNED REWARD LOCATION 86
2.7. CA2 ACTIVITY AT THE PREVIOUS REWARD LOCATION. 89
2.8. NEURONAL ACTIVITY STABILITY 91
2.9. IMPACT OF OMITTED REWARD ON SPATIAL REPRESENTATIONS 95
3. CA1 AND CA2 REGIONS ACTIVITY AT REWARD 96
3.1. ACTIVITY OF CA1 AND CA2 AROUND AND DURING REWARDED PORT NOSE-POKE ENTRY 96
3.2. INTERNEURONS ACTIVITY DURING IMMOBILITY AT REWARDED PORT. 105

CHAPTER 4: DISCUSSION AND PERSPECTIVES 111

1. LEARNING IN THE CLOCK-MAZE: A NEW BEHAVIORAL TASK TO STUDY GOAL-DIRECTED BEHAVIOR AND REWARD RESPONSES 111
2. REMAPPING DIFFERS BETWEEN CA1 AND CA2 SUBFIELDS 112
3. ACTIVITY OF CA1- AND CA2 PYR DURING IMMOBILITY 117
4. ACTIVITY OF INTERNEURONS DURING IMMOBILITY AND RUNNING 118
5. CA2 IN PATHOLOGY 122

REFERENCES 123

Table of figures

INTRODUCTION

FIGURE 1.1: ORGANIZATION OF LONG-TERM MEMORY SYSTEMS..... 19
FIGURE 1.2: THE CLASSICAL TRI-SYNAPTIC LOOP OF THE HIPPOCAMPUS..... 21
FIGURE 1.3: SCHEMATIC OF THE LAYERED ORGANIZATION OF THE HIPPOCAMPUS..... 23
FIGURE 1.4: MAIN FORMS OF INHIBITORY MICROCIRCUITS..... 24
FIGURE 1.5: A PLACE CELL..... 27
FIGURE 1.6: REWARD PREDICTION ERROR CODE IN DOPAMINERGIC NEURONS..... 34
FIGURE 1.7: LOCALIZATION OF DOPAMINE RECEPTOR SUBTYPES ALONG THE LONGITUDINAL AXIS OF THE HIPPOCAMPUS..... 37
FIGURE 1.8: DOPAMINERGIC INPUTS TO THE HIPPOCAMPUS RESHAPE SPATIAL MAPS..... 39
FIGURE 1.9: DIFFERENT MORPHOLOGY OF CA1 AND CA2 PYRAMIDAL NEURONS..... 41
FIGURE 1.10: HIPPOCAMPAL CA2 REGION CONNECTIVITY..... 47
FIGURE 1.11: SYNAPTIC PLASTICITY IN CA2 REGION..... 49

METHODS

FIGURE 2.1: HISTOLOGICAL LOCALIZATION OF IMPLANT WITH A FOUR-SHANK SILICON PROBE..... 62
FIGURE 2.2: RESULTS OF CELL-CLASSIFICATION..... 64
FIGURE 2.3: PLACE FIELD DETECTION..... 66
FIGURE 2.4: EXAMPLES OF SHUFFLING USED TO ASSESS THE SIGNIFICANCE OF SPATIAL CORRELATION VALUES OF THREE INDIVIDUAL CELLS..... 68

RESULTS

FIGURE 3.1: SCHEMATIC OF CLOCK-MAZE TASK FOR SPATIAL LEARNING OF REWARD LOCATION..... 71
FIGURE 3.2: MICE PERFORMANCE IN THE CLOCK-MAZE..... 74
FIGURE 3.3: MEAN SPEED IN THE CLOCK-MAZE..... 75
FIGURE 3.4: PROPERTIES OF PUTATIVE PYRAMIDAL CELLS IN CA1 AND CA2 REGIONS..... 78
FIGURE 3.5: PROPERTIES OF PUTATIVE INTERNEURONS (INS) IN CA1 AND CA2 REGIONS..... 79
FIGURE 3.6: CHANGE OF CA1- AND CA2-PYR ACTIVITIES DURING THE TASK..... 81
FIGURE 3.7: CHANGE OF CA1 PUTATIVE PYRAMIDAL CELLS ACTIVITY DURING THE TASK..... 84
FIGURE 3.8: CA1 ACTIVITY ALIGNED ON PREVIOUS REWARD..... 86
FIGURE 3.9: CHANGE OF CA2 PUTATIVE PYRAMIDAL CELLS ACTIVITY DURING THE TASK..... 88
FIGURE 3.10: CA2 ACTIVITY ALIGNED ON PREVIOUS REWARD..... 91
FIGURE 3.11: POPULATION VECTOR CORRELATION..... 92
FIGURE 3.12: SPATIAL ACTIVITY STABILITY DURING THE TASKS COMPARED BETWEEN REGIONS..... 94
FIGURE 3.13: SPATIAL CORRELATION BETWEEN REWARDED AND POST-OMISSION LAPS IN CA2..... 96
FIGURE 3.14: CA1- AND CA2-PYR ACTIVITY AROUND THE REWARDED PORT..... 99
FIGURE 3.15: CLUSTERING OF CA1- AND CA2-PYR BASED ON THEIR ACTIVITY AROUND THE REWARDED PORT..... 101
FIGURE 3.16: QUANTIFICATION OF THE ACTIVITY OF CA2-PYR GROUPS AROUND REWARDED PORT AND EFFECT OF OMISSIONS..... 105
FIGURE 3.17: ACTIVITY OF PUTATIVE CA1 AND CA2 INTERNEURONS AT THE REWARDED PORT..... 108
FIGURE 3.18: INTERNEURONS ACTIVITY DURING MOVEMENT, TASK 1..... 109
FIGURE 3.19: INTERNEURONS ACTIVITY DURING MOVEMENT, TASK 2..... 110

List of Abbreviations

Amb	ambiguous
AP	antero-posterior
CA	*cornu ammonis*
CaBP-ir	calbindin immunoreactive
CB	calbindin
CB1R	cannabinoid receptors of type 1
CCK	cholecystokinin
ChR2	channel rhodopsin
CPP	conditioned place preference
CR	calretinin
CS	conditioned stimulus
D receptor	dopamine receptor
DA	dopamine
DAPI	4′,6-diamidino-2-phénylindole
dCA1	dorsal ca1
DG	dentate gyrus
dHPC	dorsal hippocampus
DiI	1,1′-dioctadecyl-3,3,3′,3′-tetraméthylindocarbocyanine perchlorate
DOR	delta opioid receptor
DV	dorso-ventral
EC	entorhinal cortex
eLTP	excitatory ltp
FR	firing rate
GABA	γ-aminobutyric acid
GCL	granule cell layer
HFS	high frequency stimulation
HPC	hippocampe
i.p.	intraperitoneal
iLTD	inhibitory long-term depression
IN	inhibitory interneuron
KO	knockout
LC	locus coeruleus
LEC	lateral entorhinal cortex
LFP	local field potential
LS	lateral septum
LTP	long-term potentiation
MEC	medial entorhinal cortex
MF	mossy fibers

MFB	medial forebrain bundle
ML	medio-lateral
ML	stratum moleculare or molecular layer
MRI	magnetic resonance imaging
MRN	median raphe nucleus
MS/DB	medial septum diagonal band
MS	medial septum
MTL	medial temporal lobes
NAc	nucleus accumbens
NMDA	n-méthyl-d-aspartate
NMDAR	nmda receptor
No R	omission of the expected reward
NPY	neuropeptide y
opto	optogenetic
PETH	peri-event-histogram
PF	place fields
PFA	paraformaldehyde
PP	perforant path
Prev.	previous
PV	parvalbumin
PVN	paraventricular nucleus
PVs	population vectors
PYR	pyramidal cell
R	resultant vector lengths
REM	rapid-eye-movement
Rew.	reward
RGS14	regulator of g-protein signaling 14
RPE	reward prediction error
SC	schaffer collaterals
SI	spatial information
SL	*stratum lucidum*
SLM	*stratum lacunosum moleculare*
SO	*stratum oriens*
SOM	somatostatin
SP	*stratum pyramidale*
SR	*stratum radiatum*
SuM	supra-mammilary nucleus
SWR	sharp-wave ripples
TBS	theta burst stimulation
TH	tyrosine hydroxylase
t-SNE	t-distributed stochastic neighbor embedding

TTL	transistor–transistor logic
vCA1	ventral ca1
vCA2	ventral ca2
vHPC	ventral hippocampus
VIP	vasoactive intestinal polypeptide
VTA	ventral tegmental area

Chapter 1: Introduction

1. Hippocampus and memory

1.1. Early works on memory function

What remains of a person when this person has lost his/her memories? This disconcerting notion comes to mind when considering the experience of individuals suffering from Alzheimer's disease for instance. Beyond its contribution to our own identity, memory is a fundamental aspect of cognition that is central for survival, enabling individuals to learn and adapt their behaviour as a function of experience. Our understanding of memory function and the neuronal substrates supporting it have strongly benefitted from the early works of Brenda Millner with the patient H.M (Scoville and Milner, 1957). Since then, the hippocampal role in memory has been the centre of research for over half a century. H.M. was suffering from a severe form of epilepsy that required the ablation of his medial temporal lobes (MTL, including the hippocampus, amygdala, and the adjacent parahippocampal gyrus) in order to control the seizures. Unfortunately, the surgery left him with the inability to form memories of new experiences (anterograde amnesia) (Scoville and Milner, 1957). His memory for events that occurred immediately before the surgery was also affected but those from his childhood remained largely intact (graded retrograde amnesia). Importantly, his memory deficits were mostly restricted to personal events. For instance, he was able to learn new motor skills but could not recall how or when the acquisition occurred. Later on, H.M.'s memory impairment was mostly attributed to the near-complete removal of the hippocampal formation. However, the surgeon's original reports as well as more recent magnetic resonance imaging (MRI) analyses noted that damage was not limited to the hippocampus (Annese *et al.*, 2014). Nonetheless, works on H.M. and more specifically hippocampus – largely contributed to identify the hippocampus as a central node for episodic memory function, led to the definition of the different types of memory and highlighted the fact that memory formation involves different stages.

1.2. The different types of memory

Following studies of amnesic patients with brain lesions, a distinction was made between different forms of memory (Scoville and Milner, 1957; Milner, Corkin and Teuber, 1968;

Baddeley and Warrington, 1970). Memory types can be classified based on two key parameters: the **duration of storage** and the **nature of the stored information**. According to duration, **short-term memory** and **long-term memory** are usually distinguished (Atkinson and Shiffrin, 1968; Baddeley and Hitch, 1974; Squire and Zola, 1996a).

Short-term memory, which includes working memory, refers to the ability to temporarily hold and manipulate information relevant to immediate goals—such as keeping track of the steps in a mental math calculation or remember a phone number to dial it. In the traditional view, short-term memory transiently stores information before it is consolidated into more durable long-term memory. Short-term memory also includes sensory memory, the ability to retain impressions of sensory information after the original stimuli have ended. **Long-term memory** allows for the storage and retrieval of information over extended periods, from hours to a lifetime. This memory type will be further detailed below as it relates to my work.

Long-term memory itself can be further divided into **implicit (non-declarative)** and **explicit (declarative)** memory types (**Figure 1.1**) (Squire and Zola, 1996b; Squire, 2004) . **Implicit memory** involves learning processes that do not require conscious awareness. This type of memory was notably preserved in the patient H.M. Despite his profound amnesia for new events, he could still form implicit memories—such as performing tasks relying on procedural memory (like riding a bike), or responding to priming and conditioning paradigms (Milner, Squire and Kandel, 1998; Squire, 2004). Everyday habits, such as adding sugar to coffee, also remained intact for H.M. In contrast, **explicit memory** involves the conscious recollection of facts and events, which can be expressed verbally (Tulving, 1972). Explicit memory comprises two main types: **episodic memory** and **semantic memory**. **Episodic memory** is the ability to recall specific past experiences, binding together multimodal sensory details to form rich contextual memories—answering questions like "what, when, and where" (Tulving, 1972). Meanwhile, **semantic memory** involves general knowledge, such as historical facts or vocabulary, that is independent of the context in which it was learned. The ability to form explicit memories depends on encoding, storage, consolidation, and retrieval processes, which are influenced by factors like motivation and attention.

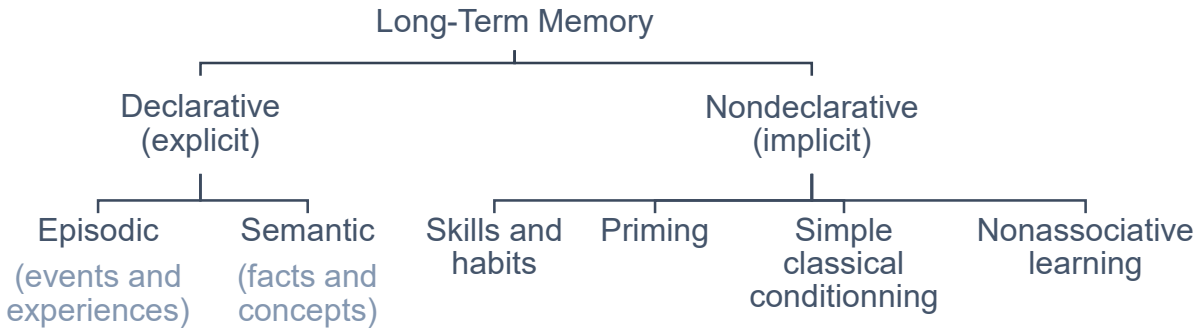

Figure 1.1: Organization of long-term memory systems.
Adapted from Squire and Zola, 1996.

Observations of patients with hippocampal lesions established the hippocampus as a key structure in the initial encoding and subsequent stabilization of long term memories through the process of consolidation (Squire, 1982; Cohen and Eichenbaum, 1994; Rudy and Sutherland, 1995).

The **two-stage model of memory consolidation** supports the idea of a transformation from labile short-term memory into more stable long-term memory, involving an initial encoding and a stabilization that comes later, during offline states (Buzsáki, 1989). Memory consolidation is supported by different types of coordinated neuronal activity, reflected in Local Field Potential (LFP). LFP represents captures the combined effects of synaptic activity, neuronal spiking, and other membrane voltage fluctuations. Hippocampal LFP presents oscillatory patterns that alternate between distinct states, correlating with different animal behaviours(Vanderwolf, 1969). The first stage of memory consolidation, **encoding**, is associated with **theta oscillations**—slow rhythmic activity (4–12 Hz in rodents) observed in the hippocampal LFP during active exploration, movement, and Rapid-Eye-Movement (REM) sleep (Vanderwolf, 1969; Kramis, Vanderwolf and Bland, 1975). Theta oscillations are thought to organize the timing of neuronal firing, acting as a temporal framework for the integration of sensory inputs and the formation of new neuronal representations (Pastalkova *et al.*, 2008; Mizuseki *et al.*, 2009; Gupta *et al.*, 2012; Colgin, 2013). The second stage, **consolidation**, occurs predominantly during non-REM sleep and is supported by sharp-wave ripples (SWRs)—brief, high-frequency oscillatory events (150–250 Hz) that reflect the synchronous reactivation of recently encoded neuronal ensembles (Wilson and McNaughton, 1994). SWRs are believed to

support the stabilization of these newly formed memories by promoting synaptic plasticity and facilitating the transfer of information to neocortical regions (Alvarez and Squire, 1994; Markram *et al.*, 1997; Nadel and Moscovitch, 1997; Buzsáki, 2015a). Accordingly, SWR suppression results in memory impairments (Ego-Stengel and Wilson, 2007a; Girardeau *et al.*, 2009; Oliva *et al.*, 2020; Jarzebowski *et al.*, 2021; Zhang *et al.*, 2021) and prolongation of SWR or additional SWR generation ameliorates memory performances (Fernández-Ruiz *et al.*, 2019; Oliva *et al.*, 2020). Together, the interplay between theta oscillations during encoding and SWRs during consolidation underscores the dynamic role of hippocampal activity in reorganizing and stabilizing memory traces across brain states.

1.3. The hippocampal circuit

In order to understand how memory is encoded, stored and recalled, it important to know about the circuits involved. The hippocampus proper, together with the subiculum and entorhinal cortex (EC), is part of the so-called hippocampal formation. The hippocampus proper is composed of several sub-regions: the dentate gyrus (DG) and four subdivisions of *cornu ammonis* (CA): CA1, CA2, CA3 and CA4 (Lorente De Nó, 1934). CA4 is not present in rodents (Amaral and Witter, 1989). Before describing the specificities of CA2 which was at the core of my work, I will briefly describe the general connectivity of hippocampal circuits.

The classical flow of information through the hippocampus is following an excitatory feed forward pathway commonly called “the trisynaptic pathway” (or loop) (**Figure 1.2**). The main glutamatergic input to the hippocampus comes from the entorhinal cortex layer II through the perforant path (PP), which synapses onto granule cells in the DG. This constitutes the first synapse of the trisynaptic loop. Granule cells then send inputs to CA3 through a distinct bundle of fibers named the Mossy Fibers (MF). Mossy fibers target the most proximal part of apical dendrites of CA3 pyramidal neurons, forming the second synapse of the tri-synaptic pathway. CA3 axons, in turn, form the Schaffer Collaterals (SC) and reach the CA1 region downstream. There, they form the third synapse of the pathway onto CA1 pyramidal cells. Beyond this tri-synaptic pathway, pyramidal cells located in the EC layer III project directly to CA1, forming the Temporo-Ammonic path. Finally, CA1 connects back to EC layer V, either directly or through the subiculum, completing a mainly unidirectional circuit (**Figure 1.2**) (Amaral and Witter, 1989).

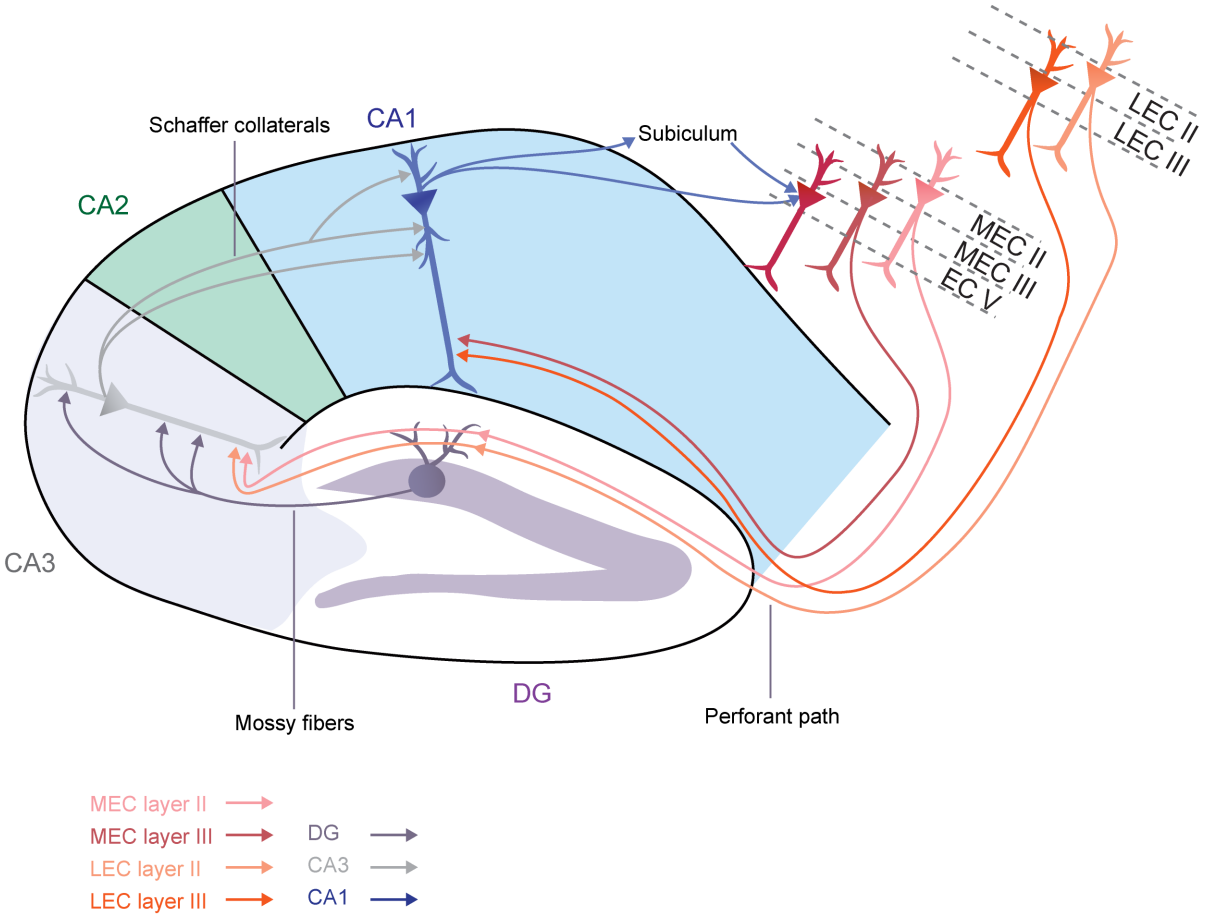

Figure 1.2: The classical tri-synaptic loop of the hippocampus.
The EC inputs reach the hippocampus via the perforant path, targeting both, the DG and, directly, CA1 region. In the DG, granule cells transmit information via mossy fiber projections to CA3-PYR, which in turn project to CA1-PYR. Finally, CA1-PYR relay hippocampal output back to the EC, directly, or via the subiculum, closing thus the tri-synaptic loop. Adapted from Oliva et al., 2023.

The integration of the region CA2 in hippocampal circuits will be further described in a dedicated section (see "4.CA2 in the Hippocampal circuit"). (Oliva, Fernandez-Ruiz and Karaba, 2023)

1.4.Hippocampal layers

The hippocampal regions follow a layered organisation (**Figure 1.3**). The different parts of the *cornu ammonis*, including CA2, are subdivided into:

- *Stratum oriens* (SO) is the deepest layer. It contains inhibitory basket cells and the dendrites of pyramidal cells.

- The *stratum pyramidale* (SP) is densely packed with the cell bodies of pyramidal cells and some interneurons. Within this layer, deep and superficial pyramidal cells also form two sublayers (Mizuseki *et al.*, 2011).
- The *stratum lucidum* (SL) contains the MF from the DG. It is only present in CA3 and CA2 where it is thinner.
- The *stratum radiatum* (SR) is superficial to the pyramidal layer. It includes the Schaeffer collaterals from CA3 and some interneurons.
- The *stratum lacunosum moleculare* (SLM) is the most superficial layer. It hosts EC inputs that arrive *via* the perforant path (or temporo-ammonic pathway in CA1) and contains inhibitory cell bodies.

A cell-free region known as the hippocampal sulcus separates the CA regions from the DG. The latter has its own laminar structure, consisting of:

- The *hilus* which contains the projections of the granule cells and many interneurons
- The *stratum granulosum* where the cell bodies of granule cells, the most numerous excitatory cells of the DG, are located. This layer is also commonly known as the granule cell layer (GCL).
- The *stratum moleculare* or molecular layer (ML) where axons from the PP connect with the dendrites of granule cells.

Hippocampal circuits have often been studied within specific subregions. However, recent works have also revealed that within a given subregion, a functional heterogeneity is present along the dorso-ventral (Fanselow and Dong, 2010), proximo-distal (Henriksen *et al.*, 2010; Fernandez-Lamo *et al.*, 2019) and deep-superficial axes (Mizuseki *et al.*, 2011; Lee *et al.*, 2014; Valero *et al.*, 2015a; Soltesz and Losonczy, 2018a).

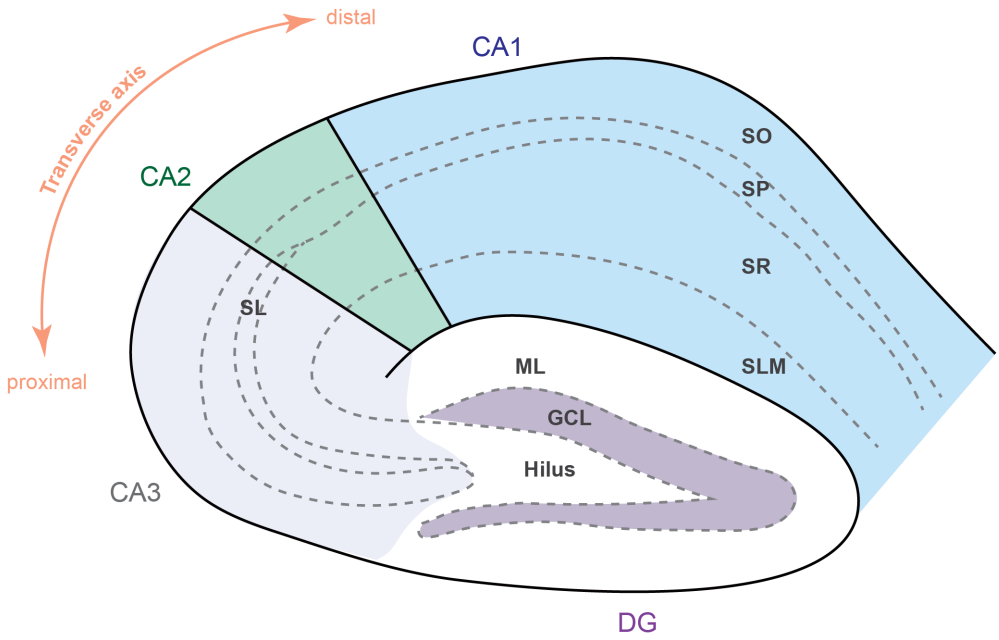

Figure 1.3: Schematic of the layered organization of the hippocampus.
Schematic of a dorsal hippocampal transverse slice with the different sublayers. SO: Stratum Oriens; SP: Stratum Pyramidale; SL: Stratum Lucidum; SR: Stratum Radiatum; SLM: Stratum Lacunosum-Moleculare; Hilus; GCL: Granule Cell Layer; ML: Molecular layer.

1.5. Hippocampal cell diversity

1.5.1. Interneuron diversity

By definition, inhibitory interneurons (INs) release γ-aminobutyric acid (GABA) as their principal neurotransmitter (Freund and Buzsáki, 1998). However, they represent the most diverse population in the hippocampus, both anatomically and functionally. More than 20 distinct classes of INs have been described in the CA1 and CA3 regions (Somogyi and Klausberger, 2005; Klausberger and Somogyi, 2008). INs are often classified based on their dendritic and axonal arborizations as well as the subcellular domain(s) of pyramidal neurons they innervate: dendrite-, soma- (perisomatic), and axonal initial segment (axo-axonic)-targeting cells (Han, 1994; Sik *et al.*, 1995; Buhl *et al.*, 1996; Cobb *et al.*, 1997). Additionally, they can be characterized by the expression of calcium-binding proteins such as parvalbumin (PV), calbindin (CB), and calretinin (CR), or by their neuropeptide content, including cholecystokinin (CCK), somatostatin (SOM), vasoactive intestinal polypeptide (VIP), and neuropeptide Y (NPY) (Somogyi and Klausberger, 2005; Fuentealba *et al.*, 2008; Ascoli *et al.*, 2009; Klausberger, 2009). This molecular and structural diversity underpins the precise roles

that interneurons play in orchestrating hippocampal network dynamics and information processing (Roux and Buzsáki, 2015).

INs can regulate the activity of pyramidal cells (PYR) in different configurations (**Figure 1.4**) (Roux and Buzsáki, 2015). First, *via* **feed-forward inhibition**, INs inhibit the PYR they receive excitatory afferents from, limiting its output spiking or competing with its dendritic excitation (Buzsaki, 1984). **Feedback inhibition** requires the PYR activating an IN that, in turn, sends inhibitory signals back to the same PYR, forming a feedback loop that controls ongoing activity (Miles, 1990). **Disinhibition** occurs when IN target and inhibit other IN, effectively releasing the PYR from inhibition and increasing its activity (Freund and Buzsáki, 1998; Lovett-Barron *et al.*, 2012; Xu *et al.*, 2013; Turi *et al.*, 2019b). These distinct microcircuits shape and coordinate the precise timing and balance of PYR signaling across networks.

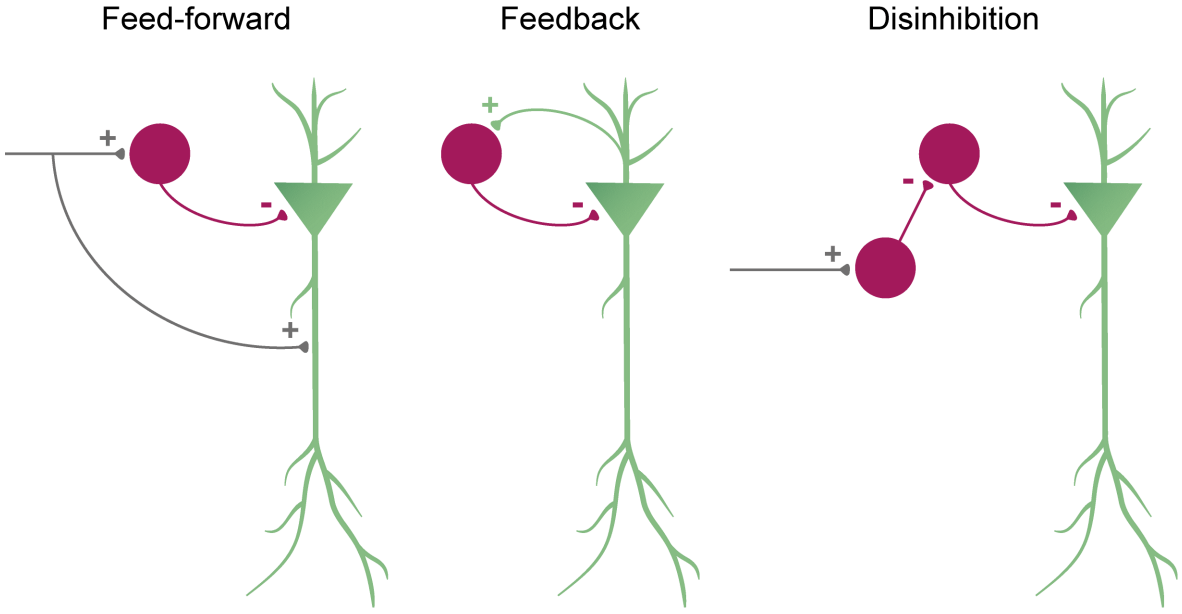

Figure 1.4: Main forms of inhibitory microcircuits.
Schematic illustrating how inhibitory interneuron (in pink) can connect on to pyramidal neuron (green), via feed-forward inhibition, feedback inhibition or engaged in a disinhibition circuit with other interneurons.

1.5.2. Pyramidal diversity

PYR which form a more homogeneous population compared to INs, nonetheless exhibit notable diversity within the hippocampus. Along the radial axis, the PYR population is typically divided into **deep** (closer to SO) and **superficial** sublayers (closer to SR). Neurons of these sublayers are generated during different periods of development, superficial pyramidal neurons are born later (Caviness, 1973; Stanfield and Cowan, 1979) and exhibit marked genetic,

morphological and functional differences (Bannister and Larkman, 1995; Dong *et al.*, 2009; Mizuseki *et al.*, 2011; Slomianka *et al.*, 2011; Valero *et al.*, 2015a; Soltesz and Losonczy, 2018a). Superficial pyramidal cells typically display more complex dendritic arbores and distinct intrinsic electrophysiological properties compared to deep-layer neurons (Bannister and Larkman, 1995). Furthermore, these two layers integrate different afferent inputs: superficial PYR primarily receive input from entorhinal cortex projections *via* the perforant path (Masurkar *et al.*, 2017), whereas deep-layer PYR are preferentially targeted by recurrent collaterals and local circuits (Danielson *et al.*, 2016a; Nasrallah *et al.*, 2019). One of the first identified marker to separate the PYR along the radial axis, and still used nowadays, is the *calbindin.* Calbindin immunoreactive (CaBP-ir) PYR are present in the densely packed superficial layer, whereas the deeper pyramidal cells lack this protein (Baimbridge and Miller, 1982; Sloviter, 1989; Valero *et al.*, 2015a).

In conclusion, the anatomical organization of the hippocampus, based on clearly identified layers, segregates cell types and specific inputs/output pathways. This structural and functional heterogeneity supports the specialized roles of these subpopulations in hippocampal information processing.

2. The hippocampal cognitive map

2.1. The hippocampal cognitive map and its cellular substrates

2.1.1. Cognitive map

A prominent model states that navigating "in space" and "in thoughts" rely on similar neuronal substrates (Buzsáki and Moser, 2013) making navigation in rodents an active focus of research. Rodents heavily rely on spatial cues to navigate in the external environment, mirroring the role of spatial and contextual information ("where?") in human episodic memory. Edward Tolman introduced the term of "**cognitive map**" in 1948, after showing that rats were capable of reaching a goal location in a maze using different paths that the ones it had previously learned. He proposed that this ability is supported by **an internal memorised representation of the physical space** that enables the animals to navigate in the environment *via* novel routes (Tolman, 1948). Later, using electrophysiological tetrode recordings from the hippocampi of freely moving rats, John O'Keefe identified **hippocampal neurons—later termed place cells—that exhibited location-specific firing** (O'Keefe and Dostrovsky, 1971; O'Keefe and

Nadel, 1978), providing a cellular substrate for the cognitive map proposed by Tolman. Additionally, a hippocampal lesion study showed a disruption in rats' spatial memory (Morris *et al.*, 1982). Since it was already known that the hippocampus supports episodic memory in humans, notably thanks to works on H.M., spatial navigation paradigms in rodents became a model of choice to understand the neural mechanisms underpinning episodic memory.

Accordingly, numerous behavioural tasks were developed over the years. One of the most famous is the Morris water maze, where rodents swimming in a pool must find the location of a hidden safe platform (Morris *et al.*, 1982; Moser *et al.*, 1995). Other tasks include object recognition memory tasks, the cheeseboard maze task (Dupret *et al.*, 2010a; Roux *et al.*, 2017a) or the continuous spatial alternation task (Kim and Frank, 2009).

2.1.2. Hippocampal place cells

Our understanding of place cells comes from extracellular recordings in rodents using electrodes implanted chronically in the dorsal hippocampus and allowing the animal to freely explore an environment. The activity of individual neurons is paired with simultaneous animal's position tracking, allowing to determine in the position of the animal whenever an action potential of the cell occurs. The number of spikes in each location (or spatial bin) is counted and normalized by the occupancy (i.e. how much time the animal spent in that bin), allowing to extract a rate map for each cell. Rate maps can be computed for single cell or for a population of cells, providing a global view of neuronal activity across the explored environment. From the rate maps of individual cells are defined the so-called "**place fields" which are the locations in space where the cell is the most active (Figure 1.5)**. Place fields emerge rapidly the first time an animal explores an environment (Hill, 1978) and with exploration, the animal's spatial cognitive map becomes more stable (Frank, Stanley and Brown, 2004). Active engagement in spatial exploration (such as when animals are looking for a reward) may increase the stability of the place map (Kentros *et al.*, 2004a). With extended exposure to the environment, the place cells also increase their spatial specificity, their information content, and fire more reliably in a given location (Cacucci *et al.*, 2007; Roux *et al.*, 2017a).

Place cells have been identified in the main excitatory neuron populations from all of the hippocampal subfields, including CA1, CA2, CA3 and DG (O'Keefe and Dostrovsky, 1971; Jung and McNaughton, 1993; Leutgeb *et al.*, 2007; Lu *et al.*, 2015a; Mankin *et al.*, 2015a; Oliva, Fernández-Ruiz, *et al.*, 2016). However, the properties of place cells are not homogeneous within and across the hippocampus subfields.

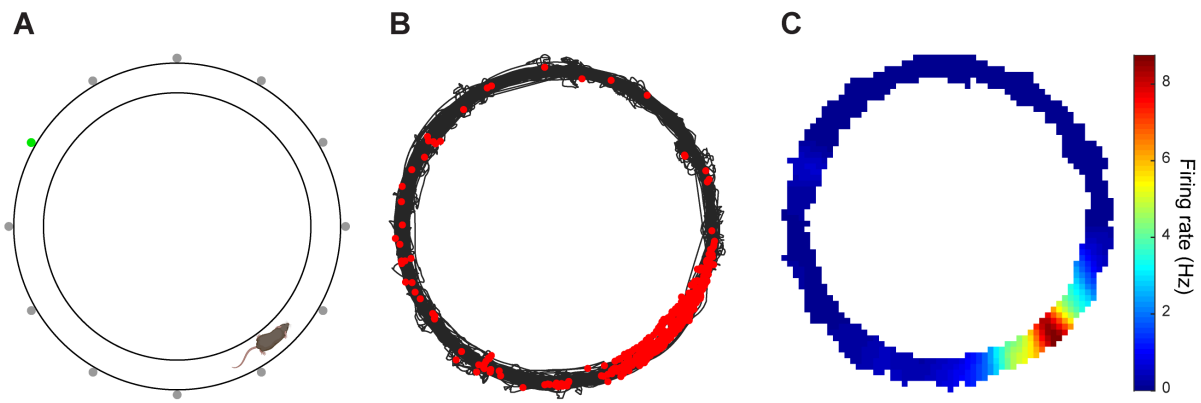

Figure 1.5: A place cell.
(A) A mouse running in a circular corridor. Cells in dorsal hippocampus and animal's position are recorded simultaneously. (B) The black line represents the mouse's trajectory; red dots represent the positions where spikes from a putative pyramidal cell from dorsal CA1 were detected. (D) A firing rate map produced from the spiking of the recorded cell, showing high firing rates (warmer colors) only in a localized space of the maze, forming the so-called place field.

A proximo-distal topography quickly emerged as a major organizational principle of intra-hippocampal connectivity (Witter *et al.*, 2000) and this is reflected in the organization of place fields. In CA1, place fields tend to be sharper and more spatially specific in the proximal region (closer to CA2) (Henriksen *et al.*, 2010). This gradient in spatial tuning is thought to reflect differential inputs from the medial and lateral entorhinal cortices, with the medial entorhinal cortex (MEC) and its grid cells projecting to proximal CA1 (Naber, Lopes Da Silva and Witter, 2001; Zhang *et al.*, 2013)and the lateral entorhinal cortex (LEC) projecting to distal CA1 (Burke *et al.*, 2011; Nakamura *et al.*, 2013; Igarashi *et al.*, 2014). Similar gradients in spatial coding are observed in CA3, where proximal CA3 PYR support a more precise spatial representation compared to distal CA3 PYR that shows broader place fields (Leutgeb *et al.*, 2007; Lu *et al.*, 2015a), possibly due to increased recurrent connectivity in this part (Li *et al.*, 1994; Ishizuka, Cowan and Amaral, 1995). In the dentate gyrus (DG), granule cells also display place-related firing patterns, though their place fields are generally smaller and sparser than those in CA1 and CA3, consistent with the DG's role in pattern separation (Leutgeb *et al.*, 2007). **Note: CA2 spatial properties will be discussed in section 4.6.**

A heterogeneity in spatial encoding is also present along the dorso-ventral axis. While dCA1 exhibit pronounced spatial coding, progressively along the dorso-ventral axis, spatially-tuned neurons become fewer. In ventral CA1 (vCA1) they have larger place fields and carry

lower information about the animal's position than dorsal CA1 (dCA1) neurons (Jung and McNaughton, 1993; Ciocchi *et al.*, 2015; Chockanathan and Padmanabhan, 2021). vCA1 has been linked to anxiety and social cognition (Henke, 1990; Moser and Moser, 1998; Fanselow and Dong, 2010; Okuyama *et al.*, 2016), consistent with the fact that it receives direct inputs from the amygdala and the hypothalamus (Swanson and Cowan, 1977) unlike dCA1. Differences between dorsal and ventral CA1 are more broadly reviewed in (Fanselow and Dong, 2010).

Several studies have explored how hippocampal interneurons encode spatial information. To a lesser extent than PYR, INs show some degree of spatially selectivity and their stability is dependent on the subclass (Geiller *et al.*, 2020a). However, Geiller et *al.* were able to decode animal's position from interneuron activity above chance level. Marshall et al. (2002) showed that interneurons receiving putative monosynaptic inputs from simultaneously recorded pyramidal cells tend to inherit the spatial firing patterns of these pyramidal neurons. This suggests that interneurons can adopt the spatial modulation of their afferent place cells, including the phase shift in their firing relative to the hippocampal theta rhythm as the animal moves through the place field (known as "phase precession") (Marshall *et al.*, 2002a). Building on this, it has been demonstrated that certain CA1 interneurons themselves exhibit spatially modulated firing patterns and phase precession (Maurer *et al.*, 2006a). Furthermore, Royer and al showed that suppressing inhibition selectively *via* optogenetics increases the firing of pyramidal neurons within their place fields. Additionally, optogenetic manipulations of different types of INs induced place field modulation and subsequently spatial learning, indicating a fine-tuned control of spatial coding by interneurons (Royer *et al.*, 2012; Turi *et al.*, 2019a, 2019a; Dudok, Szoboszlay, *et al.*, 2021; Rolotti *et al.*, 2022a). Taken together, these findings suggest that that interneurons actively contribute to spatial representations.

Altogether, these variations underscore the heterogeneity of spatial coding within the hippocampus and highlight how anatomical and functional specialization along the proximo-distal and transverse axes contribute to distinct roles in memory processing and navigation.

2.2. Modulation of the cognitive map

Importantly, the cognitive maps can undergo different types of changes over time or when the environment is modified. These reconfigurations in spatial firing patterns are collectively referred to as ***remapping***. The term remapping encompasses both **global remapping**, in which place cells change their place field locations or become silent/active in a new environment, and **rate remapping**, where the spatial firing locations remain stable but the firing rates of place cells are modulated in response to contextual or sensory changes (Wood, Dudchenko and Eichenbaum, 1999; Anderson and Jeffery, 2003; Leutgeb *et al.*, 2005; Fyhn *et al.*, 2007). It was shown for instance that when an animal is moved form a circular arena to a square one, place cells undergo a global remapping, a new subset of the place cell-population was recruited (Muller and Kubie, 1987). These changes corroborate the idea that the spatial cognitive map is a mental representation of the surrounding environment.

Interestingly, gradual changes in place cell representations can also occur in the same familiar environment. Such representational drift can be observed over days (Ziv *et al.*, 2013a) or hours (Mankin *et al.*, 2012), when animals are placed in the same arena across different sessions. It seems that the speed at which representations are drifting is not identical between the different hippocampal subfields. Indeed, the drift was observed in both CA1 and CA3, but it is slower in CA3, suggesting greater stability in this subregion (Mankin *et al.*, 2012). Similarly, Ziv et al. (2013) used calcium imaging to demonstrate that although individual CA1 neurons' activity changes over weeks, a subset of neurons remains consistently active, preserving a stable spatial representation. Together, these studies highlight that hippocampal subfields differ in the stability of their spatial codes.

2.3. Place cells can causally drive behaviour

As a population, place cells form a cognitive map that could enable memory-based navigation in physical space. However, directly establishing the causal role of place cell activity in driving spatial behaviour has remained a significant challenge for decades. Notably, two elegant studies using optical and electrophysiological approaches have recently begun to address this question.

The first work, conducted by de Lavilléon et al., in 2015, demonstrated that stimulating the medial forebrain bundle (MFB) during the firing of specific place cell during sleep could create an artificial place-reward association. Upon wakening, these mice showed an increased

preference for the place field linked to the stimulated place cell (De Lavilléon *et al.*, 2015). In a complementary study using an all-optical approach, optical activation of place cells whose fields corresponded to a reward location in a virtual environment evoked licking behaviour in mice (an indicator of reward expectation) within the region where the stimulation was performed (different from the actual reward location) (Robinson *et al.*, 2020).

Together, these studies provide compelling evidence that hippocampal place cells play an active and causal role in representing specific location and forming spatial memories both during wakefulness and sleep.

3. Modulation of the hippocampal cognitive map by rewards

Animals' survival largely depends on their ability to navigate towards places of interest such as food locations or home. As mentioned before, hippocampal "place cells" are active in particular locations in space during active exploration called their "place fields" - (O'Keefe and Nadel, 1978). However, the cognitive spatial map is not a homogeneous representation of the physical environment. (Hollup *et al.*, 2001a; Dupret *et al.*, 2010a; Mamad *et al.*, 2017a; Zaremba *et al.*, 2017a; Kaufman, Geiller and Losonczy, 2020a; Jarzebowski *et al.*, 2022a).

The following section explores how reward might be represented within the hippocampus and how it may influence or reshape hippocampal activity patterns.

3.1. Goal over-representation

Some studies focusing on spatial cognitive maps during goal-oriented learning led to an important observation: **place field density of dorsal CA1 (dCA1) place cells can – in some conditions - increase at learned reward locations. This phenomenon is now commonly called "goal-oriented remapping"**. Although it is not systematic and may depend on specific experimental conditions (see section 3.2, and review (Nyberg *et al.*, 2022)), goal-oriented remapping was revealed and studied in different spatial navigation tasks. In freely moving rodents for instance, it was shown in the cheeseboard maze task (Dupret *et al.*, 2010a; Jarzebowski *et al.*, 2021), in a T-maze task (Mamad *et al.*, 2017a), in the Morris water maze (Hollup *et al.*, 2001a) and the 8 arm radial maze (Xu *et al.*, 2019). In head-restrained mice, it

was shown using a linear track in a virtual environment (Gauthier and Tank, 2018; Lee *et al.*, 2020; Robinson *et al.*, 2020; Sato *et al.*, 2020a) and a treadmill with tactile cues (Danielson *et al.*, 2016a; Zaremba *et al.*, 2017a, 2017a; Turi *et al.*, 2019a). Across all these studies, different types of reward were used: food (Dupret *et al.*, 2010a; Mamad *et al.*, 2017a; Xiao, Lin and Fellous, 2020), water (Danielson *et al.*, 2016a; Zaremba *et al.*, 2017a; Turi *et al.*, 2019a; Kaufman, Geiller and Losonczy, 2020a), intracranial stimulation of the Medial Forebrain Bundle (MFB, the main pathway of dopaminergic axons) (Kobayashi *et al.*, 1997, 2003) and an safety platform for the Morris water maze (Hollup *et al.*, 2001a).

Complementarily, it was observed that place fields density increases when animals approach the reward (Zaremba *et al.*, 2017a; Kaufman, Geiller and Losonczy, 2020a). The observed place field accumulation at the reward is both due to existing place fields shifting towards the reward and to previously non-spatially modulated cells becoming consistently active at the reward location (Mizuta *et al.*, 2021a; Sosa, Plitt and Giocomo, 2023). The accumulation at reward happens gradually with learning (Dupret *et al.*, 2010a; Sosa, Plitt and Giocomo, 2023). This phenomenon has also been observed in the hippocampus of other species: for instance, an increase in goal representation was also revealed in bats (Sarel *et al.*, 2017).

3.2. Remapping only occurs in particular conditions: the importance of conscious navigation

Importantly, place field remapping directed towards goal locations was only observed in certain conditions. For instance, no place field accumulation was observed when the rewarded well was indicated by a visual cue in the cheeseboard maze (Dupret *et al.*, 2010a) or in a foraging task with rewards delivered at different places (Kentros *et al.*, 2004a). These observations indicate the importance of the cognitive engagement and learning requirement for goal-oriented remapping in the hippocampus.

Accumulation of place fields at the goal location has also been shown to be absent when the goal and the reward were separated in time and space: this was demonstrated in the experiment from Hok at al. (2007) where the animal had to wait few seconds in a goal location in order to receive a food pallet that was delivered in a random place of the arena (Hok *et al.*, 2007). Along the same lines, when animals have to remember a goal position but find new routes towards it, goal-oriented remapping was not observed (Jeffery *et al.*, 2003; Hok *et al.*, 2007; Pfeiffer and Foster, 2013; Spiers, Olafsdottir and Lever, 2018; Duvelle *et al.*, 2019). One explanation for these results might be the heterogeneity of CA1 cells. In fact, deep CA1 place

cells remap and stabilize at reward locations while the most superficial ones are more likely to stay spatially tuned to their initial place field (Danielson 2016). Interestingly, extra-field firing at the goal was observed after arrival at goal locations (Hok *et al.*, 2007; Hayashi, Sawa and Hikida, 2016; Duvelle *et al.*, 2019), meaning that coding of goal locations could be independent from the place fields observed elsewhere on the maze.

It is also important to note that remapping can be animal-dependant, with different animals showing different levels of remapping in the same conditions, and during different behaviours (Bostock, Muller and Kubie, 1991; Anderson and Jeffery, 2003; Kentros *et al.*, 2004a). This inter-animal variability could be related to diverse attentional or stress levels as well as differences in individual behaviours.

3.3. Reward cells in the hippocampus

More strikingly, Gauthier and Tank, using calcium imaging in mice running in a virtual environment, showed in 2018 that 1-5% of neurons respond to rewards in dCA1 and subiculum (0.8% of all place cells). This means that they were consistently active upon reward consumption, regardless of its location in the virtual environment. Importantly, another study does not support this finding (Lee *et al.*, 2020). These differences may be due to the experimental conditions that slightly differed between the two studies: while both were using virtual reality, Gauthier and Tank had only one active reward that was moved within the same 2-4m environment. In contrast, Lee used several active goals in a large environment (40m).
A more recent study based on two-photon calcium imaging reported reward-related cells that follow reward displacement: these were shown to be active at a specific distance relative to the reward, regardless of its location, with each cell having its own preferred distance (Sosa, Plitt and Giocomo, 2023).

Together, these findings suggest that hippocampal representations can encode information about reward locations (or distance to reward locations), but this encoding appears to be more robust in simplified, mostly one-dimensional environments with consistent, stereotypical goal-directed behaviours.

3.4. Reward signals in the hippocampus

3.4.1. Reward and reward expectation

Dopamine was initially studied for its role in initiating movements, a function that is impaired in patients with Parkinson's disease due do degeneration of dopaminergic neurons in the *substantia nigra pars compacta*. However, not all dopaminergic neuron activity was consistent with movement initiation, leading Romo and Shultz (1990) to address the discrepancy observed between movement initiation and conditioned stimuli responses. They realized a study where monkeys performed two tasks: in one, they self-initiated an arm movement to retrieve a hidden reward, and in the other, a cue predicted the reward delivery. In the self-initiated task, dopaminergic neurons increased their firing upon reward consumption, and decreased firing when the reward was unexpectedly absent. In the cue-driven task, the increase in activity was linked to the predictive stimulus, not to the actual consumption of the reward (**Figure 1.6**). These findings were key in formulating the **Reward Prediction Error (RPE)** hypothesis defined as the signal that codes for the difference between the expected and received reward. It implies the presence of a teaching signal that shifts the behavior and neuronal activity from the reward itself to a predictive signal (Montague, Dayan and Sejnowski, 1996).

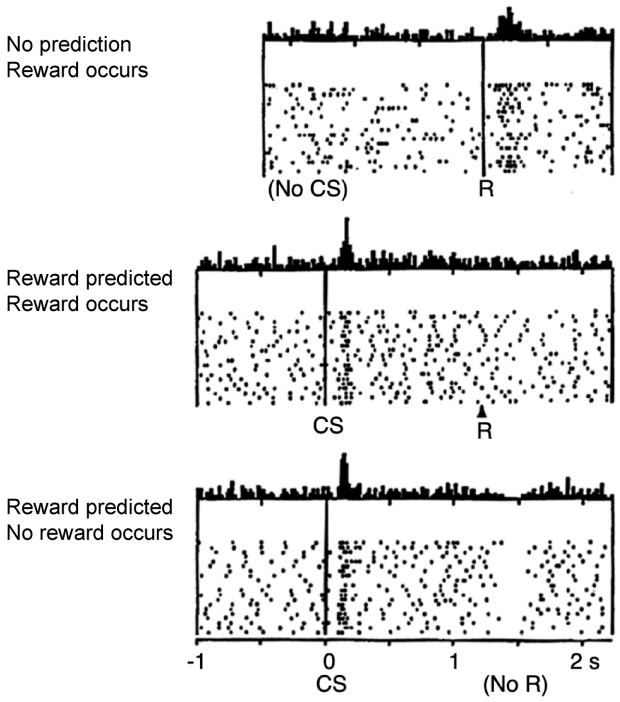

Figure 1.6: Reward prediction error code in dopaminergic neurons.
First evidence of RPE coding by dopaminergic neurons in monkey. Raster plots and peristimulus histogram of a single dopamine neuron. ***Top****: the neuron demonstrates a positive prediction error response when an unpredicted reward was delivered at time 'R'.* ***Middle****: The reward delivery was paired with a conditioned stimulus (CS). Neuron response shifts to time of CS and no response is observed at time of reward delivery 'R'.* ***Bottom****: CS is emitted but no reward is delivered. The neuron still responds positively after the CS, but decreases in activity after the omission of the expected reward (No R), exhibiting a negative prediction error response. Adapted from Schultz et al., 1997.*

These insights laid the groundwork for understanding how RPE signals can update an animal's internal representation of the environment and inform future actions (Watabe-Uchida, Eshel and Uchida, 2017; Berke, 2018) (Watabe Uchiada 2017, Berke 2018). As described in previous sections, the hippocampus spatial representations reorganize in goal-oriented tasks, goal-oriented remapping, and researchers have been trying to uncover the mechanisms behind it. This process likely relies on the interaction between spatial and reward signals, notably, from dopaminergic neurons that potentially modulate the salience of goals and could drive adaptive changes into hippocampal maps. Exploring this interplay provides an important framework for understanding how the hippocampus encodes flexible, goal-directed behaviors. In the next section, I will describe what has been uncovered about dopaminergic modulation of hippocampal memory.

It is important to note that the sources of dopamine projections are not solely VTA and LC, and conversely, the hippocampus (HPC) is far to be the only target of dopaminergic

projections. In fact, the HPC is a relatively small output for the VTA, compared for example to the nucleus accumbens (NAc) which constitutes one of its main output structure (Beier *et al.*, 2015).

3.4.2. Dopaminergic modulation of hippocampal memory

Initially, pharmacological studies have shown that dopamine (DA) critically modulates hippocampus-dependant memory processes, particularly through dopamine receptors (D1/D5), belonging to the metabotropic G-protein-coupled receptor family. Systemic or local administration of D1/D5 receptor agonists, has been shown to **enhance spatial memory performance** in tasks like the **Barnes maze** and **alternating T-maze**, including in aged mice (Bach *et al.*, 1999; Kern *et al.*, 2015). On the other hand, blocking D1-like receptors impairs performance of hippocampal-dependent tasks, including **nicotine-induced conditioned place preference** and **novel object recognition** (Tang and Dani, 2009; Yang *et al.*, 2017). Intrahippocampal infusion of D1/D5 receptor antagonist disrupts both **memory retrieval** in delayed matching-to-place tasks and **consolidation** of spatial memory in the Morris water maze, whereas D1/D5 receptor activation improves retention (O'Carroll *et al.*, 2006; Silva *et al.*, 2012). Blocking locally D1/5 receptors in the hippocampus also prevents the learning of a new spatial navigation strategy leading towards the goal in a multi-well appetitive task (Retailleau and Morris, 2018).

Interestingly, it was observed that **spatial learning** increases dopamine levels in the **dentate gyrus (DG)**, and this effect is abolished by D1/D5 receptor blockade (Wang, Foster and Pfeiffer, 2020).

Genetic deletion studies reinforce these pharmacological findings. **D1 receptor knockout (KO) mice** exhibit significant deficits in spatial memory tasks such as the Morris water maze and the Barnes maze (El-Ghundi *et al.*, 1999; Granado *et al.*, 2008; Xing *et al.*, 2010). Recordings from **D1 KO mice** revealed **impairments in place cell global-remapping** when the distal cues of a familiar environment were rotated (Tran *et al.*, 2008). Interestingly, while D1 KO mice showed no differences in the number of spatially modulated cells in a familiar environment compared to wild-type mice, **D2 KO mice place cells displayed reduced spatial tuning**, lower intra-field firing rates, and diminished stability of place fields (Nguyen *et al.*, 2014). Furthermore, unlike in D1 KO mice, place cells in D2 KO mice responded to displacements of both distal and proximal cues in familiar and novel environments—similar to

the responses seen in wild-type mice—yet their place fields remained less stable overall (Nguyen *et al.*, 2014)

3.4.3. Dopamine receptor expression profiles

The hippocampus expresses a high density of dopamine receptors, particularly the D1-like (D1, D5) and D2-like (D2) subtypes. Immunohistochemical and autoradiographic studies have revealed the presence of D1 and D5 receptors throughout the hippocampal formation, with a higher expression in the dorsal hippocampus compared to the ventral portion (Savasta, Dubois and Scatton, 1986; Wamsley *et al.*, 1992; Devoto *et al.*, 2001; Edelmann and Lessmann, 2018). Furthermore, studies have described a dorso-ventral gradient of D2 receptor expression, increasing toward the ventral part (**Figure 1.7**) (Gangarossa *et al.*, 2012; Puighermanal *et al.*, 2015; Edelmann and Lessmann, 2018; Dubovyk and Manahan-Vaughan, 2019). The apical dendrites (in layers SR and SLM) of the ventral CA2 region also exhibited higher D2R expression compared to the dorsal pole (Dubovyk and Manahan-Vaughan, 2019). Dopamine receptors are located on both pyramidal neurons and interneurons, suggesting a broad role in modulating hippocampal circuits (Puighermanal *et al.*, 2017) .

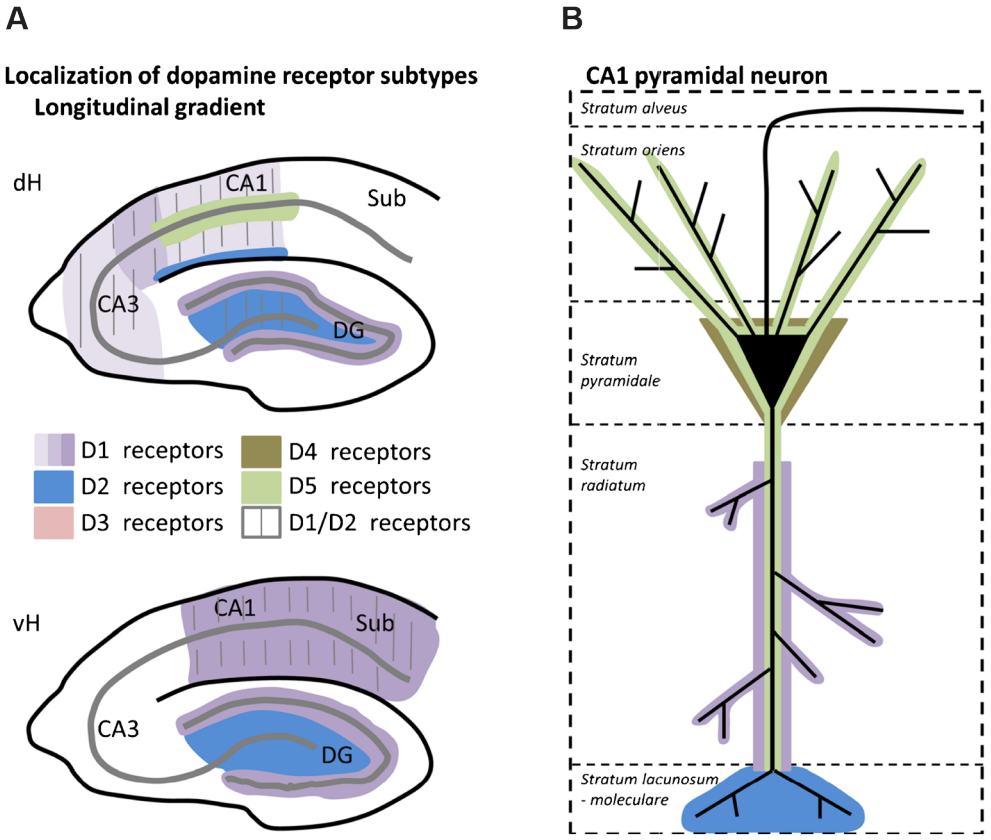

Figure 1.7: Localization of dopamine receptor subtypes along the longitudinal axis of the hippocampus.
*(**A**) Dopamine receptor density in the different subregions of the dorsal hippocamus (dH) and ventral hippocampus (vH). For different receptor subtypes, see color code. Lighter purple depicts lower, darker purple higher abundance of D1 dopamine receptors. CA1, CA3 cornu ammonis region 1 or 3, DG dentate gyrus, Sub subiculum. (**B**) Expression pattern of different members of the dopamine receptor family along the dendrites and at the soma of an individual CA1 pyramidal neuron. Meaning of color codes is identical to A. For D2Rs in stratum lacunosum moleculare, the possible presence in presynaptic and/or postsynaptic structures was not resolved. Figure from Edelamann and Lessmann, 2018.*
This schematic could be complemented with recent work (Dubovyk&Manahan-Vaughan, 2019) that revealed higher expression of D2 receptors in vCA2 layers SR and SLM, compared to dCA2.

3.4.4. Sources of dopamine in the HPC

There are two main sources of dopamine (DA) in the hippocampus: one arises from the **ventral tegmental area** (VTA) of the midbrain, and the other from the **locus coeruleus (LC)** (Duszkiewicz *et al.*, 2019). Although, VTA dopaminergic projections **to the dorsal hippocampus** were revealed by anterograde and retrograde tracing studies, these projections are **sparse** (Gasbarri, Sulli and Packard, 1997; McNamara *et al.*, 2014; Tsetsenis *et al.*, 2021). Recent studies using viral tracing and optogenetics (*via* channelrhodopsin) confirmed the presence of **TH+ (tyrosine hydroxylase-positive) fibers** from the VTA in the **stratum oriens and stratum radiatum** of CA1 (Broussard *et al.*, 2016; Tsetsenis *et al.*, 2021; Tsetsenis, Broussard and Dani, 2023). In contrast, the **LC**, traditionally associated with norepinephrine release, has emerged as an important alternative source of hippocampal dopamine. LC neurons synthesize DA as a precursor to norepinephrine and can **co-release dopamine and norepinephrine** in the hippocampus (Devoto *et al.*, 2001; Kempadoo *et al.*, 2016; Smith *et al.*, 2016; Takeuchi *et al.*, 2016).

These two structures related to dopamine function exert strong influence on hippocampal circuits during reward-based spatial learning.

Altogether, these studies highlight the important contribution of hippocampal D1/D5 receptor signaling to the encoding of spatial memory and to the flexibility of cognitive maps, which adapt to changes in the external environment through place field remapping. However, these pharmacological and genetic studies, cannot provide information about the origin of the dopaminergic signal and the sources that are activated during these cognitive processes.

3.5. Manipulation of dopaminergic inputs to reshape goal-directed behaviour

Recent studies have demonstrated that **manipulating dopaminergic inputs to the hippocampus can reshape goal-directed behaviour and spatial representations**, highlighting the previously reported dopamine's modulatory role in learning and memory.

For instance, **optogenetic stimulation of dopaminergic fibers from the locus coeruleus (LC) to dorsal CA1** enhances spatial learning and promotes **overrepresentation of goal locations** in place cell activity during reward-based tasks (Kempadoo *et al.*, 2016; Takeuchi *et al.*, 2016; Kaufman, Geiller and Losonczy, 2020a). This was elegantly shown by Kaufman et al. (2020), who combined two-photon calcium imaging of CA1 with LC axonal recordings and found that LC axon activity increases near the reward location, leading to stronger place cell recruitment in that zone. Indeed, optogenetic suppression of LC inputs reduced place cell accumulation near the reward zone while optogenetic activation did the opposite. Similarly, **post-encoding LC activation** improved long-term memory for the previously learned spatial goals. This effect was blocked by D1/D5 receptor antagonist infusion in the hippocampus, confirming an effect mainly mediated by LC-derived dopamine **(Figure 1.8)** (Takeuchi *et al.*, 2016).

Parallel studies demonstrated VTA dopaminergic implication in rewarded-guided spatial navigation tasks and spatial coding. **Direct optogenetic stimulation of VTA fibers during learning stabilizes newly formed hippocampal** place fields and enhances memory retention for reward locations (McNamara *et al.*, 2014; Mamad *et al.*, 2017a; Tamatsu *et al.*, 2023). Not only does VTA activation stabilizes place cell activity, it also inhibits interneurons in CA1 and can **shift place fields towards** the site where the stimulation took place mimicking natural reward-related remapping **(Figure 1.8)**. Conversely, suppression of VTA inputs can elicit **place avoidance behaviors** and induce remapping of place fields, shifting spatial population vectors towards the non-opto-modulated arm (Mamad *et al.*, 2017a). Moreover, **Tamatsu et al. (2023)** recently showed that the **VTA–hippocampal dopaminergic pathway enables rapid updating** of spatial goals: its disruption impairs the recall of reward locations and its activation accelerates adaptation to new goal positions in a circular maze task.

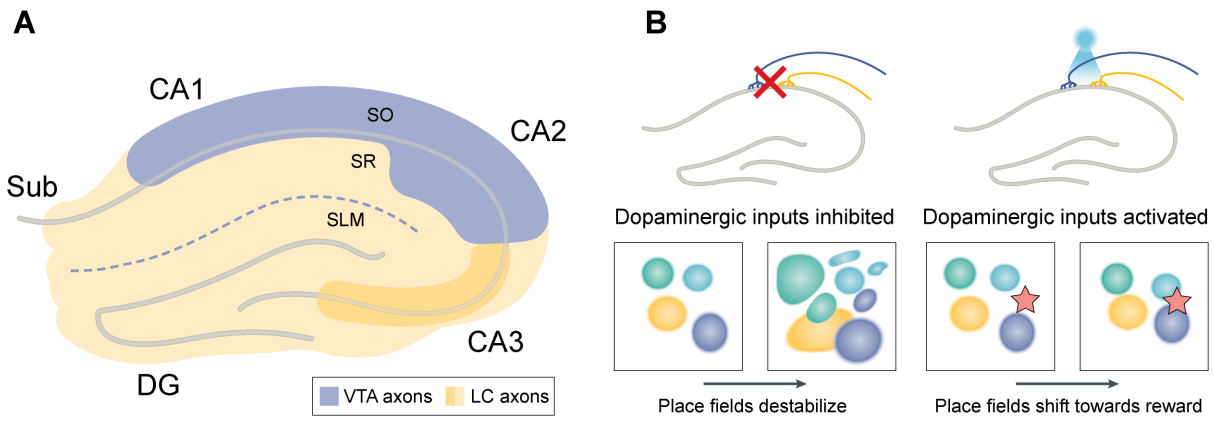

Figure 1.8: Dopaminergic inputs to the hippocampus reshape spatial maps.
*(**A**) Schematic distribution of VTA (in blue) and LC (in yellow) projections in the hippocampus. Darker yellow indicates greater density of LC axons in CA3. (**B** Summarized effects of dopaminergic input inactivation or activation on four hippocampal place fields (colored blobs). **Left**: LC or VTA axon inhibition (colors as in part c), or dopamine antagonism in the hippocampus, destabilizes place fields in sequential exposures to the same square environment. **Right**: LC or VTA axon activation with optogenetics (shown as a blue light) promotes the shift of place fields towards a goal location (pink star). DG, dentate gyrus; SLM, stratum lacunosum moleculare, SO, stratum oriens; SR, stratum radiatum; Sub, subiculum. Adapted from Sosa et al., 2021.*

Altogether, these studies underscore a **causal role for dopaminergic modulation**—both from **VTA and LC projections**—in shaping hippocampal spatial representations and **promoting flexible, goal-directed memory**. However, the mechanisms through which these two regions participate in spatial memory is still a matter of debate. LC is thought to contribute to hippocampal coding via increasing **attentional mechanisms** towards salient cues, notably via noradrenaline (Lemon *et al.*, 2009), while VTA is believed to provide a **rewarding signal** to the hippocampus via dopamine (Schultz, Dayan and Montague, 1997; Tsai *et al.*, 2009).The complexity of these neuromodulatory systems and their complementary actions will require further investigations to fully capture their respective roles in shaping hippocampal function.

Nevertheless, the hippocampus appears to integrate both reward signals and spatial information, relaying this integrated information to guide goal-directed behavior. Indeed, dorsal hippocampus (dHPC) projections to the nucleus accumbens (NAc) have been shown to support memory-guided behavior in sucrose-conditioned place preference (CPP) tasks (Trouche *et al.*, 2019). Furthermore, these dHPC-NAc projections were not only necessary but also sufficient for spatial memory-related appetitive behavior (Barnstedt, Mocellin and Remy, 2024). Notably, the subpopulation of hippocampal neurons projecting to the NAc contains a higher proportion of place cells and their activity is modulated during goal-related behaviors, such as deceleration

and anticipatory licking, suggesting that these neurons are more likely to encode spatial information about the goal (Barnstedt, Mocellin and Remy, 2024).

Despite these findings, the precise mechanisms through which the hippocampus integrates information and interacts with downstream targets to support spatial memory remain to be further explored.

4. CA2 in the hippocampal circuits

4.1. A distinct region of the HPC morphologically and physiologically

4.1.1. A distinct morphology

Originally described in 1934 by Lorente de Nó, CA2 is historically defined as the area located between the CA3 and CA1 regions with large pyramidal cells that, in contrast with the ones from CA3, lack thorny excrescences (complex spines) on their apical dendrites and lack innervation from the DG (Lorente De Nó, 1934; Tamamaki, Abe and Nojyo, 1988; Ishizuka, Cowan and Amaral, 1995). Recent research progress has further contributed to describe CA2 as a morphologically, physiologically and functionally unique region of the hippocampus proper (Jones and McHugh, 2011; Benoy, Dasgupta and Sajikumar, 2018; Piskorowski and Chevaleyre, 2018; Chevaleyre and Piskorowski, 2023).

CA2 distinguishes itself from other CA regions by the larger size of its pyramidal neurons and a thicker somatic layer (Chevaleyre and Siegelbaum, 2010). Along its radial axis, similarly to CA1 and CA3, CA2 is organized in different layers that align to different parts of principal cells parallel dendritic arborization. Among these layers, we can distinguish: the *stratum oriens* (localization of the basal dendrites, the deepest layer compared to the pyramidal layer), the *stratum pyramidale* (that contains the soma of the pyramidal cells); the apical dendrites are longer than the basal ones and successively cross the *stratum lucidum*, the *stratum radiatum* (that receives Schaffer collateral projections from CA3) and the *stratum lacunosum moleculare* (that contains the inputs from the EC). The layer called *stratum lacidum* houses the mossy fiber projections and is present only in regions CA3 and CA2. DG granule cells send mossy fibers to the proximal apical dendrites of CA3 pyramidal neurons, where they form characteristic synaptic connections *via* giant mossy fiber boutons that envelop the complex dendritic spines of CA3—structures known as thorny excrescences (Amaral and Dent, 1981;

Rollenhagen *et al.*, 2007). Early works from Lorente de Nó and Ramon y Cajal showed that CA2 lacks this type of synaptic connections characteristic of DG-CA3 synapses. This led to think that DG does not form connections with CA2 but we will see later that this is not the case (see later the section on CA2 inputs). Thanks to its morphological characteristics, CA2 is easily identifiable in transverse hippocampal slices as a cell-dense triangle that begins approximately where the end of the mossy fiber projections are located.

As mentioned above, pyramidal neurons of the different CA regions share common features: numerous short basal dendrites and a long apical dendrite that terminates with a dendritic tuft. However, few distinctions among the different CA subfields can be mentioned: CA1 pyramids typically have a single apical dendrite that usually does not bifurcate, or if it does, this occurs away from the soma. Yet, they have numerous secondary oblique dendrites located in the SR (Ishizuka, Cowan and Amaral, 1995). In contrast, CA2 apical dendrite bifurcates closes to the soma into two or three dendrites that reach to the SLM, and CA2 pyramids have very few secondary oblique dendrites. The apical dendrite of CA2 pyramidal neurons divides into more branches in SLM than CA1 or CA3 (Ishizuka, Cowan and Amaral, 1995; Chevaleyre and Siegelbaum, 2010; Sun *et al.*, 2014) which results in an overall larger distal dendritic arborization. Morphologies of CA1- and CA2-PYR are illustrated in **Figure 1.9.** The organization of the dendritic arborization of CA2 pyramidal cells has a direct influence on their firing and on the inputs type and number that they receive (Helton *et al.*, 2019).

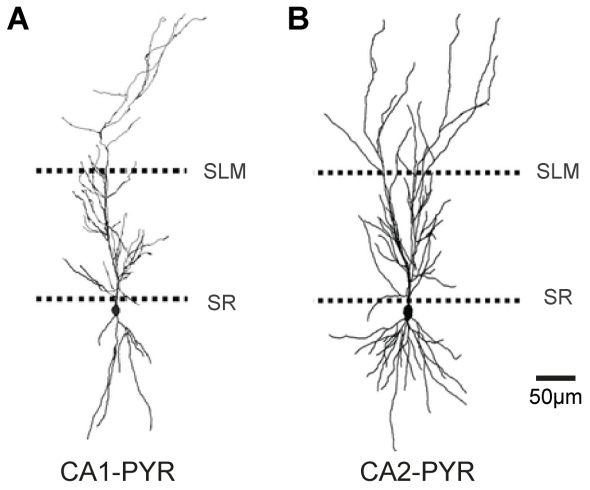

Figure 1.9: Different morphology of CA1 and CA2 pyramidal neurons.
*Representative Neurolucida drawing of mouse CA1-PYR (**A**) and CA2-PYR (**B**). Border of stratum radiatum (SR) and stratum lacunosum moleculare (SLM) denoted by dashed lines. Scale bar equivalent to 50 µm. Adapted from Helton et al. 2019.*

4.1.2. Pyramids with a distinct genetic profile

Since the initial morphological studies describing the region CA2, several recent works further redefined CA2 as a distinct region from CA1 and CA3. Several studies indicated an enrichment of specific proteins in area CA2. Among these, I can cite: **cacng5** (Fukaya *et al.*, 2005), **STEP** (Boulanger *et al.*, 1995), **TREK-1** (Talley *et al.*, 2001), **Adenosine receptor 1** (Ochiishi *et al.*, 1999), **calbindin** (Leranth and Ribak, 1991), **RGS14** (Lee *et al.*, 2010), **α actinin, PCP4** , **fibroblast growth factor** (Woodward *et al.*, 1992; Gómez-Pinilla, Lee and Cotman, 1994), **Mapk3** (Lein, Zhao and Gage, 2004) and **neurotrophin 3** (Phillips *et al.*, 1990). A recent RNA-seq database provided a more detailed genetic profile of CA2 pyramidal neurons (PYR) (Cembrowski *et al.*, 2016). This analysis confirmed previously known genetic markers and identified novel ones, with a total set of 41 genes exhibiting over threefold enrichment in CA2 compared to CA1 and CA3. These findings strongly supported the idea that CA2 constitutes a molecularly distinct hippocampal subregion, rather than merely representing a transitional zone between CA1 and CA3. More recently, a Drop-seq single-cell transcriptomic analysis further dissected the molecular diversity of CA2-PYR, revealing eight distinct subclusters based on the expression of six CA2-specific marker genes (Bienkowski, 2023), thus underscoring the **cellular heterogeneity** within this region.

Additional transcriptomic studies refined the CA2 boundaries along the dorsal-ventral hippocampal axis (Lein *et al.*, 2005) and proximo-distal axis (Sun *et al.*, 2017; Fernandez-Lamo *et al.*, 2019; Radzicki, Chong and Dudek, 2023). These studies demonstrated **a more subtle transition between region CA3 and CA2**, by showing that the distal part of CA3 (CA3a) is genetically and functionally more similar to CA2 principal cells (Piskorowski and Chevaleyre, 2012; Lu *et al.*, 2015a; Fernandez-Lamo *et al.*, 2019).

The fine genetic characterization of the region CA2 in the past years has allowed the generation of specific mouse lines expressing the Cre recombinase under CA2-specific promoters, enabling the targeting of CA2 PYR. Among them, the following lines have been used: *Amigo2-cre* (Hitti and Siegelbaum, 2014a), *MapK 315-Cre 5* (Kohara *et al.*, 2014a; MacDonald and Tonegawa, 2021), *Avpr1b-cre* (Smith *et al.*, 2016) and the *Cacng5-cre* (Boehringer *et al.*, 2017a).

4.1.3. Pyramids with a distinct physiology both *ex vivo* and *in vivo*

Beyond their unique genetic profile, CA2 PYR distinguish themselves from their neighbors by their intrinsic properties. CA2 PYR were reported to have a **more hyperpolarized resting membrane potential** (from -76 mV to -74mV, on average in adult mice) (Zhao *et al.*, 2007; Chevaleyre and Siegelbaum, 2010; Sun *et al.*, 2014, 2017; Boehringer *et al.*, 2017a; Srinivas *et al.*, 2017). Because of their larger size and their numerous apical dendrites, CA2 PYR have a **larger membrane capacitance** than CA1 PYR, with values that are more similar to CA3 PYR (Zhao *et al.*, 2007; Chevaleyre and Siegelbaum, 2010; Sun *et al.*, 2017). They also have **a lower membrane resistance** in part due to the overexpression of "leak" channels (TREK (Talley *et al.*, 2001)). In awake behaving animals, CA2 has been reported to have a **higher firing rate than** CA1 and CA3 (Mankin *et al.*, 2015a; Oliva, Fernández-Ruiz, *et al.*, 2016). During slow wave sleep, CA2 PYR show different patterns of activation relative to the so-called sharp-wave ripples (SWR) depending on their location in the pyramidal cell layer. Deep CA2 PYR defined as "ramping cells" enhance in their firing rate ~100 milliseconds before SWR. In contrast, superficial CA2 PYR, defined as "phasic cells", increase in their firing rate during SWR (like their peers in CA1 and CA3) (Oliva, Fernández-Ruiz, *et al.*, 2016; Karaba *et al.*, 2024a).

Together, the research of the past twenty years, demonstrated that CA2 is more than just a continuum between CA3 and CA1. Its distinctive properties may play a different role in the hippocampal memory processing.

4.2. CA2: a "hidden" hub inside of the hippocampus

4.2.1. Intra-hippocampal connectivity

CA2 has long been considered as a simple transition zone between CA3 and CA1. Yet, it slowly gets to be integrated in the already established circuits of information processing within the hippocampus. CA2 distinguish itself not only morphologically and genetically but also by its unique connectivity (**Figure 1.10**) (Oliva, Fernandez-Ruiz and Karaba, 2023).

i) Inputs from the DG

Although, CA2 was initially described as lacking thorny excrescences (No 1934), some CA2 PYR do receive functional monosynaptic inputs from the DG *via* the mossy fibers, as shown

via optogenetic stimulations by Kohara *et al*. in 2014. Direct projections from both mature and adult-born granule cells were observed (Llorens-Martín *et al.*, 2015; Laham *et al.*, 2024). Morphologically distinct from the classical DG-CA3 synapses, the DG-CA2 connections are also weaker than DG-CA3 (Sun *et al.*, 2014). Indeed, these inputs were shown to engage feedforward inhibition within CA2. Curiously, this connection was neither identified in rats by retrograde tracing (Cui, Gerfen and Young, 2013)nor in the Amigo2-Cre mouse line (Hitti and Siegelbaum, 2014a), meanwhile Kohara *et al*. used the MAP3K15-cre line. The differences may be due to the specificities of the vectors and transgenic mouse lines, which may sometimes not fully capture the heterogeneity of CA2 populations.

ii) Inputs from CA3

CA2 receives direct excitatory inputs from CA3 as shown by conventional and rabies-based retrograde labelling, as well as by direct electrical stimulation in brain slices (Chevaleyre and Siegelbaum, 2010; Cui, Gerfen and Young, 2013; Hitti and Siegelbaum, 2014a). Schaffer collaterals (SC) inputs to CA2 are relatively weak compared to SC-CA1, and they are **strongly dominated by powerful feed-forward inhibition** in acute slices from mice. Important plasticity mechanisms control this powerful inhibition (see paragraph 4.4 below). While projections from CA2 to CA1 are unilateral, **CA2 and CA3 connectivity is bidirectional** (Chevaleyre and Siegelbaum, 2010; Piskorowski and Chevaleyre, 2013; Nasrallah, Piskorowski and Chevaleyre, 2015a; Boehringer *et al.*, 2017a)

iii) Outputs from CA2

In 2004, Bartesaghi *et al*. demonstrated that CA2 can activate directly CA1, independently of CA3 (Bartesaghi and Gessi, 2004). Later Cui et al., reported that CA2 project ipsi- and contra-laterally to CA1, CA2 and CA3. CA2 PYR send projections mainly in the SO layer of CA1 and principally to deep pyramidal cells (Shinohara *et al.*, 2012a; Kohara *et al.*, 2014a; Valero *et al.*, 2015a; Oliva, Fernández-Ruiz, *et al.*, 2016; Soltesz and Losonczy, 2018a) . In contrast, CA3 PYR principally sent inputs in the SR of CA1 (Hitti and Siegelbaum, 2014a). Challenging paired recordings realized by Vivien Chevaleyre in 2010, revealed that the excitatory drive brought about by CA2 to CA1 through excitatory monosynaptic connections was way stronger than the one observed at CA3 to CA1 connections. On the contrary to CA1 excitation, the CA2 to CA3 connection in the SR is dominated by feedforward inhibition (Boehringer *et al.*, 2017a).

Notably and in a unique manner for the hippocampus, CA2 projects both to the ventral and dorsal HPC (Okuyama *et al.*, 2016; Meira *et al.*, 2018). On top of these projections, CA2 show

an important level of recurrent excitation (Cui, Gerfen and Young, 2013; Okamoto and Ikegaya, 2019).

Therefore, within the hippocampus, CA2 occupies a unique role, controlling the excitatory and inhibitory balance of the tri synaptic circuit.

4.2.2. Extra-hippocampal inputs :

i) Cortical inputs

The dense dendritic arborisation of CA2 in the SLM receives direct inputs from the EC II (Bartesaghi and Gessi, 2004; Bartesaghi, Migliore and Gessi, 2006; Chevaleyre and Siegelbaum, 2010; Cui, Gerfen and Young, 2013; Hitti and Siegelbaum, 2014a; Kohara *et al.*, 2014a; Srinivas *et al.*, 2017). Bartesaghi and al. showed that *in vivo*, in guinea pigs, CA2 is the first region to be activated after EC stimulation (i.e. before CA1 and CA3). Furthermore, in acute mouse brain slice recordings, it was demonstrated that the EC inputs to CA2 PYR provide a stronger excitatory drive than EC inputs to the distal dendrites of CA1 PYR (Chevaleyre and Siegelbaum, 2010). Thus, the entorhinal information arrives through three parallel pathways to CA1: (1) by direct inputs from EC (layer III) but also through CA2, and (3) indirectly *via* CA3 and the trisynaptic loop (**Figure 1.10**). The functional differences of these parallel circuits are yet to be discovered.

ii) Other inputs to CA2

CA2 receives inputs from the paraventricular nucleus of the hypothalamus (**PVN**) (inputs containing vasopressin) (Cui, Gerfen and Young, 2013). Another hypothalamic nucleus sending its projections to CA2 is the **Supra-mammilary nucleus** (SuM) (Haglund, Swanson and Köhler, 1984; Vertes, 1992). The lateral part of the SuM sent projections to CA2 and DG. However, the medial SuM was reported to project exclusively to CA2, highlighting again the distinction of this region from the rest of the HPC (**Figure 1.10**) (Haglund, Swanson and Köhler, 1984; Chen *et al.*, 2020a). These projections are glutamatergic but contain also substance P or calretinin, mostly targeting the soma of CA2 PYR (Haglund, Swanson and Köhler, 1984; Maglóczky, Acsády and Freund, 1994). However, these projections were shown to recruit large feedforward inhibition (Chen *et al.*, 2020a).

Additionally, retrograde tracing injection into CA2 labeled projections from **medial septum/the diagonal band of Broca, and the median raphe nucleus** (Cui, Gerfen and Young, 2013). Last but not least, CA2 receives inputs from two major regions involved in reward processing: **the Ventral Tegmental Area (VTA) and the Locus Coeruleus (LC**) (Ntamati and Lüscher, 2016; Takeuchi *et al.*, 2016). The nature of their cellular targets within CA2 remains however unclear.

iii) Outputs:

Anterograde tracings have shown that CA2 projects to the SuM, the medial septum (MS), and the diagonal band of Broca, thereby forming reciprocal connections with each of these regions (Ishizuka, Cowan and Amaral, 1995; Cui, Gerfen and Young, 2013; Leroy *et al.*, 2018). Interestingly, although projections from CA2 PYR to the lateral septum were reported previously (Cui, Gerfen and Young, 2013), studies using the Amigo2-Cre line—expected to label most CA2 PYR (Bienkowski, 2023)—failed at reporting these extra-hippocampal outputs (Hitti and Siegelbaum, 2014a). It is therefore likely that the Amigo2-Cre mouse line is missing a subpopulation of PYR that target the lateral septum.

CA2 and EC may also be bidirectionally connected, as a projection from CA2 back to the EC was observed with retrograde tracing based on a non-cell-specific retrograde labelling (Rowland *et al.*, 2013).

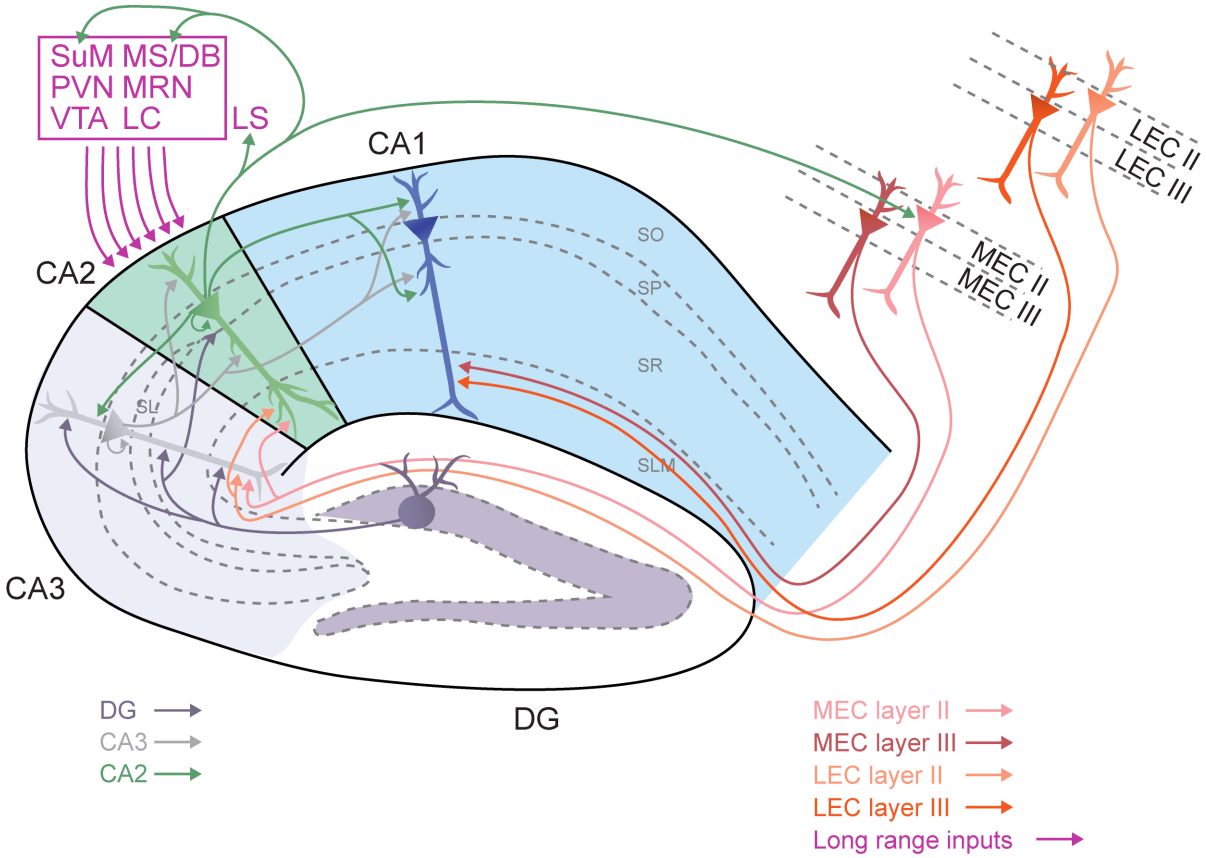

Figure 1.10: Hippocampal CA2 region connectivity.
Intra-hippocampal connections: CA2 PNs receive afferents from SCs in SR, from the EC II (medial and lateral) in SLM and can also receive MF input in SL. CA2 PNs project back onto CA3 PNs in SR and project to CA1 PNs in SO, and back to layer II in MEC. Extra-hippocampal connections: CA2 receives long range inputs from different regions including supramammilary nucleus (SuM), paraventricular nucleus (PVN), median raphe nucleus (MRN), medial septum diagonal band (MS/DB), the ventral tegmental area (VTA), and lateral septum (LS). CA2 sends back axons to the SuM as well as to the MS/DB.
Schematic adapted from Oliva et al. 2023.

4.3. Interneurons of CA2

As in CA1 and CA3, CA2 interneurons (INs) are distributed among layers. However, CA2 distinguishes from its neighbouring regions, by **a higher density of INs** (Botcher *et al.*, 2014a). Notably, in the pyramidal layer, CA2 has a significantly higher proportion of paravalbumin positive (PV+) INs than CA1, along with a higher proportion of cholecystokinin positive (CCK+) and reelin+ INs in SR. These studies suggest that CA2-PYR activity might be tightly controlled by inhibitory transmission. In fact, disruption of inhibitory circuits in this region was linked with several neuronal pathologies such as schizophrenia in mouse-model and

humans(Zhang and Reynolds, 2002; Benes *et al.*, 2008; Piskorowski *et al.*, 2016), epilepsy (Whitebirch *et al.*, 2022), or Alzheimer disease (Rey *et al.*, 2022a).

4.4. Modulation of CA2 activity and synaptic plasticity

Describing CA2 connectivity in the hippocampal and brain circuits questions its role in information processing and transmission and how does this small region integrate into the well described tri-synaptic pathway.

For a long time, it was believed that CA2 was unable to form long-term potentiation (LTP) at the CA3-CA2 synapse, unlike the one largely described at the CA3-CA1 connection. Specifically, Zhao and *al.* reported that they failed at evoking LTP at CA3-CA2 synapses using high frequency stimulation (HFS, 100 pulses at 100Hz) or pairing-protocol (simultaneous depolarisation of the PYR while stimulating SC inputs). These protocols are usually used to evoke robust LTP in CA1 region (Zhao *et al.*, 2007; Simons *et al.*, 2009). The properties of the SC to CA2 connections contrast considerably with the strong direct excitation that CA2 receives from the EC (Chevaleyre and Siegelbaum, 2010). In fact, the EC-CA2 excitatory connection can undergo NMDA receptor (NMDAR)-dependent LTP as shown by whole-cell and field recordings (Chafai *et al.*, 2012; Chevaleyre and Piskorowski, 2016; Dasgupta *et al.*, 2020). This intriguing singularity of CA2 network, led to a series of studies to disentangle the mechanisms ruling CA2 activity.

CA2 have been reported to have a higher density of interneurons than neighboring regions (Botcher *et al.*, 2014a). It was demonstrated that the stimulation of CA3-SC in the SR on acute slices from mice induces a strong feedforward inhibition (Chevaleyre and Siegelbaum, 2010).If an excitatory LTP is unlikely to occur at SC-CA2 synapses, it was shown that CA3 excitatory input could elicit CA2 PYR spiking in conditions where inhibition is reduced (CA2 PYR spiking following SC stimulation does not occur otherwise). Two types of so-called **inhibitory long-term depression** (iLTD) were discovered. The first plasticity is mediated by **delta opioid receptor (DOR)** activation and defined as DOR-mediated plasticity (Piskorowski and Chevaleyre, 2013). The excitatory transmission from CA3 to CA2 was shown to double upon iLTD induction (Nasrallah, Piskorowski and Chevaleyre, 2015a). This **reduction of feedforward inhibition** was shown to allow for CA3 to effectively drive action potential firing

in CA2 PYR, thus recruiting CA2 into the tri-synaptic loop(Nasrallah, Piskorowski and Chevaleyre, 2017; Nasrallah *et al.*, 2019). The DOR-dependent disinhibitory increase in SC transmission was also confirmed using a paired activation of EC inputs 20-40ms prior SC inputs (Leroy *et al.*, 2017), a phenomena called input-timing-dependent-plasticity, previously described in CA1 (Basu *et al.*, 2013).

Later on, the same team demonstrated that DOR-mediated plasticity can be followed by a second iLTD, mediated by the **cannabinoid receptors of type 1** (CB1R iLTD) (Loisy *et al.*, 2022).These two plasticities were shown to be essential for social-memory formation (Loisy *et al.*, 2022). Different types of plasticity described in CA2 are illustrated in **Figure 1.11.**

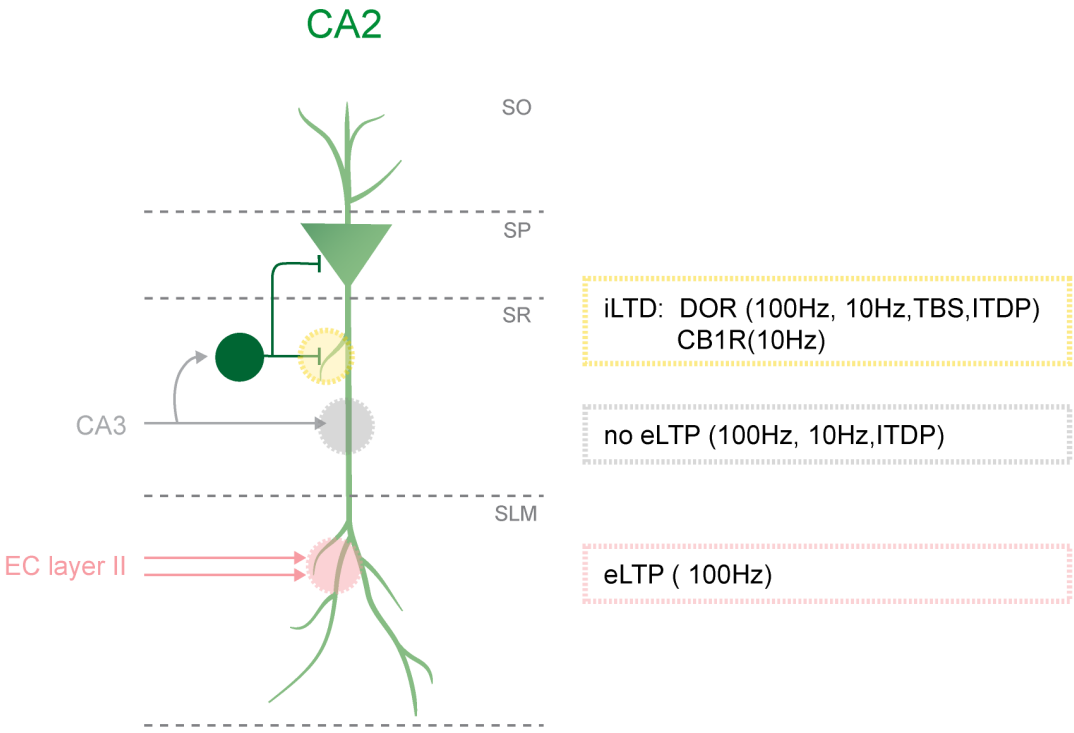

Figure 1.11: Synaptic plasticity in CA2 region.
Left*: schematic of CA2-PYR (green), a CA2-IN (dark green), CA3 excitatory inputs (grey), EC II excitatory inputs (pink).* ***Right****: Cortical inputs can undergo an excitatory long-term potentiation (eLTP) following tetanic stimulation (100 pulses at 100 Hz, repeated twice). Excitatory inputs from CA3 do not express LTP following tetanic stimulation or a pairing protocol (stimulation of CA3 inputs coupled to depolarization of the pyramidal neuron). Inhibitory inputs from Parvalbumin-expressing interneurons express a long-term depression (iLTD) following tetanic stimulation, 10 Hz stimulation (100 pulses twice), theta burst stimulation (TBS) or a pairing stimulation of cortical and CA3 inputs (ITDP). Under conditions of decreased inhibition, inhibitory inputs from CCK+ INs can undergo iLTD following a 10 Hz stimulation protocol and allowing action potential generation in the postsynaptic CA2 PYR.*

The unique connectivity, gene expression patterns, and cellular plasticity of CA2 suggest that its role in memory processing is distinct from those of other hippocampal subregions. The following sections will mention the recent studies demonstrating the role of CA2 in encoding social, temporal and contextual memory.

4.5.CA2 role in social memory

We have seen that CA2 is well placed to integrate sensory information from EC. In the last decade, CA2 was shown to play a key role in social memory, defined in rodents as the ability to discriminate between novel and familiar conspecifics (Hitti and Siegelbaum, 2014a).Since the seminal study of Hitti and colleagues, several studies corroborated the importance of CA2 in social memory encoding (Stevenson and Caldwell, 2014; Meira *et al.*, 2018; Oliva *et al.*, 2020; Loisy *et al.*, 2022).

First evidence of the implication of CA2 in social memory came from the observation that the receptors for the neuropeptides vasopressin and oxytocin, known to be involved in social behaviors, are strongly expressed in this region. It was shown, that mice lacking the vasopressine V1b receptor, which is selectively enriched in CA2 neurons (Young *et al.*, 2006), have more troubles to discriminate between novel and familiar stimulus mice than wild type mice (10min exposure, every 5min, repeated 10 times). Furthermore, two lesions' studies published close in time, demonstrated the necessity of CA2 region in a social memory recognition task. Hitti *et al*. used the transgenic mouse line Amigo2-Cre to express a tetanus toxin specifically in almost all CA2 PYR in order to block neuronal transmission form these cells. Stevenson Caldwell 2014 chronically used NMDA excitotoxic injections in the CA2 region of rats (Stevenson and Caldwell, 2014). Hitti *et al*. a performed a habituation/dishabituation task with 4 presentations of 1minute familiarization to social stimulus, and a 5th presentation of a novel stimulus. Stevenson and Caldwell performed a 2-trials test, with first 5min exposure to a familiar juvenile and 30min after to the same familiar and a novel juveniles). Both studies reported impaired social memory, evidenced by the fact that the animals spent equal amounts of time exploring both familiar and novel stimuli. Importantly, both works, reported that memory impairment was not due to a decrease in sociability. Conversely, optogenetic activation of PVN vasopressinergic projections to CA2 was shown to enhance social recognition memory: animals that underwent opto-stimulation during the encounter of the social stimulus, showed a significantly decreased interest towards it,

compared to a non-stimulation condition, after 2h, 24h and 7 days presentation (Smith *et al.*, 2016)

In 2020, Oliva *et al*. showed that silencing CA2 activity in the Amigo2-Cre mouse line during long periods of time (~30s every two minutes) during sleep, decreased the number of SWRs, which resulted in social memory deficits. Using previously described optogenetic methods (Stark *et al.*, 2015; Fernández-Ruiz *et al.*, 2019), additional SWRs generation selectively in CA2 during post-experience, was sufficient to extend social memory recall in mice a 24h. To show the specificity of CA2 in social memory consolidation, the researchers also triggered SWRs from the CA3 region (using Grik-4 animals, which express the Cre recombinase in CA3 pyramidal cells), and showed that it has no impact on social memory.
Additionally, using on extracellular CA2 recordings collected during social recognition tasks, it is possible to predict if the encountered individual is familiar or novel (Donegan *et al.*, 2020a). Furthermore, in 2023, Hassan et al. demonstrated that **CA2-PYR activity codes for the social odors of distinct conspecifics**. Hassan et al., using a Bayesian decoder, showed indeed that CA2 activity also discriminates the identities of social and non-social odors (Hassan, Bigler and Siegelbaum, 2023).

Interestingly, **dorsal CA3** (Chiang *et al.*, 2018) or **dorsal CA1** do not seem to participate in social recognition memory (Okuyama *et al.*, 2016; Meira *et al.*, 2018; Oliva *et al.*, 2020).This finding suggests that the social memory processing in the HPC might involve a parallel pathway routing through CA2 and not the classical tri-synaptic loop. The direct LEC > dorsal CA2 > ventral CA1 pathway has been suggested as a crucial conduit for conveying social information in the HPC (Lopez-Rojas *et al.*, 2022). Nevertheless, synaptic connections from CA3 to CA2 have also been shown to be potentiated during social interactions (Loisy *et al.*, 2022), showing that HPC network processing involves complex parallel supporting mechanism.

While the role of CA2 in social memory has been extensively studied and is now well established, its contribution to spatial memory has long been considered minimal or negligible. Early studies, such as those involving vasopressin receptor knockouts (Wersinger *et al.*, 2002; DeVito *et al.*, 2009) or selective silencing of CA2 pyramidal neurons (Hitti and Siegelbaum, 2014a), reported no significant impairments in spatial or contextual memory tasks, reinforcing the view that CA2 is primarily dedicated to social information processing. However, this interpretation warrants re-evaluation. Emerging evidence suggests that CA2 pyramidal cells

may also exhibit spatial properties that have been overlooked or minimized. In the following section, I will examine latest works, offering a more nuanced perspective on CA2's role in episodic memory.

4.6. CA2 beyond social memory

Naturally, several studies have investigated spatial properties of the CA2 region (Lu *et al.*, 2015a; Mankin *et al.*, 2015a; Alexander *et al.*, 2016a; Oliva, Fernández-Ruiz, *et al.*, 2016; Bhasin and Nair, 2022a).

Place cell characterization

Mankin et al. 2015 observed that CA2 place cells have a higher mean firing rate (FR), more place fields (PF) per cell, and larger place fields (24,5% bigger than CA1), lower spatial information (bits/spike) than CA1 or CA3 place cells. These observations were corroborated by several other studies (Lu *et al.*, 2015a; Alexander *et al.*, 2016a; Oliva, Fernández-Ruiz, *et al.*, 2016).

Remapping in CA2

CA2 place cell were shown to remap following contextual changes ((Wintzer *et al.*, 2014a); shown by cfos activation) and presentation of social stimuli (Alexander *et al.*, 2016; shown with unit recordings). However, CA2-PYR seem to be less sensitive to small contextual changes, and do not remap (rate remapping) following changes in the enclosure features (color or shape), in contrast to CA1-PYR (Lu *et al.*, 2015a; Mankin *et al.*, 2015a). This relative stability of CA2 was also observed following the displacement of spatial cue (Lee *et al.*, 2015). Contrasting with these results, Alexander *et al.* showed that CA2 spatial correlation decreases with the introduction of a familiar or novel mouse. The sensitivity of CA2 to environmental changes may depends on the nature of these changes and in particular their salience for the animal.

Time-dependent drift in CA2 spatial representation

In contrast to this apparent stability with regards to environmental changes, CA-PYR appears less stable when considering the passage of time. The Mankin study showed that CA2 place cells change their firing pattern across repeated exposures to the same familiar environment: CA2 place fields were less stable across trials than CA3 and CA1, when trials are separated by

several hours (6h hour interval). Alexander et al. 2016 also showed that CA2 spatial correlation decreases over time. Overall, these observations lead to question the role of CA2 in spatial memory processing and the encoding of unique episodes.

An apparent lower spatial content questioning its role in spatial memory

After the first establishments of a decreased spatial coding in CA2 as compared to its neighbouring regions, its role in spatial memory was often overshadowed by its undeniable importance in social memory. Indeed, the chronic suppression of CA2 PYR synaptic transmission in the Amigo2-Cre line did not evoke an important impairment in spatial memory when tested with the Morris water maze task (Hitti and Siegelbaum, 2014a). However, these results were revisited (Lehr *et al.*, 2023) and showed that animals with chronic inhibition of CA2-PYR transmission showed a delayed learning the Morris water maze. Therefore, **the role of CA2 in the plasticity of memory circuits during spatial learning remains an open question** (Lehr *et al.*, 2021)**.**

What remains unclear, however, is the advantage conferred by having a CA2 representation of space that remaps gradually over time to a greater extent than its neighbors.

CA2 regulates spatial encoding in other hippocampal regions

Due to the powerful feedforward inhibition that CA2 normally exerts on CA3, chronic suppression of CA2 has been shown to induce hyperexcitability of the hippocampal network, leading to decreases in the spatial information of place cells in all CA regions. Acute inhibition of CA2, *via* inhibitory DREADD expression, leads to an impaired spatial coding precision in the HPC (Boehringer *et al.*, 2017a). This disruption underscores CA2's critical role in maintaining the excitatory-inhibitory balance within hippocampal circuits.

Further investigations have revealed that CA2 activity contributes to the fidelity of experience-dependent hippocampal replay. Specifically, inhibition of CA2 reduces the precision of hippocampal assembly reactivation during SWRs, which are essential for memory consolidation (He *et al.*, 2021).

Encoding of animal position during immobility

An important study from Kay and colleagues (2016) investigated the role of CA2 in a hippocampus-dependent spatial memory task. The animals were trained to alternate between

three reward locations in a W-shaped maze. *In vivo* recordings of the hippocampus during the task revealed the presence of a heterogeneous population of units in CA2: among them, a subpopulation of principal units (~25% of recorded CA2 principal units) was firing continuously at higher rates during immobility at specific locations in the maze. This observation led to the conclusion that CA2 neurons code for the animal position during immobility intervals. Interestingly, periods of immobility in this work were concomitant to reward consumption, suggesting that this subpopulation might also be involved in reward coding. Supporting this idea, it was shown that pairing odors with rewards enhanced the decoding accuracy of stimulus identity — both social and non-social odors — from CA2 activity (Hassan, Bigler and Siegelbaum, 2023). Together, these findings suggest that CA2 may integrate spatial, sensory and reward information to support associative learning.

CA2 sensitivity to novelty

Moreover, CA2 has emerged as particularly sensitive to novelty, with place cells in CA2 exhibiting remapping in response to contextual changes, social novelty (Wintzer *et al.*, 2014b; Alexander *et al.*, 2016a; Donegan *et al.*, 2020b; Bhasin and Nair, 2022b). Recent studies suggest that this novelty sensitivity may be linked to unique inputs from the supramammillary nucleus (SuM) of the hypothalamus, which acts as a "novelty hub" routing distinct types of novelty signals to the hippocampus (Chen *et al.*, 2020a). SuM projections to CA2 are preferentially engaged by social novelty and are largely glutamatergic, offering a content-specific modulation of CA2's activity.

Collectively, these findings highlight that while CA2's role in social memory has received significant attention, its contributions to spatial coding and memory processing are under-investigated. CA2's unique physiological and anatomical properties – including its powerful feedforward inhibition of CA3, its distinct remapping and temporal drift profiles, and its sensitivity to salient and social novelty – position it as an essential regulator of hippocampal network dynamics. Notably, CA2 activity ensures the fidelity of spatial representations in downstream hippocampal areas, impacting spatial coding precision and memory replay. These insights suggest that CA2 acts as more than a social memory hub: it has a central position to play a role in the fine-tuning of hippocampal circuits that support adaptive spatial memory and flexible cognitive mapping.

5. Hypotheses and aims of the PhD project

While much of our understanding of reward-driven changes in spatial coding comes from studies of CA1 and CA3, the role played by CA2 remains poorly understood. As recent findings showed that CA2 is active during immobility epochs hosting reward consumption events (Kay *et al.*, 2016) and given CA2 sensitivity to novelty signals (Wintzer *et al.*, 2014a; Alexander *et al.*, 2016b; Bhasin and Nair, 2022b), we made the hypothesis that CA2 contributes to representations of new rewarded locations, potentially leading to the known goal-oriented remapping of CA1 populations (Dupret *et al.*, 2010b; Mamad *et al.*, 2017b; Zaremba *et al.*, 2017b; Kaufman, Geiller and Losonczy, 2020b). This hypothesis is consistent with the fact that the deep CA1 pyramidal neurons, in contrast to their superficial peers, preferentially remap towards rewards (Danielson *et al.*, 2016b) and also happen to be the primary targets of CA2 pyramidal cells (Shinohara *et al.*, 2012b; Kohara *et al.*, 2014b; Valero *et al.*, 2015b; Oliva, Fernández-Ruiz, *et al.*, 2016; Soltesz and Losonczy, 2018b). Yet, whether goal-oriented remapping is present in CA2 and whether CA2 presents specific responses during reward consumption is unknown. The general goal of my PhD project was therefore to test the role of CA2 in reward coding and goal-oriented remapping.

The specific aims of my thesis were the following:

- **To developed a spatial learning task that allows the study of goal-oriented remapping and responses to reward delivery in freely moving mice implanted with silicon probes.**
- **To explore neuronal activity in CA2 in this new spatial learning task and test for the presence of goal-oriented remapping in CA2.**
- **To describe CA2 activity during immobility and reward consumption.**
- **To address the specificity of CA2 activity when compared to CA1's when recorded in the same behavioural task.**

Chapter 2: Material and methods

1. Animals

All experimental procedures were performed in accordance with standard ethical guidelines (European Communities Directive 86/60-EEC) and approved by the local committee on animal health and care of Bordeaux and the French ministry of agriculture and forestry (authorization numbers 18625, 19746 / facility agreements A33063940 and A33 063 943). All behavioural experiments were performed during the light phase. Animals were kept in individual cages after surgery under a 12 h light/dark cycle (temperature and hygrometry within the following ranges: 20–24 °C and 50–70, respectively). Surgeries were performed on adult male mice (*Amigo 2 – Cre* F1ICR B6).

2. Behavioral paradigm and setup

Clock maze:

For my PhD project, I designed and custom-built the behavioural setup myself (**Figure 3.1**). Kay et al. (2016) proposed that some neurons of CA2 are more active during immobility. Yet, this was not observed everywhere in the environment but only in restricted places that were specific for each neuron (similar to "immobility place fields"). The first requirement for me was therefore to create a behavioural protocol/apparatus where the animal can stop at multiple locations. Then, in order to test whether the presence of a reward is driving activity in CA2, a second requirement was the possibility to provide rewards in some trials and omit rewards in some others. Finally, because the accumulation of place fields at reward was mostly observed in 1-dimension environments in the mouse (Hollup et al. 2001), (Zaremba et al. 2017), a third requirement was to use a track or a corridor. Based on these requirements, I built a **circular corridor** (6.5 cm wide, 180cm of circumference) with **12 equally spaced wells for reward delivery** located every 30°: **the "Clock" maze**. The nose ports were 3D printed with grey resin, in circular shape and that could fit the nose poke detector. I made the Clock-maze an automated reward-delivery maze: the 12 wells were equipped with infrared sensors: when the light beam is broken it sends at TTL signal to the Arduino that drives the activation of *Clippard* pinch valves with a fixed delay. For omission trials, **a mock valve** was activated to compensate for a possible sound-related response. A movement detector was included, in order to impose a

directionality to animal's movement, the animal could get a new reward only if it completed a full lap.

All ports were equipped with nose poke detectors, the signals of which were acquired by the Intan recording system (RDH 2000, Intan Technologies), along with valves opening command signals.

The times of the valve opening valves were set to 200ms after calibration to deliver approximatively 4µL of liquid. The reward consisted of diluted condensate milk (1:5 in drinkable water).

Behavioural task:

Each day, the mice ran two sessions, Task 1 and Task 2, during which they had to learn the location of a new rewarded port. During each Task, mice could visit this port up to 90 times after completing a full lap in the same direction. First, the animals completed ten laps in which the reward was systematically delivered. After, the reward was pseudo-randomly omitted in 25% of the laps, with the condition that an omission trial cannot be followed by a second omission.

The omission trials were meant to compare CA2 activity with or without reward consumption, while keeping the position of the mouse during immobility identical. Rest recordings of 90 minutes were performed before and after the tasks in the home cage where the mice usually fell asleep. The animal position was tracked in 3D throughout the sessions using reflective markers and the Optitrack camera system.

Pre-implantation training

Prior to the implantation, the animals were trained to perform the Clock-maze task.

Animals first tasted the condensed milk in their home cage. After, for two/three days they were habituated to the Clock-maze, to turn in one direction and retrieve rewards in different wells. Then, there were food restricted, and trained twice per day to reach 90 trials with only one rewarded location. **Animals achieving 90 laps per task session were implanted.**

Food restriction:

The mice were habituated to the food reward of condensed milk and the Clock-maze before food restriction started. Mice were kept on a restricted feeding schedule for the duration of behavioural testing to maintain at least 85% of their ad libitum-fed body weight. The food restriction was adjusted daily depending on animals' weight and motivation. For the pre-

training, animals were kept together. Implantation surgery was performed after the animals recovered their full body weight. After the surgery, animals were individually housed, and food restriction started again, gradually, after one week of post-surgical recovery.

Improving the Clock maze

In the first version of the Clock maze, the reward was delivered by the experimenter into the chosen well. This method presented several issues. First, we could imagine that the animal found the rewarded port solely based on olfactory cues (the smell of condensed milk) and not on spatial memory, although I made sure to put some residual odor in all the wells. That could have been a problem because, as shown in the literature before, place fields do not accumulate in reward locations when these are indicated by local cues (Dupret et al. 2010) and because responses could simply represent olfactory responses (Fischler-Ruiz et al. 2021). Second, we could not precisely determine the time of the consumption of the reward, since we had only access to the position of the animal next to the rewarded well and did not monitor port entry nor reward delivery. To address the first issue, we automatized the delivery of reward using a pinch valve activated by a beam-crossing due nose port entry. This way, the reward was present in the well only after the animal placed its nose in the selected port and the mouse could not base its navigation on olfactory cues. This installation enables us to precisely know when the animal is at the rewarded well but also to introduce a precise time delay between nose entry and the delivery of reward to later be able to disambiguate reward expectation from reward consumption.

3. Implantation surgeries

As it is difficult to locate the shanks located in CA1 from those located in CA2 using traditionally used stereotaxic coordinates, we have tried identifying CA2 pyramidal neurons by "opto-tagging", expressing channel rhodopsin (ChR2) in Amigo2-Cre positive cells. I have learned to build the opto-probes and successfully recorded light-responsive units together with indirectly-suppressed neuronal populations. However, we struggled with cell death and increased cases of post-surgical bleeding while lowering the silicon-probe (due to the size of the optic fiber and the fact that CA2 is highly vascularised). Moreover, the results were not very conclusive due to the indirect effects of the optogenetic stimulations.

Therefore, we aimed for more anterior and medial coordinates of CA2, where all the shanks would be in that region: AP = -1,1 mm, ML = +/- 0.5mm, DV = - 0.7 mm from skull

surface (see Histology section). These coordinates have the advantage of having a flat cell layer of pyramidal neurones.

A total of 5 mice were successfully implanted and recorded in the CA2 region during behaviour, and 3 mice in dCA1.

Dorsal CA1 was targeted with the following coordinates: AP = -1.8mm, ML = +/- 1.4mm, DV = - 0.7 from skull surface.

For surgery, mice were anesthetized using isoflurane (induced 3 min at 4% - maintenance at 1.5% for the duration of surgery) and received an intraperitoneal (i.p.) injection of metacam (5 mg/kg). After being placed on a stereotaxic apparatus (RWD), local anesthesia (lidocaine 5mg/kg) above the skull was performed, followed by a midline skin incision. Vitals and body temperature were tracked at all times using PhysioSuite (Kent Scientific), and i.p injections of NaCl 0.9% was given if necessary to avoid dehydration. Before insertion, silicon probes were dipped into DiI solution, to stain the shanks and help to identify the tracks during histology. Craniotomies were protected with silicon (3-4680, Dow corning). One stainless steel screw placed above the cerebellum was used as a reference for the electrodes. Finally, a Faraday cage was custom-made with a 3D-printer and attached to the skull with dental cement and connected to the ground screw. Animals recovered for at least one week with *ad libitum* food and water, they were placed in individual cages before the start of behavioral experiments. During post-surgical recovery, probes were gradually lowered to reach the target position. The presence of sharp wave ripple oscillations during sleep was used as a landmark for the hippocampus pyramidal cell layer (Buzsáki, 2015b). Recording locations were systematically confirmed by electrical electrolytic lesions (10 μA for 10 s) and histology.

Mouse ID	Region	Inclusion in the analysis	Outcome	Implant
3C313	CA1	Yes	**Recorded**	4-shank 32 channels Neuronexus
3C308	CA2	Yes	**Recorded**	Janus probe, 4 shank, 128 channels (64- double sided) Diagnostic Biochips
3C305	CA1	Yes	**Recorded**	6-shank 64 channels Neuronexus
3C303	CA1	Yes	**Recorded**	6-shank 64 channels Neuronexus
3C300	CA2	Yes	Recorded, few sessions	4-shank 32 channels Neuronexus
3C294	CA2	Yes	**Recorded**	4-shank 32 channels Neuronexus
3C292	CA2	No	Probe broke	4-shank 32 channels Neuronexus
3C289	CA2	Yes	**Recorded**	4-shank 32 channels Neuronexus
3C286	CA2	Yes	**Recorded**	4-shank 32 channels Neuronexus
3C283	CA2	Yes	**Recorded**	4-shank 32 channels Neuronexus
3C276	CA1	No	No mock valves	6-shank 64 channels Neuronexus
3C275	CA1	No	No mock valves	6-shank 64 channels Neuronexus
3C268	CA2	No	No mock valves	4-shank 32 channels Cambridge Neurotech
3C266	CA2	No	No mock valves	4-shank 32 channels Cambridge Neurotech

Table 2.1: Table of implanted and recorded animals.

4. Histology

At the end of experiments, mice underwent electrolytic lesioning under isoflurane anaesthesia (1.5%) of 1 site per shank (10µA for 10s, A365RC Stimulus isolator from World Precision Instruments) to facilitate electrode placement validation. After a minimum of 48h following the lesions, mice were sacrificed by intracardiac perfusion of 4% paraformaldehyde (PFA) after having received a lethal dose of ketamine/xylazine (100mg/kg and 20mg/kg, respectively). After 24h in 4% PFA, brains were sliced in 60 µm coronal sections using a vibratome (Leica,

VT 1200S). After a 17-hour incubation in RGS14 (1:500, UC Davis/NIH NeuroMab Facility) antibody, secondary antibody incubation and 4′,6-diamidino-2-phénylindole (DAPI) staining (1:10 000, Fisher scientific), floating slices were washed and mounted under coverslips for visualization under the epifluorescence microscope (Eclipse Ni-U, Nikon). Electrode positions were then confirmed by the combination of electrolytic lesion visualization and/or probe track visualization (silicon probes shanks were dipped into DiI solution prior insertion in the brain) combined with region identification (with RGS14 for CA2). Images were taken SP8 LIGHTNING Confocal microscope, Leica.

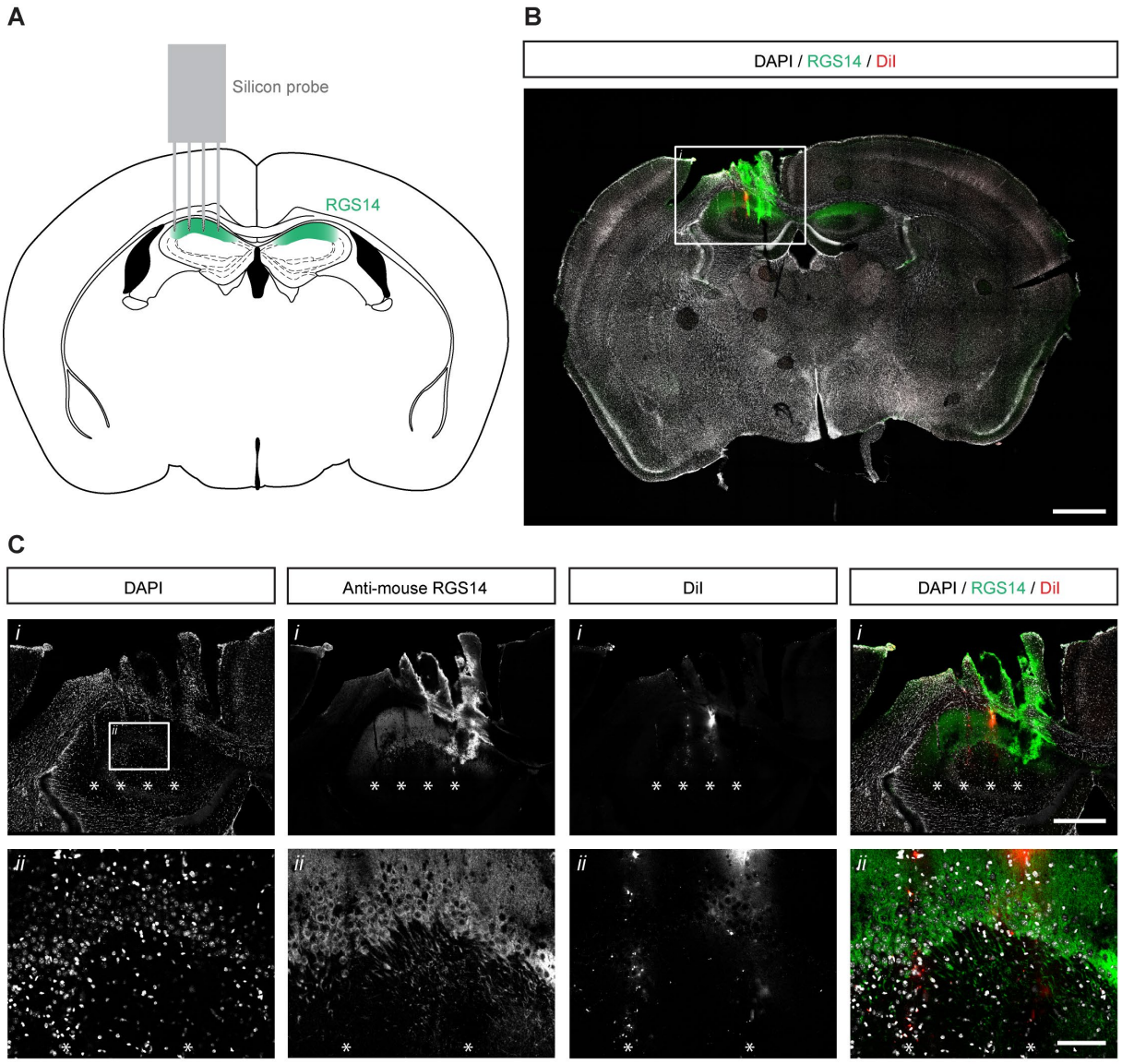

Figure 2.1: Histological localization of implant with a four-shank silicon probe.
*(**A**) Schematic illustrating the implantation site of a four-shank silicon probe targeting the antero-dorsal CA2 region, highlighted in green. (**B**) Representative coronal brain section stained with DAPI (grey), anti-RGS14 (green) to identify the CA2 region, and DiI (red) marking the probe tracks. The white rectangle indicates the region shown in panel (C). Scale bar = 1000µm. (**C**) Higher magnification of the region outlined in (B), showing individual staining channels from left to right: DAPI, anti-RGS14, DiI, and the merged image (DAPI/RGS14/DiI). (i) Overview images showing the four shank tracks (indicated by asterisks *). Scale bar = 500 µm. (ii) Zoomed-in views of the boxed region in (i), illustrating cellular detail and the track localization of two shanks. Scale bar = 100 µm.*

5. Electrophysiological recordings

Signals were acquired continuously at 20 kHz with an Intan RHD2000 interface board and 32- or 64-channel digital headstages (Intan Technologies). Data were visualized with Neuroscope79 (Neurosuite, http://neurosuite.sourceforge.net).

6. Electrophysiology data analysis

Preprocessing – spike sorting and unit classification

All analyses were performed using Matlab (The MathWorks), the Freely Moving Animal FMAToolbox (http://fmatoolbox.sourceforge.net/), Buzsaki lab toolbox – Buzcode (https://github.com/buzsakilab/buzcode), and custom-written scripts (generated mostly by Joe Moore, Giulio Casali, Evan Harrel and other team members). Electrophysiological signals were acquired continuously at 20 kHz on an Intan RHD2000 interface board and amplified by 32 and 64-channel digital headstages (Intan Technologies). Data were then visualized with Neuroscope (Neurosuite, http://neurosuite.sourceforge.net, (Hazan et al., 2006). Spike sorting was performed semi-automatically with KiloSort (Pachitariu et al., 2016), https://github.com/cortex-lab/KiloSort) followed by manual clustering with Phy (Phy 2.0 beta, https://github.com/cortex-lab/phy) with the help of custom-designed plugins (https://github.com/petersenpeter/phy-plugins).

Putative excitatory and inhibitory HPC units were separated on the basis of a Gaussian-mixture model using two waveform features: trough-to-peak and spike width (Stark *et al.*, 2013) (**Figure 2.2**). Only units showing a high classification confidence ($p < 0.01$) were used for the study and the remaining units were excluded from the analysis (65 ambiguous neurons).

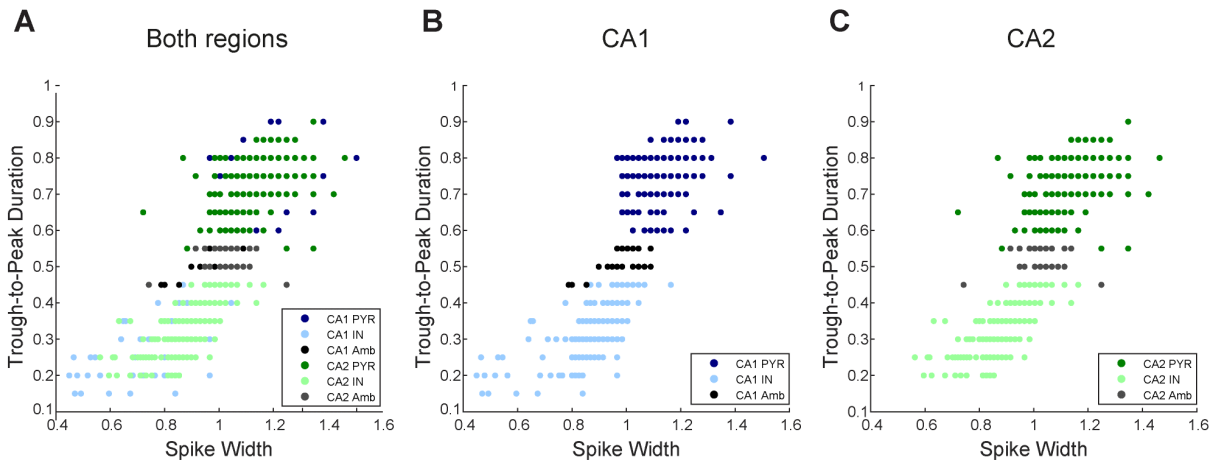

Figure 2.2: Results of cell-classification.
*(**A**) Spike waveform features of units recorded in both dorsal CA1 and CA2. Units were classified into putative pyramidal cells (PYR) or putative PV-like interneurons (INs) based on a classifier as in Stark et al. 2013. Units with low classification confidence were assigned to the Ambiguous (Amb) category. Putative PYR from CA1 are in dark blue, CA1-INs in light blue, CA1-Amb in black. CA2-PYR in dark green, CA2-INs in light green, CA2-Amb in grey. (**B**) Spike waveform features of units recorded in CA1 only. (**C**) Spike waveform features of units recorded in CA2 only. Results from 24 **sessions** for CA1, 35 sessions for CA2.* $n_{CA1\text{-}PYR} = 883$, $n_{CA2\text{-}PYR} = 943$, $n_{CA1\text{-}INs} = 215$, $n_{CA2\text{-}INs} = 235$, $n_{CA2\text{-}Amb} = 32$, $n_{CA2\text{-}Amb} = 33$.

Spatial coding analysis

Movement directionality

As rate maps can be different depending on the directionality of the movement (Wood *et al.*, 2000), the direction of the movement along the circular maze was computed by: calculating the movement vector of the animal for each available position and the vector of the tangent to the circular maze in the clockwise direction at this position. The sign of the dot product of these two vectors gave the directionality, positive = clockwise, negative = anti-clockwise. Only movement in the imposed direction (anti-clockwise) was considered in the analysis.

Circular to linear rate maps

To assess how spatial locations modulated the cell activity, its place map was calculated. To facilitate analysis and comparison between different recording sessions, the circular maze was linearized to represent it as a 1D environment. The circular maze was divided into 72 equal sectors with angles of 5° (and representing around 2,5 cm of the maze track). For each cell, firing rate maps were constructed by dividing the number of spikes in each spatial bin by the

occupancy time, including only activity during movement (speed > 3 cm/s) in the same direction. All the spatial analysis is done based on linearized rate maps.

Spatial information

Spatial information (SI) measures how much information about the animal's location is carried by one spike (Skaggs, McNaughton and Gothard, 1993), and was calculated using the following equation:

$$SI(bits/spike) = \sum_i P_i \left(\frac{R_i}{R}\right) ln\left(\frac{R_i}{R}\right)$$

Where i represents the bin number in the firing rate map, P_i is the probability that bin i is occupied, R_i is the mean firing rate in bin i, and R is the overall mean firing rate.

Sparsity

Sparsity measures the proportion of the area the mouse explored in which spikes from a cell/cluster occurred. This was calculated using the formula:

$$Sparsity = \sum \frac{(P_i {R_i}^2)}{R^2}$$

Where i represents the bin number in the firing rate map, P_i is the probability that bin i is occupied, R_i is the mean firing rate in bin i, and R is the overall mean firing rate.

Place cell detection and analysis

Place fields were defined using the Matlab function, **findpeaks**, applied to each cell's linearised rate map, to find local peaks in the spatial firing data. The linear ratemaps were repeated for this calculation to account for the circularity of the maze, so that peaks at the "end" of the maze would be adjacent to their neighbouring points at the "start". To qualify as a valid peak, the firing rate at that bin had to exceed a minimum threshold of 2 Hz and exhibit a prominence of at least 2, meaning the peak stood out from surrounding bins by at least that amount. Additionally, a minimum peak-to-peak distance of 4 spatial bins was imposed to prevent the detection of fragmented or closely spaced peaks that could reflect the same underlying field. Each identified peak was then evaluated to define its associated place field. The field was defined as the contiguous regions of at least 3 bins surrounding the peak in which the firing rate remained above 40% of the peak value. Fields that did not meet the following size constraints were excluded.

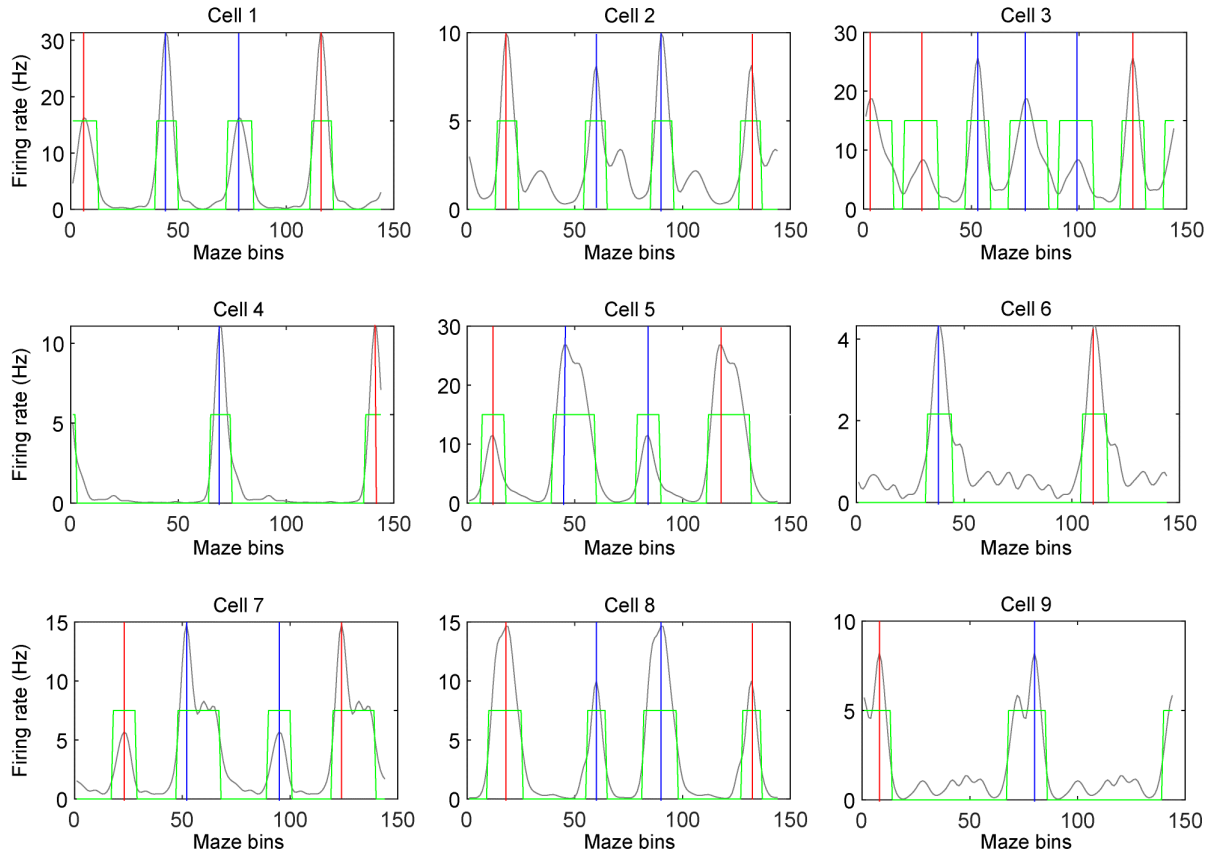

Figure 2.3: Place field detection.
Example for 9 different cells. Since the maze was circular and place filed detection was performed on linearized rate-maps, the bins were duplicated and concatenated in order to be able to detect place fields at the limits of linearize map. Blue lines indicate the detections of the peaks that were considered to define place fields (i.e. valid peaks); red lines represent peaks that have already been detected due to the duplication and are not considered for place field analysis. Green lines indicate the areas that can be considered as place field when centered on a valid peak.

Place field density, and difference

To assess how the spatial distribution of place fields evolved over the course of the task, the **place field density** was calculated by computing, for each spatial bin of the circular maze, the **proportion of pyramidal cells (PYR) with a place field peak including that bin**. This analysis was performed separately for the **first ten laps** and the **last ten laps** of the task. The resulting distributions were then **subtracted bin-by-bin** to yield a difference vector representing spatial changes in place field density across learning, from the first laps when the animal is naive, to the last laps when the animal has learned the reward location. To determine whether these changes were **biased towards a certain part of the maze**, the **preferred direction** of the difference was quantified by computing the **resultant vector angle**, a circular

measure of where the greatest changes in place field density occurred. To evaluate the statistical significance of the observed directional bias, a **bootstrap-based permutation test** was performed. Specifically, the bin-wise field density values were **randomly shuffled across bins** 10,000 times to generate a null distribution of **resultant vector lengths** (*R*) under the assumption of no directional preference. The actual *R* value obtained from the empirical data was then compared to this null distribution. The **p-value** was defined as the proportion of shuffled *R* values that exceeded the actual *R*, reflecting the probability that a directional bias of equal or greater magnitude could arise by chance. For example, if only 0.5% of shuffled *R* values exceeded the observed *R*, this corresponded to a p-value of 0.005, indicating a statistically significant directional bias.

Population vector analysis

Spatial representations were quantified by computing population vectors (PVs) for each spatial bin of the maze, where each PV consists of the firing rates of all recorded pyramidal cells within that bin. Rate maps were generated using non-overlapping blocks of 5 laps, and PVs were computed separately for each block. The Pearson correlation coefficient (r) was then calculated between the PVs of all pairwise lap blocks across Task 1 and Task 2.

Spatial correlation analysis

For each cell, spatial stability was assessed as the Pearson's correlation coefficient (r) resulting from the comparison between the mean spatial rate maps obtained from two subsets of laps depending on the three following conditions;

- **Intra-task** — stability between spatial maps from the **first vs last 10 laps** of the same task (Task 1 or Task 2).
- **Inter-task similarity** — stability between spatial maps from the **last 10 laps of Task 1** vs **first 10 laps of Task 2.**
- **Omission response** – stability between spatial maps from the laps **preceding a reward omission** with those **immediately following** the omission.

To assess statistical significance of the observed correlation value of each cell, a **permutation-based shuffling procedure** generating a **null distribution of shuffled correlation values** was performed as follows:

1) For each iteration (n = 1000), lap labels from the two groups were pooled;

2) **Lap identities were randomly permuted;**
3) Shuffled lap identities were then reassigned to two new pseudo-groups of same size generating novel shuffled spatial rate maps for each iteration
4) The Pearson correlation between two spatial rate maps was recomputed for each iteration.

Two statistical assessments were next computed. **Firstly,** the **Kolmogorov–Smirnov test** was used to compare the cumulative distribution of observed correlations across cells against that of the shuffled data. Secondly, for each individual cell, the **p-value representing the probability of a significant change in the spatial stability between the two subsets of laps was determined as the inverse percentile** of its observed correlation coefficient relative to the shuffled distribution of the same cell. Cell was classified as:

- **Significantly positively correlated** if the observed $r > 0$ and $p < 0.001$,
- **Significantly negatively correlated** if the observed $r < 0$ and $p < 0.001$,
- Or **not significantly different** (n.s.) otherwise.

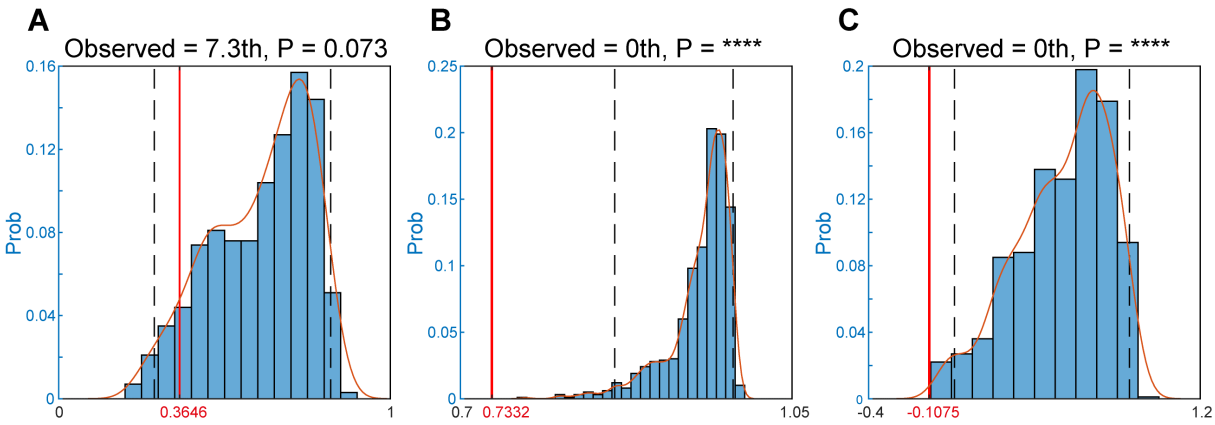

Figure 2.4: Examples of shuffling used to assess the significance of spatial correlation values of three individual cells.
Histograms represent the distribution of the correlations values obtained for 1000 iterations of shuffles for 3 different units (A-C). Red line represents the observed correlation value for

Hippocampal pyramidal cells clustering

PYR from the CA1 and CA2 regions of the hippocampus were pooled together for analysis. To identify potential subtypes or functional groupings, we employed unsupervised clustering using the k-means algorithm. The number of clusters was set to five.

For visualization of the high-dimensional data, we used t-distributed stochastic neighbor embedding (t-SNE) to project the clustered data into a two-dimensional space. This allowed us to visually inspect and validate the separation and grouping of the pyramidal cell populations.

7. Quantification and statistical analysis

Statistical analyses were performed using MATLAB scripts and GraphPad PRISM. Most comparisons were performed using linear mixed model tests to account for difference in batch sizes. Additional nonparametric tests (Mann-Whitney U tests or Wilcoxon signed rank tests in the two-tailed configuration) were conducted for non-paired and paired data. Significance was set with alpha = 0.05, unless stated otherwise, and was represented on graphs as the following: * = $P < 0.05$, ** = $P < 0.01$, ***= $P < 0.001$, **** = $P < 0.0001$. As mentioned in the figure legends, box plots representing 25- 77th percentile and median, moustaches representing 10th and 90th percentile of distribution.

Chapter 3: Results

1. Learning in the « Clock-maze » task

To characterize CA2 neuronal populations' activity during spatial navigation towards a reward and during reward consumption itself, I collected extracellular electrophysiological recordings using silicon probes chronically implanted in the dorsal CA2 (CA2) in mice. For comparison, I also recorded neuronal populations in the dorsal part of CA1 (CA1). This section describes the behavior and learning performance of the animals during the new task I have set up using a circular arena that we called the "Clock-maze". The data in this section comes from eight implanted animals: five in CA2 and three in CA1.

1.1. The Clock-maze task

Kay *et al.* (2016) showed that a subset of neurons from CA2 are more active during immobility. Yet, this was not observed everywhere in the environment but only in restricted places that were specific for each of these neurons (similar to "immobility place fields"). Interestingly, many of these identified place fields corresponded to rewarded locations in this work, raising the question of whether CA2 homogeneously code for space during immobility and/or shows specific activation in presence of rewards. To test for these possibilities, the first requirement was to create a behavioral paradigm and apparatus where the animal must stop and get a reward at different locations. Then, to discern whether the rewarded location or the reward itself influences, a second requirement was the possibility to provide a reward in some trials and omit the reward in some others. Finally, to facilitate data analysis and to be able to compare our data to previous studies showing accumulation of place fields close to rewards (Hollup *et al.*, 2001b; Zaremba *et al.*, 2017b) , a third requirement was to use of an environment with only 1-dimension, e.g. a track. Based on these requirements, I built a circular corridor with 12 side-wall ports for reward delivery, located every 30°: the "Clock-maze" (**Figure 3.1A**).

In this task, food-restricted mice can collect a drop of sweet condensate milk-solution (the reward) in one of the side-wall ports, the position of which changes at every session (**Figure 3.1B**). Thanks to infrared detectors placed at the nose-port entrances, the reward was automatically delivered following a fixed one-second delay after nose-poke detection. This delay was meant to temporally separate the nose-poke from the reward the reward consumption itself and to impose a fix immobility period at the port.

Each day, mice ran two sessions, Task 1 and Task 2, during which they had to learn the location of a newly rewarded port. During each Task, they could visit this port up to 90 times after completing a full lap in the same direction. First, the animals completed ten laps in which the reward was systematically delivered. After, the reward was pseudo-randomly omitted in 25% of the laps, with the condition that an omission trial could not be followed by a second omission (**Figure 3.1C**). The omission trials were meant to compare CA2 activity with or without reward consumption, while keeping the position of the mouse during immobility identical. Rest recordings were performed before and after the tasks in the home cage where mice usually fell asleep. The animal position was tracked in 3D throughout the sessions using reflective markers and an Optitrack camera system.

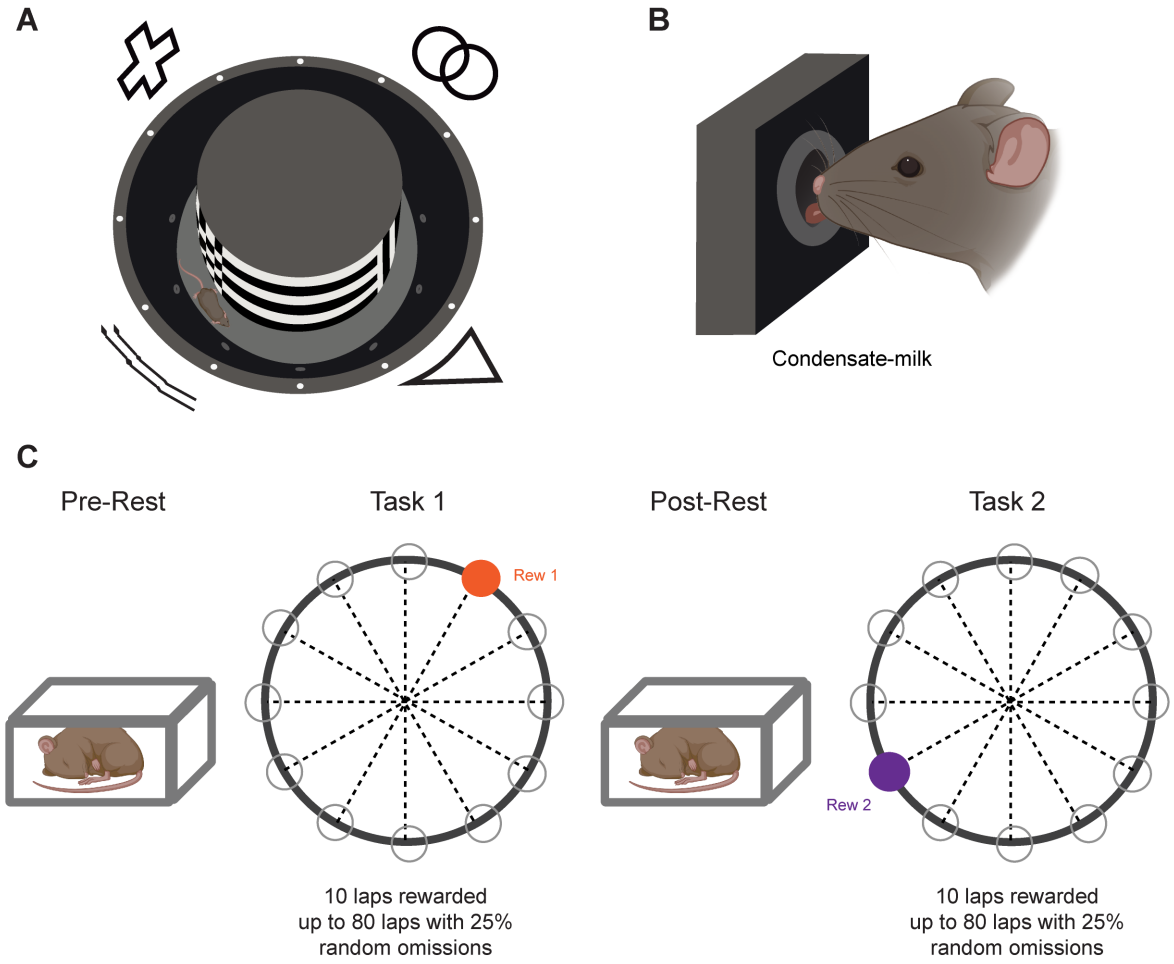

Figure 3.1: Schematic of Clock-maze task for spatial learning of reward location.
(A) *Schematic of the Clock-maze and* ***(B)*** *zoom on the nose-port.* ***(C)*** *After a period of rest, mice were trained to find the rewarded port out of the twelve available ones. The reward (1:5 diluted condensate milk) was delivered following one-second delay after nose-poke initiation. For the ten first laps, the reward was systematically delivered. In the following task period, the reward was randomly omitted in 25% of the laps. The rewarded port was changed after a second rest session. The maze location remained fixed relative to the room's visual cues across all learning trials.*

1.2. Learning in the Clock maze task

To assess rewarded location learning during the task, I analyzed the lap-by-lap performance from sessions with simultaneous electrophysiological recordings. Learning was quantified by comparing performance during the first and last ten laps of each task session. Behavioural performance was measured with three parameters: **lap duration, number of non-rewarded ports visited, and time spent at non-rewarded ports**. **Figure 2A**, is an example of one mouse: we can observe that the lap trajectories after learning become straighter and include fewer periods of immobility along the corridor (immobility positions are shown in red). The occupancy, shown as a linearized version of the circular corridor, was concentrated at the rewarded-port. Yet, we can observe that for a given mouse, the lap duration during the task can be very variable from one trial to the next. (**Figure 3.2A-*iii***). The mean curve (in black) however shows a progressive decrease in the lap duration, rapidly reaching a plateau (after 10-15 laps).

Recorded mice showed variable learning progression (**Figure 3.2B-*i*, C-*i*, D-*i***) that did not seem to differ between the first and second Task of each day (**Figure 3.2B-*ii*, C-*ii*, D-*ii***). Although trial duration was variable both within and across animals, most mice exhibited a progressive decrease in lap duration, with performance stabilizing after approximately 10–15 laps (**Figure 3.2B-*i***). This was evident at both the individual (colored lines) and population level (black mean curve). A two-way repeated measures ANOVA confirmed a significant main effect of learning stage ($p < 0.0001$), with an average decrease of 7.5 seconds between the first and last ten laps (mean final lap duration: 18.12 ± 0.81 sec, n = 118 sessions). There was also a significant interaction between learning stage and mouse identity ($p = 0.0093$), reflecting inter-animal variability (**Figure 3.2B-*iii***).

A similar pattern was observed for the number of non-rewarded ports visited per lap (**Figure 3.2C-*i***). Mice initially explored several ports per lap but quickly reduced visits to unrewarded ports. A significant main effect of learning was observed ($p < 0.0001$), with a mean reduction of 0.32 ports per lap. The interaction between learning stage and individual mouse was also significant ($p < 0.0001$), again highlighting inter-subject variability (**Figure 3.2C-*iii***).

Finally, the time spent at non-rewarded ports (**Figure 3.2D-*i***) also declined across laps. A significant main effect of learning was detected ($p = 0.0007$), with a mean reduction of 0.54 seconds, alongside a significant interaction with mouse identity ($p = 0.0027$) (**Figure 3.2D-*iii***).

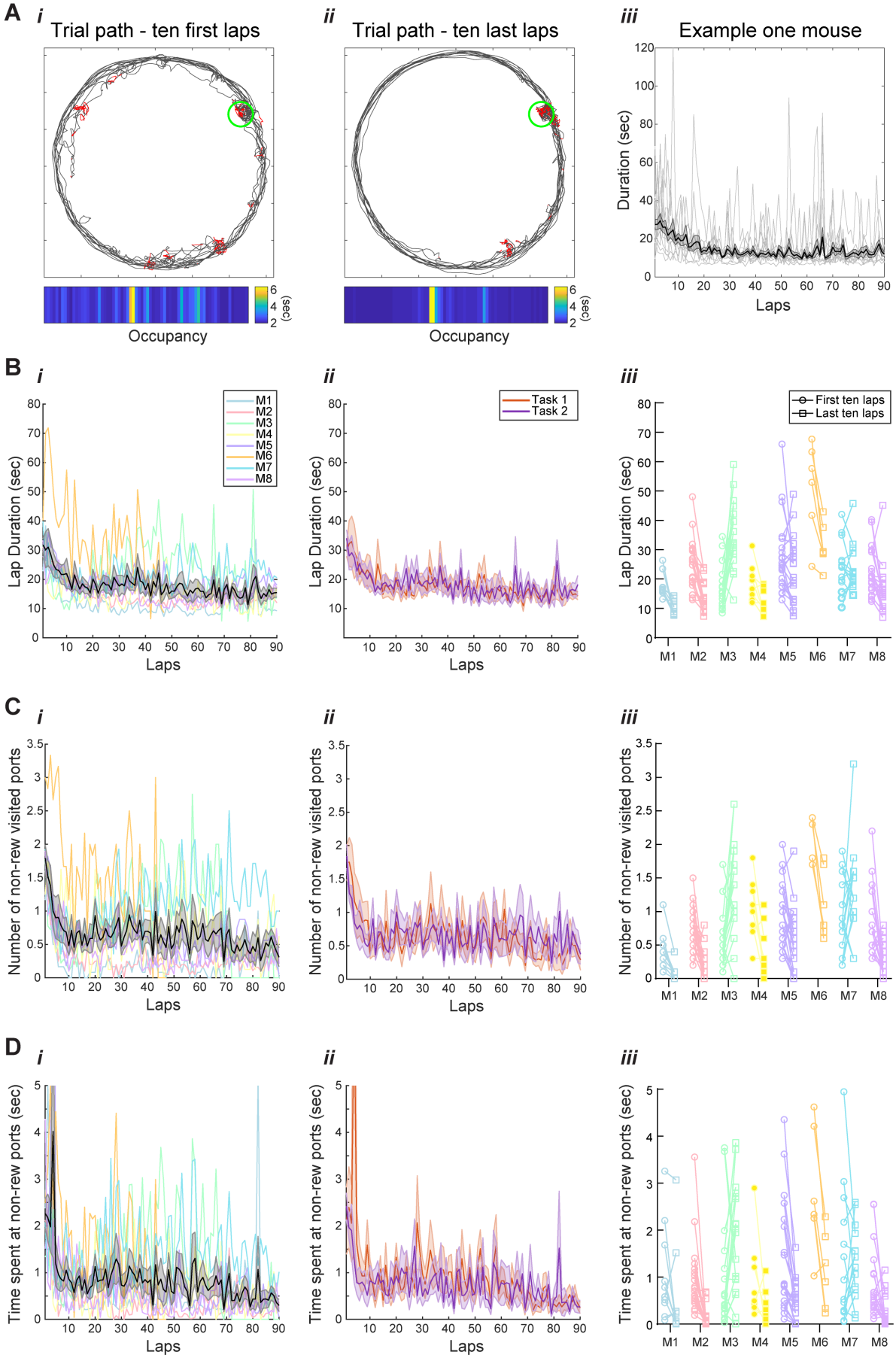
A
i
Trial path - ten first laps
Occupancy
6
4
2
(sec)
ii
Trial path - ten last laps
Occupancy
6
4
2
(sec)
iii
Example one mouse
Duration (sec)
Laps
B
i
Lap Duration (sec)
Laps
M1
M2
M3
M4
M5
M6
M7
M8
ii
Lap Duration (sec)
Laps
Task 1
Task 2
iii
Lap Duration (sec)
First ten laps
Last ten laps
M1 M2 M3 M4 M5 M6 M7 M8
C
i
Number of non-rew visited ports
Laps
ii
Number of non-rew visited ports
Laps
iii
Number of non-rew visited ports
M1 M2 M3 M4 M5 M6 M7 M8
D
i
Time spent at non-rew ports (sec)
Laps
ii
Time spent at non-rew ports (sec)
Laps
iii
Time spent at non-rew ports (sec)
M1 M2 M3 M4 M5 M6 M7 M8

Figure 3.2: Mice performance in the Clock-maze.
(A) *Examples for one mouse.* ***(i)*** *Trajectories during the first ten laps (**left**) and ten last laps (**right**) of a Task. Grey lines: trajectories during movement (speed > 3 cm/sec). Red line: mouse position during immobility periods (speed < 3 cm/sec). Green circle: reward position. Beneath is represented the occupancy in the linearized representation of the circular corridor.* ***(ii)*** *Learning curves assessed by lap durations. In grey are represented the curves of individual sessions and the mean curve is shown in black with SEM (shaded area).* ***(B) (i)*** *Learning curves assessed by **lap durations**. Data collected from 8 implanted animals (5 in dCA2 and 3 dCA1), 118 recording sessions in total (Task 1 and 2 included). The black curve represents the mean across mice with SEM (shaded area) while the colored curves represent the mean across days for individual mice.* ***(ii)*** *The orange curve represents the mean across mice for Task 1 and the purple one for Task 2.* ***(iii)*** *Comparison between the mean lap duration in the first ten and the last ten laps of each task for individual mice. A two-way repeated measures ANOVA revealed significant effects of mouse identity (****p < 0.0001), learning stage (****p < 0.0001; mean difference of lap duration: 7,50 sec), and a significant interaction between mouse and learning stage (**p = 0.0093).* ***(C) (i) Numbers of non-rewarded ports visited*** *across laps for each mouse,* ***(ii)*** *across Task 1 and 2.* ***(iii)*** *A two-way repeated measures ANOVA revealed significant effects of mouse identity (****p < 0.0001), learning stage (****p < 0.0001; mean difference in the number of ports visited: 0.32), and a significant interaction between mouse and learning stage (****p < 0.0001).* ***(D) (i) Time spent at non-rewarded ports*** *across laps for each mouse or,* ***(ii)*** *across Task 1 and 2.* ***(iii)*** *A two-way repeated measures ANOVA revealed significant effects of mouse identity (**p = 0.0035), learning stage (***p = 0.0007; mean difference time spent: 0.51 sec), interaction (**p = 0.0027). N= 118 sessions in 8 mice.*

While each mouse showed its own speed profile (**Figure 3.3B**), they all tended to accelerate as approaching the rewarded port. The speed in the **three seconds that precede the arrival** at the rewarded port significantly increased between the first ten and the last ten laps (difference in mean speed: **5.9 cm/sec**; two-way repeated measures ANOVA: learning stage, $p < 0.0001$; mouse identity, $p = 0.0004$; interaction, $p < 0.0001$) (**Figure 3.3A**). I also observed that reward omission induced a faster departure from the port (two-way repeated measures ANOVA: type of lap, $p < 0.0001$; mouse identity: $p < 0.0001$; interaction, $p = 0.0005$; difference of mean speed: 5.9 cm/sec) (**Figure 3.3C**).

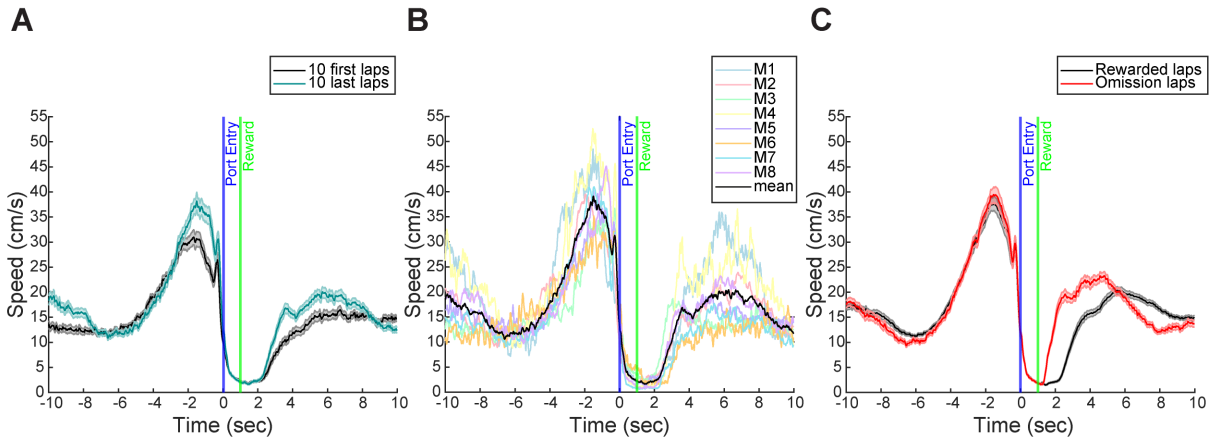

Figure 3.3: Mean speed in the Clock-maze.
(A) *Mean speed for the first ten laps and last ten laps aligned on rewarded-port entry (time 0). Mean and SEM (shaded area) were calculated over all mice and sessions (n=118 sessions in 8 mice).* ***(B)*** *Mean speed of individual mice (colored curves) and mean across mice (black), for the ten last trials of all sessions.* ***(C)*** *Mean speed for rewarded trials (black) and omission laps (red). Mean and SEM (shaded area) were calculated over all mice and sessions (n=118 sessions in 8 mice).*

Altogether, these behavioral metrics indicate that mice rapidly learned the task structure, showing shorter lap durations, more directed trajectories, and less exploration of non-rewarded ports over time, consistent with goal-directed learning.

2. Spatial coding in the CA1 and CA2 regions during Clock-maze task

The properties of pyramidal units (PYR) in CA2 and CA1 were compared previously and CA2 PYR are generally reported to be less spatially tuned (Mankin *et al.*, 2015b; Alexander *et al.*, 2016b; Kay *et al.*, 2016; Oliva, Fernández-Ruiz, *et al.*, 2016). Yet, since the Clock-maze is a new task, I first wanted to describe and compare the unit properties in dCA1 and dCA2 regions to test whether previous observations hold in this new behavioral paradigm. In the following sections, I have focused on **Task 1** and investigated hippocampal activity **during movement** (speed > 3cm/s), unless stated otherwise.

2.1. Properties of PYR in CA1 and CA2 regions in the Clock-maze task.

The position of the probes in dCA1 and dCA2 was verified by histology (**Figure 2.1**) and units were classified into putative pyramidal units (PYR) or putative interneurons (INs; with

properties corresponding to parvalbumin-positive interneurons) based on their spike waveform features (Stark et al. 2014). Units for which the classifier showed low confidence were labelled as Ambiguous. I recorded a total of 883 PYR (CA1-PYR), 215 interneurons (CA1-IN) and 32 Ambiguous (CA1-Amb) from dorsal CA1 of 3 mice and 943 CA2-PYR, 252 CA2-INs and 33 CA2-Amb from dorsal CA2 in 5 other mice (**Figure 2.2**). To compute rate maps, the Clock maze was divided into 72 radial bins (~5°) (**Figure 3.4A, B**).

In agreement with previous studies (Mankin *et al.*, 2015b; Alexander *et al.*, 2016b; Oliva, Fernández-Ruiz, *et al.*, 2016), I found that CA2-PYR have a significantly higher firing rate during running, compared to CA1-PYR (Mann Whitney test, $p < 0.0001$, difference of medians = 0.7 Hz) (**Figure 3.4C**). CA2-PYR also displayed lower spatial information than CA1-PYR (Mann Whitney, $p < 0.0001$, difference: -0.5) (**Figure 3.4D**). The sparsity of recorded CA2-PYR reached higher values than CA1-PYR (Mann Whitney, $p < 0.0001$, median sparsity difference = 0.24). Seventy-two percent of the recorded CA1-PYR had at least one place field (PF) whereas this percentage only reached 40 % in CA2-PYR (two-sided chi-square test, $p < 0.0001$). When units had place fields these were significantly larger in CA2 (Mann Whitney, $p < 0.0001$, difference of median = 1.5 bin, corresponding to ~10% of the median CA1 PF size) (**Figure 3.4F**).

Because INs are also spatially-tuned in the hippocampus (Marshall *et al.*, 2002b; Maurer *et al.*, 2006b; Geiller *et al.*, 2020a) and have been seldom studied *in vivo* in CA2 despite their high proportions – higher than in other hippocampus subfields (Mercer, Botcher, *et al.*, 2012; Mercer, Eastlake, *et al.*, 2012; Botcher *et al.*, 2014b) - and their important roles revealed *ex vivo* (Piskorowski and Chevaleyre, 2013; Nasrallah, Piskorowski and Chevaleyre, 2015b; Loisy *et al.*, 2022; Rey *et al.*, 2022b), I wondered about possible differences when comparing INs of CA1 and CA2.

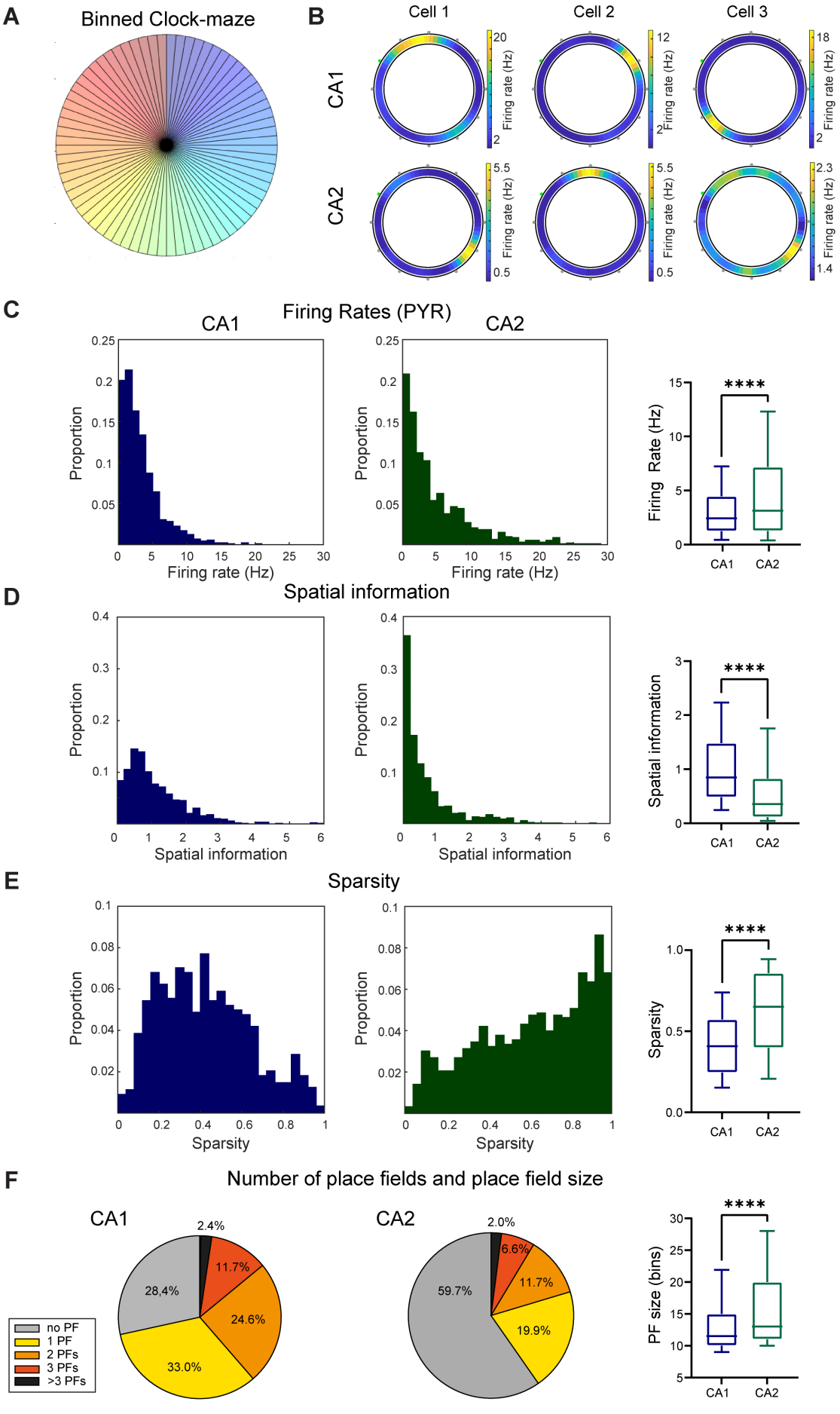
A
Binned Clock-maze
B
Cell 1
Cell 2
Cell 3
CA1
CA2
Firing rate (Hz)
20
2
12
2
18
2
5.5
0.5
5.5
0.5
2.3
1.4
C
Firing Rates (PYR)
CA1
CA2
Proportion
Firing rate (Hz)
Firing Rate (Hz)
****
D
Spatial information
Spatial information
E
Sparsity
Sparsity
F
Number of place fields and place field size
CA1
CA2
2.4%
11.7%
28,4%
24.6%
33.0%
2.0%
6.6%
59.7%
11.7%
19.9%
no PF
1 PF
2 PFs
3 PFs
>3 PFs
PF size (bins)

Figure 3.4: Properties of putative pyramidal cells in CA1 and CA2 regions.
(A) *To generate the rate maps the clock maze was binned into 72 bins (~5degrees).* ***(B)*** *Examples of rate maps for individual PYR recorded in CA1 and CA2 in Task 1.* ***(C)*** *Distribution of the mean firing rates of all recorded PYR in CA1 (blue) and CA2 (green) during movement (speed > 3cm/sec) in Task 1.* ***(D)*** *Distribution of the spatial information encoded by these units.* ***(E)*** *Distribution of their sparsity.* ***(F)*** *Distribution of the recorded PYR as a function of their number of place fields (PF) and mean size of these PF in CA1 and CA2. CA1 n= 883 PYR; CA2 n= 943 PYR. Boxplots represent median and 25-75 percentiles, whiskers represent 10-90 percentiles. Two-tailed Mann-Whitney tests were used to assess significance. **** $p < 0.0001$. Similar observations were done for Task2 (not shown).*

2.2. Properties of putative interneurons in CA1 and CA2 regions.

When considering all the units recorded (1130 units in CA1 and 1228 units in CA2), the CA1 and CA2 regions had similar proportions of interneurons (**Figure 3.5AC;** 215 INs in CA1 – CA1-INs – and 252 INs in CA2 – CA2-INs), although CA2 showed sessions with the largest IN proportions (up to 27% of INs, a level never observed in CA1). I observed that CA2-INs, like CA1-INs, show some degree of spatial tuning in the Clock-maze (**Figure 3.5B**) Interestingly, CA2-INs had a significantly higher firing rate than compared to CA1-INs (**Figure 3.5E**) (Mann-Whitney, $p < 0.0001$) although they were both identified as 'parvalbumin-like' by our classifier (Stark 2014).

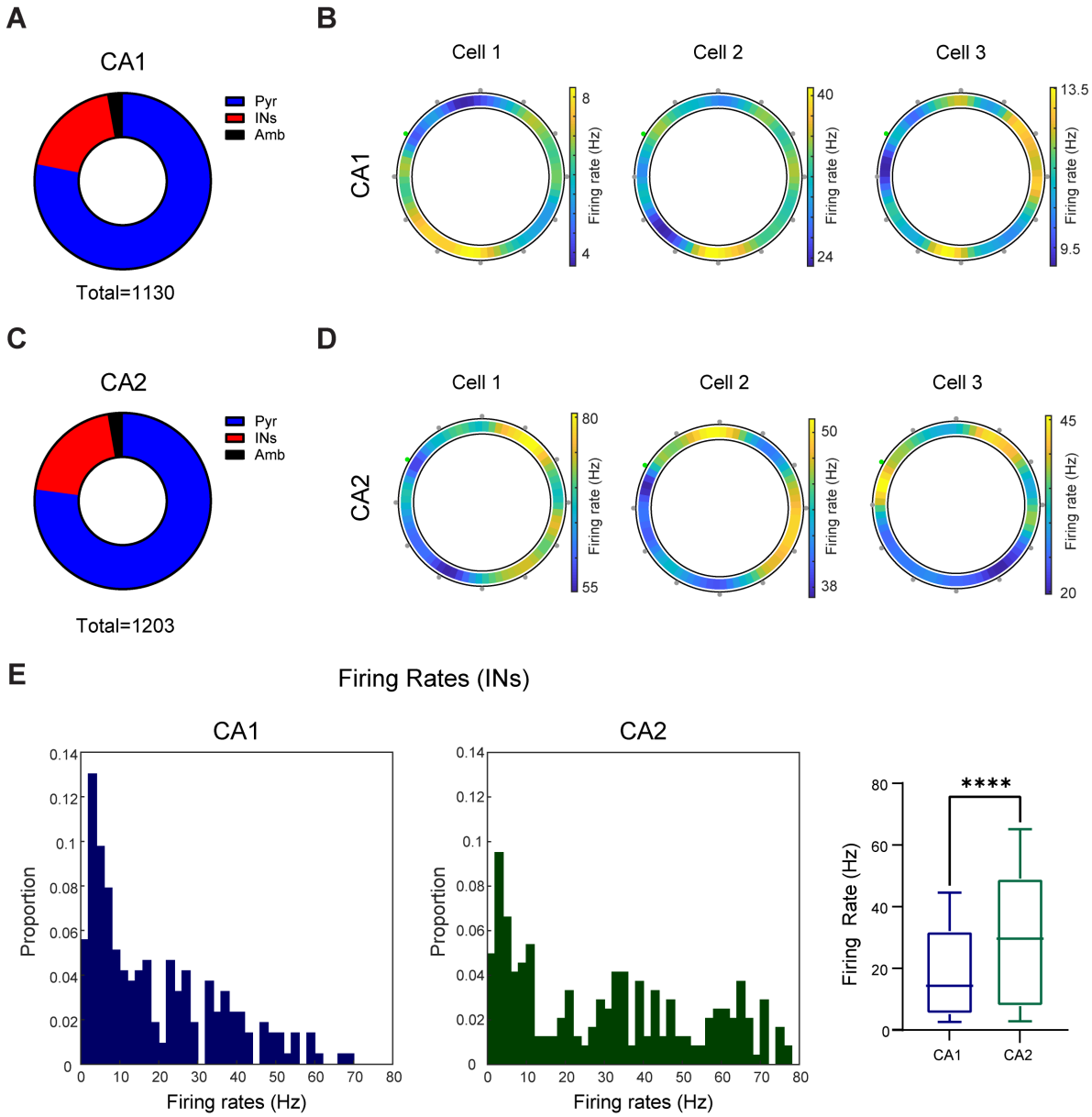

Figure 3.5: Properties of putative interneurons (INs) in CA1 and CA2 regions.
(A) *Distribution of recorded cell types in CA1. Units were classified as putative pyramidal cells (PYR) and parvalbumin-like interneurons (INs) as in Stark et al., 2014. Unclassified units were labeled as Ambiguous (Amb).* ***(B)*** *Examples of rate maps computed for putative INs of CA2.* ***(C)*** *Same as is* ***(A)*** *but for CA1.* ***(D)*** *Same as in* ***(B)*** *but for CA1.* ***(E)*** *Distribution of the mean firing rates of all recorded INs in CA1 (blue) and CA2 (green) during movement (speed > 3cm/sec) in Task 1. n = 247 INs; CA2 n = 285 INs. Boxplots represent median and 25-75 percentiles, whiskers represent 10-90 percentiles. Two-tailed Mann-Whitney tests were used to assess significance. **** $p < 0.0001$. Similar observations were done for Task2 (not shown).*

2.3. Global increase in PYR activity during the task

After describing the general cell properties, I wanted to see how spatial coding evolves in the hippocampal subregions during learning. I have first compared the mean firing rate of all recorded PYR in each region between the first and the last 10 laps of the task (n = 883 CA1-PYR and 943 CA2-PYR) (**Figure 3.6A**). To compare populations of different size, linear mixed model analysis was used. Statistical analysis revealed a significant increase in PYR firing rates from the first to the 10 last laps, with a larger firing rate change in CA2 as compared to CA1 (task phase factor: $p < 0.001$, region factor: $p < 0.001$, phase of the task x region interaction: $p < 0.001$).

Furthermore, the mean number of place fields per PYR was increased at the end of the task in both regions (**Figure 3.6B**) (task phase factor: $p < 0.0001$, region factor: $p = 0.0016$, phase of the task x region interaction: $p = 0.9634$). Likewise, the proportion of PYR with multiple place fields increased in both regions similarly (task phase factor: $p < 0.0001$, region factor: $p = 0.8285$, phase of the task x region interaction: $p = 0.4220$).

These changes suggest that both regions undergo a general activity change as the task progresses, with CA2-PYR showing a larger increase in firing rates than CA1-PYR.

Knowing that PF number increases during the course of the Task, I then wondered whether they are homogeneously distributed along the circular maze or whether they tend to cluster around the 12 ports or, alternatively, near the reward. The position of all PYR place field peaks, detected for the 10 last laps of the Task, rather showed a homogenous distribution along the track, both for CA1 and CA2 regions (**Figure 3.6D, E**).

To further investigate the spatial reorganization during the task, I decided to study how place fields of the different regions evolve, with a particular focus on the reward zone.

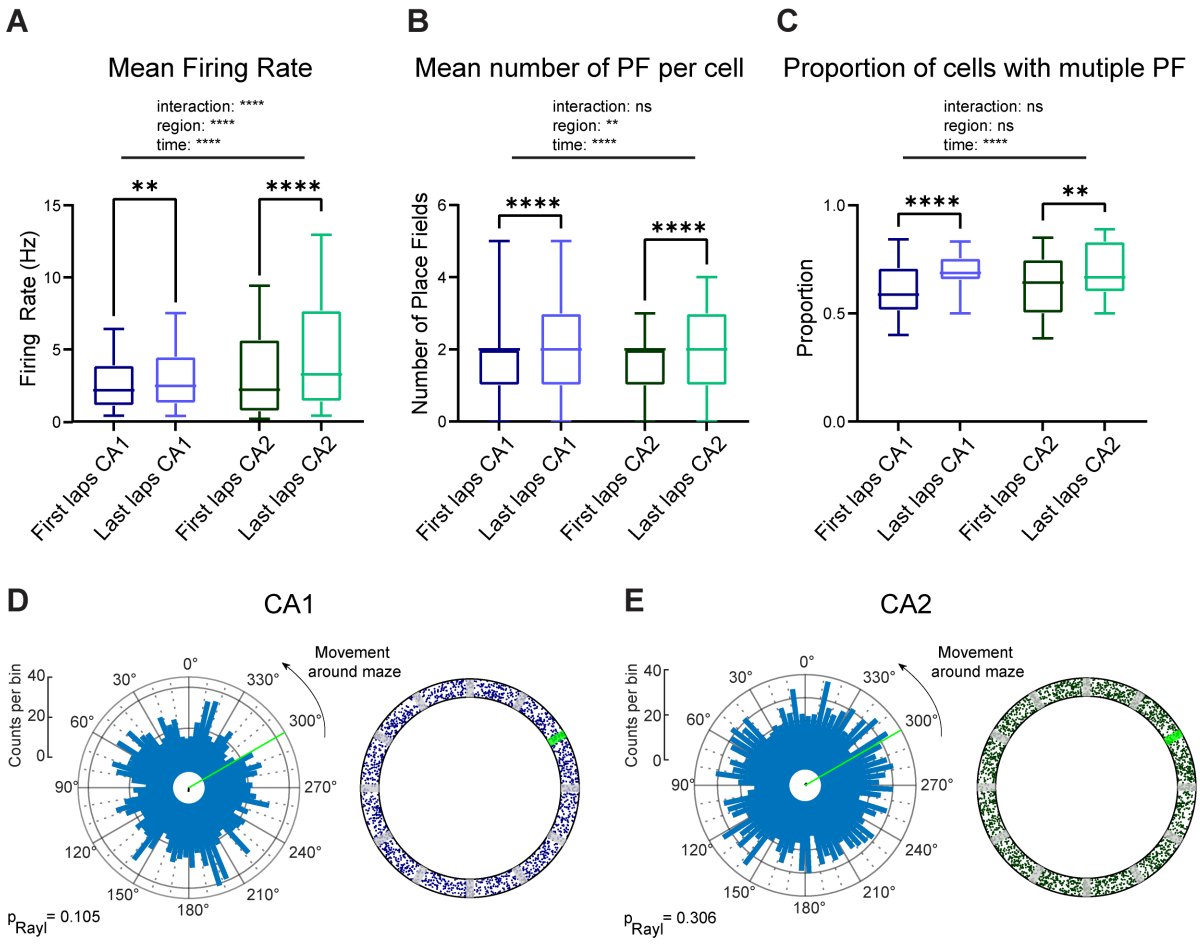

Figure 3.6: Change of CA1- and CA2-PYR activities during the task.
(A) *Changes in the mean firing rates from the first to last 10 laps of Task 1 of all recorded PYR in CA1 (blue) and CA2 (green). CA1 n = 883 PYR. CA2 n = 943 PYR. Two-tailed Wilcoxon was performed to assess significance intra-region. CA1: **p = 0.0078, CA2: ****p < 0.0001. A linear mixed-effects model revealed significant effects of hippocampal region (****p < 0.0001), task phase (****p < 0.0001), and a significant interaction between region and task phase (****p = 0.0001).* ***(B)*** *Comparison of the mean number of place field per cell between first and last 10 lap and across regions. Two-tailed Wilcoxon was performed to assess significance intra-region. CA1: ****p < 0.0001, CA2: ****p < 0.0001. A linear mixed-effects model revealed significant effect of task phase (****p < 0.0001), hippocampal region (**p < 0.0016), and no interaction between region and task phase (p = 0.9634).* ***(C)*** *Proportion of cells with multiple place fields between first and last 10 lap and across regions. Two-tailed Wilcoxon was performed to assess significance intra-region. CA1: ****p < 0.0001, CA2: **p = 0.0078. A linear mixed-effects model revealed significant effect of task phase (****p < 0.0001), no effect was observed for hippocampal region (p = 0.8285), and no interaction between region and task phase (p = 0.4220).* ***(D) Left:*** *Circular histogram representing the distribution of place field peaks during the last ten laps of Task 1. Green line: Task reward position.* ***Right:*** *Schematic of the clock-maze, with dots representing place fields peaks of all individual CA1-PYR. Nose-ports are represented in gray except the rewarded one that is shown in green.* ***(E)*** *Same as (D) but for CA2-PYR.* ***Boxplots*** *represent median and 25-75 percentiles, whiskers represent 10-90 percentiles.*

2.4. Accumulation of CA1 place fields near the learned reward location

I first investigated how PYR-CA1 activity change during course of the task in the reward zone (defined as the 12 bins surrounding the rewarded location). To do so, I compared the activity during the 10 first laps versus the 10 last laps of the Task 1 (similar observations were made for Task 2).

When sorting CA1-PYR by the location of their peak firing rate on the circular maze, no striking clustering of place field peaks was observed near the reward location (green line) at either time point of the task (**Figure 3.7A, B**). CA1-PYR significantly increased their average firing rate within the reward zone from early to late laps (n = 883, Wilcoxon test, $**p < 0.0054$, median of differences = 0.009) (**Figure 3.7C, *i***). This result reflects the general increase in neuronal excitability shown previously (**Figure 3.6A**) rather than a reward-specific modulation. A significant increase in the proportion of CA1-PYR with place field peaks in the reward zone was observed between the first and last laps (n = 24 recorded sessions, two-tailed Wilcoxon signed-rank test, *** $p < 0.0006$, median of differences = 0.12) (**Figure 3.7C, *ii***). The distance from the reward location to the closest place field also significantly decreased (n = 744 PYR with at least one place field for both conditions, ****p<0,0001, median= -1 bin) (**Figure 3.7C, *iii***), consistent with the general increase in place field number shown earlier (**Figure 3.6B**).
Place field peak distribution is homogeneous along the maze (**Figure 3.6D**). Yet, as the peak does not reflect the full extent of a given place field, it remained possible that the place field density (i.e. the proportion of units showing a place field in a given spatial bin) increases in the reward zone, as previously described in CA1 by Dupret et al. 2010. I therefore computed the proportion of CA1-PYR with place fields within each spatial bin during the first and last stages of the task and plotted them as circular distributions along the maze (**Figure 3.7D, Left**). The difference in field density between early and late laps revealed a subtle increase in the density of place fields near the reward zone (**Figure 3.7D, Right**). A resultant vector angle was computed from this difference distribution and tested for significance against a shuffled distribution (10,000 iterations, see Methods). The distribution of place field changes showed a significant directional bias toward the reward (mean angle 319°, reward at 300°, p <0,0001). These findings suggest that, consistent with previous work (Hollup *et al.*, 2001b; Dupret *et al.*, 2010b), the distribution of place fields in CA1 is pulled towards the rewarded location over the course of the task.

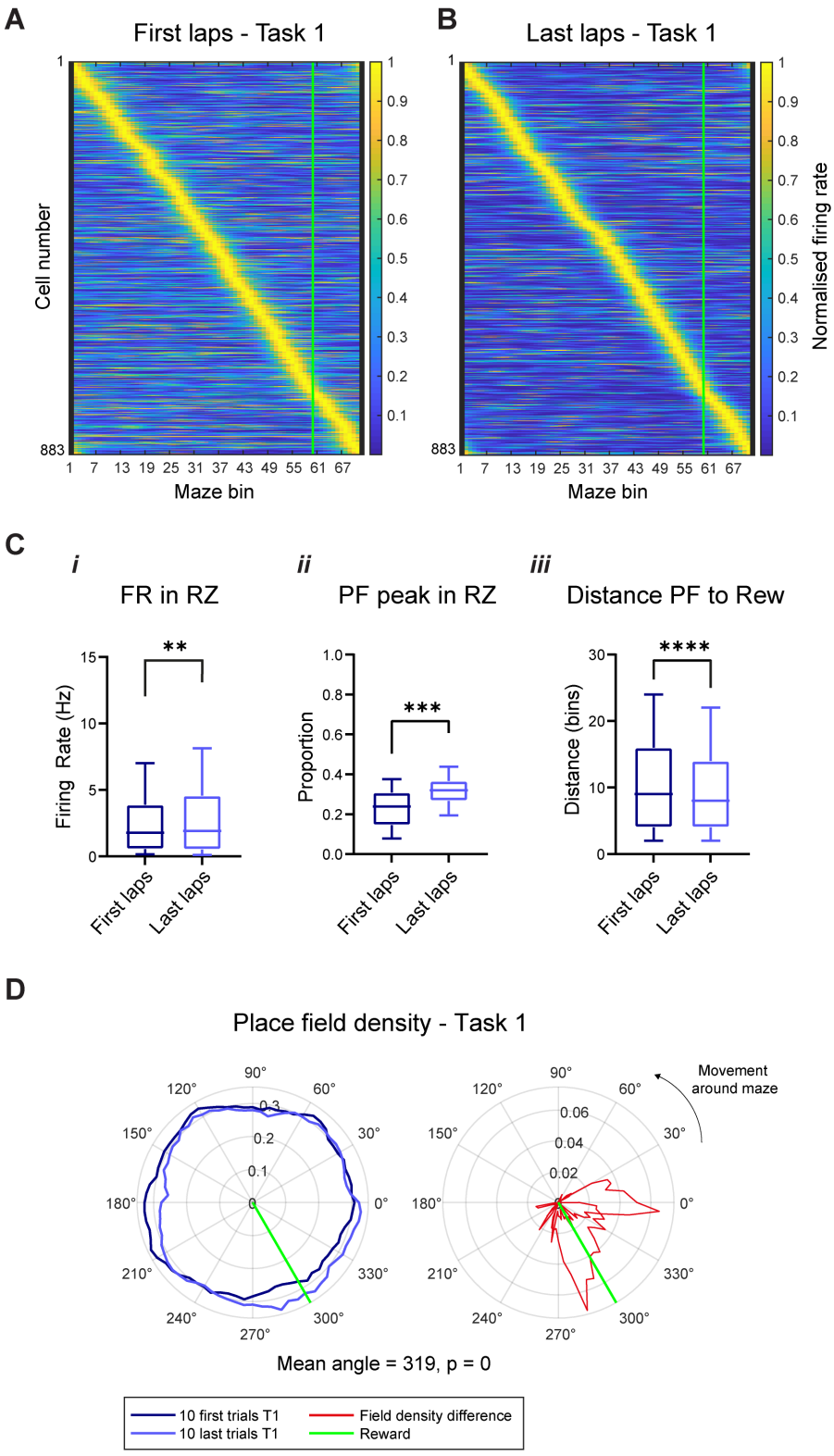
A
First laps - Task 1
B
Last laps - Task 1
Cell number
Maze bin
Normalised firing rate
C
i
FR in RZ
ii
PF peak in RZ
iii
Distance PF to Rew
Firing Rate (Hz)
Proportion
Distance (bins)
First laps
Last laps
D
Place field density - Task 1
Movement around maze
Mean angle = 319, p = 0
10 first trials T1
10 last trials T1
Field density difference
Reward

Figure 3.7: Change of CA1 putative pyramidal cells activity during the task.
(A) *Linearized rate maps of all CA1-PYR during the ten first laps of Task 1.* ***(B)*** *Same for the ten last laps.* ***(C) (i)*** *Comparison of the average firing rates in reward zone (RZ) between the first and last 10 laps of Task 1. n = 883 CA1-PYR. Boxplots represent median and 25-75 percentiles, whiskers represent 10-90 percentiles. ** p = 0.0054 (Two-tailed Wilcoxon).* ***(ii)*** *For each session, proportions of recorded CA1-PYR with a place field (PF) peak in reward zone compared between the first and last 10 laps of Task 1. n = 24 sessions. Bars represent mean ± SEM. ***p = 0.0006 (Two-tailed Wilcoxon test).* ***(iii)*** *Distance between the reward and the closest place field calculated for the first and last 10 laps of Task 1. Boxplots represent median and 25-75 percentiles, whiskers represent 10-90 percentiles. **** p < 0.0001 (Two-tailed Wilcoxon).* ***(D) Left:*** *Polar plots showing the proportion of CA1-PYR with place fields in each spatial bin during the first (dark blue line) and last (lighter blue line) laps of Task 1, along the circular maze. Green line: Task reward position.* ***Right****: The difference between the two distributions is plotted in red. The preferred direction of the difference was computed as the resultant vector angle. Significance was assessed via a bootstrap test (10,000 iterations), yielding p < 0.0001. Similar observations were done for Task2 (not shown).*

2.5.CA1 activity at the previous reward location.

In many studies, goal-oriented remapping is assessed during probe trials when the reward is absent at the learned goal, in order collect place cells activity during movement at this location (Dupret *et al.*, 2010b; Jarzebowski *et al.*, 2022b).Those test-trials are usually performed after the period of rest. In my experiment, the beginning of Task 2, when the reward has been moved to a different location, can be used to assess place cell activity during movement around the goal location of Task 1. Specifically, I wondered if this old salient location is over-represented at the beginning of Task 2, following 90 minutes of rest in the home cage, and as the animal is adapting to the new reward location within Task 2.

Sorting CA1-PYR by the location of their peak firing rate along the maze, during the first ten laps of Task 2, revealed no clear accumulation of place fields at the previous reward location (orange line), as illustrated by the population linearized rate maps (**Figure 3.8A**), as it was the case during Task 1 (**Figure 3.7A**). Quantitatively, there was a slight decrease in the proportion of CA1-PYR with place field peaks in the previously rewarded zone during the early laps of Task 2 (in grey) compared to last laps of Task 1 (in blue) (n = 24 recorded Tasks, two-tailed Wilcoxon test, *p = 0.011, median of differences = -0.06) (**Figure 3.8B-*ii***). Yet, this proportion was similar to the beginning of Task 1 (data not shown). The mean firing rate, in the previously rewarded zone, significantly decreased from the ten last laps of Task 1 to the first ones of Task 2 (n = 883, Wilcoxon test, *p = 0.013, median of differences = -0.07) (**Figure**

3.8B-*i*) but were no different from the first 10 laps of Task 1 (data not shown). Furthermore, the distance between the former reward location and the nearest place field significantly increased at the onset of Task 2, following the rest period (n = 727 PYR with at least one PF in both conditions, two-tailed Wilcoxon, **p* = 0.019, median of differences = 1 bin) (**Figure 3.8B-*iii***). This distance was however similar to the beginning of Task 1 (data not shown).

As previously in **Figure 3.7D**, the proportion of CA1-PYR with place field at each spatial bin was calculated for the two stages of **Task 2** (ten first and ten last laps), aligned on the previous reward position, and represented as circular distribution along the circular maze (**Figure 3.8C**). The difference in place field density between the first and last laps was then computed and revealed no angular preference (mean angle = 164, previous reward at 300°, *p* = 0.5584) (**Figure 3.8C**).

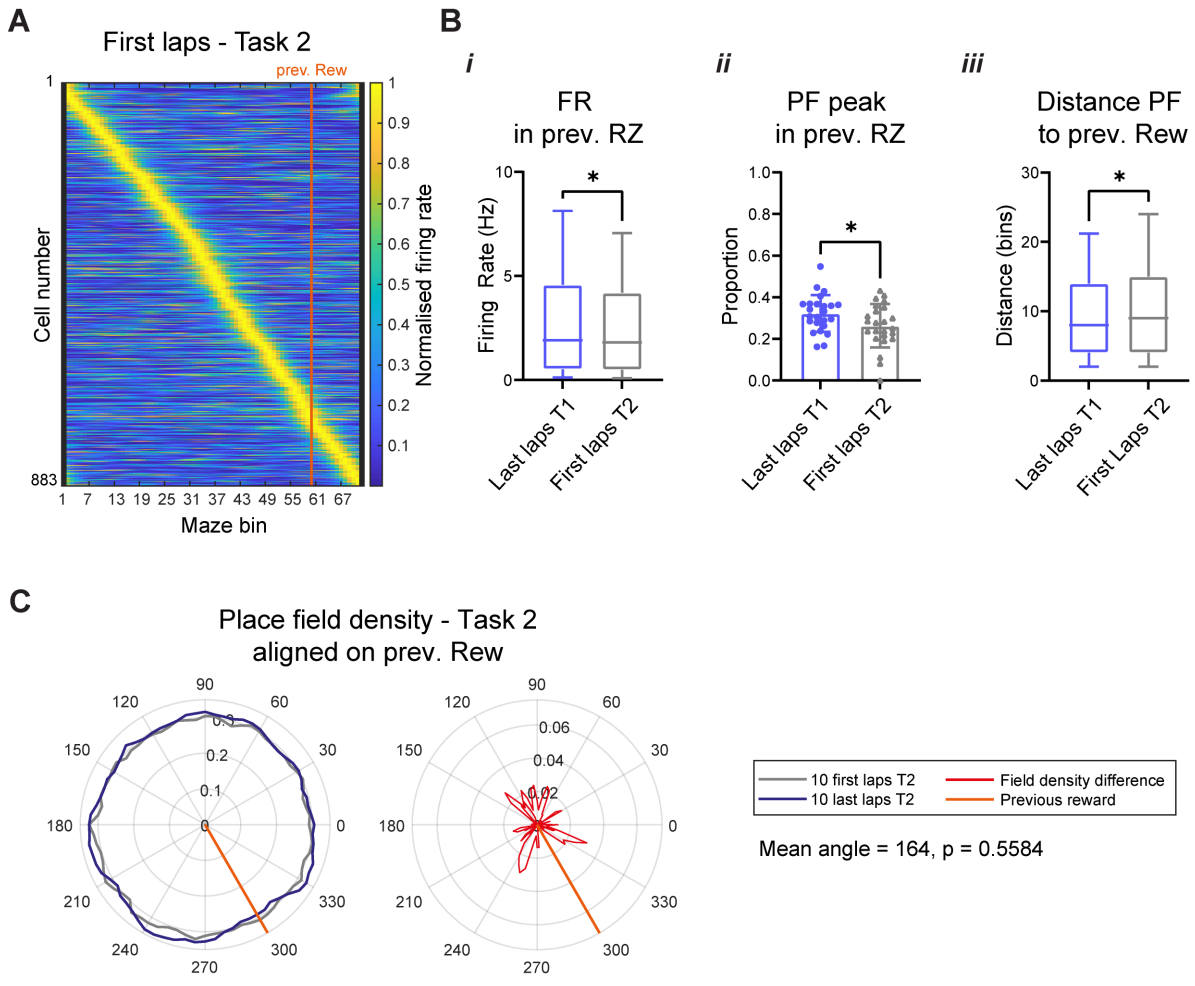

Figure 3.8: CA1 activity aligned on previous reward.
(A) *Linearized rate maps of all CA1-PYR during the ten first laps of Task 2, aligned on the previous Reward (prev. Rew, orange line).* ***(B) (i)*** *Comparison of the average firing rates in previous reward zone (prev. RZ). n = 883 CA1-PYR. Boxplots represent median and 25-75 percentiles, whiskers represent 10-90 percentiles. * p=0.0131 (Two-tailed Wilcoxon).* ***(ii)*** *Proportions of recorded CA1-PYR with a place field (PF) peak in prev. RZ compared between the last ten laps of Trial 1 (in blue) and the first ten laps of Task 2 (in grey). n = 24 sessions. Bar represents mean ± SEM. *p= 0.0113 (Two-tailed Wilcoxon).* ***(iii)*** *Distance between the previous reward and the closest PF calculated for last 10 laps of Task 1 and first 10 laps of Task 2. Boxplots represent median and 25-75 percentiles, whiskers represent 10-90 percentiles. *p = 0.0194 (Two-tailed Wilcoxon**). (D) Left:*** *Polar plots showing the proportion of CA1-PYR with PF in each spatial bin during the first (grey line) laps of Task 1 and last (dark blue line) laps of Task 2, along the circular maze. Previous reward position is indicated by the orange line.* ***Right****: The difference between the two distributions is plotted in red. The preferred direction of the difference was computed as the resultant vector angle. Significance was assessed via a bootstrap test (10,000 iterations), yielding p = 0.5584.*

These results indicate that after rest in CA1, the neuronal representation is not spatially anchored to the previous reward location at the population-level, likely due to the emergence of the new goal location and/or a global reorganization at the onset of Task 2. This suggests that CA1 place fields flexibly update their position in response to a shift in the reward location.

I next investigated how the location of CA2 place fields evolves over the course of the tasks. As for CA1, I compared neuronal activity during the first ten laps to that of the last ten laps of Task 1 (similar observations were made for Task 2).

2.6. Accumulation of CA2 place fields around the learned reward location

When sorting CA2-PYR based on the location of their maximal peak firing rate on the maze, no apparent accumulation of place field peaks was observed at the reward (green line), neither in the first 10 laps, nor in the last ones, as shown in the linearized rate maps of the recorded population (**Figure 3.9A, B**). However, the proportion of CA2-PYR with place field peaks in reward zone slightly increased (n = 35 recorded Tasks, two-tailed Wilcoxon test, $p < 0.0002$, median of differences = 0.07) (**Figure 3.9C-*i***). Similarly, CA2-PYR increased their average firing rate in the rewarded zone when comparing the first and the last laps (n = 943, two-tailed Wilcoxon, $p < 0.0001$, median of differences = 0.65) (**Figure 3.9C-*ii***). The distance between the reward and the closest place field of individual CA2-PYR significantly decreased during the task (n = 703 PYR with at least one place field, two-tailed Wilcoxon, $p = 0.04$). However, like for CA1-PYR, these changes could potentially lack specificity for the reward

zone as we have observed a general increase in firing rate during the course of the Task (**Figure 3.6**). To test for reward-oriented bias of place fields' densities, the proportion of PYR with a place field within each spatial bin was calculated for the two stages of the Task (ten first and ten last laps) and represented as circular distribution along the circular maze (**Figure 3.9D, Left**). The difference in place field density between the first and last laps was then computed and revealed a slight shift towards the reward zone (**Figure 3.9D, Right**). This directional bias was quantified by calculating the resultant vector angle of the distribution and testing its significance against a shuffled distribution (10,000 iterations, see Methods). In Task 1, CA2-PYR place field density change showed a significant directional bias (mean angle 282°, reward at 300°, $p = 0.0001$), consistent with place fields accumulating before the reward location, or at least in the quadrant of the maze that contains the rewarded port.

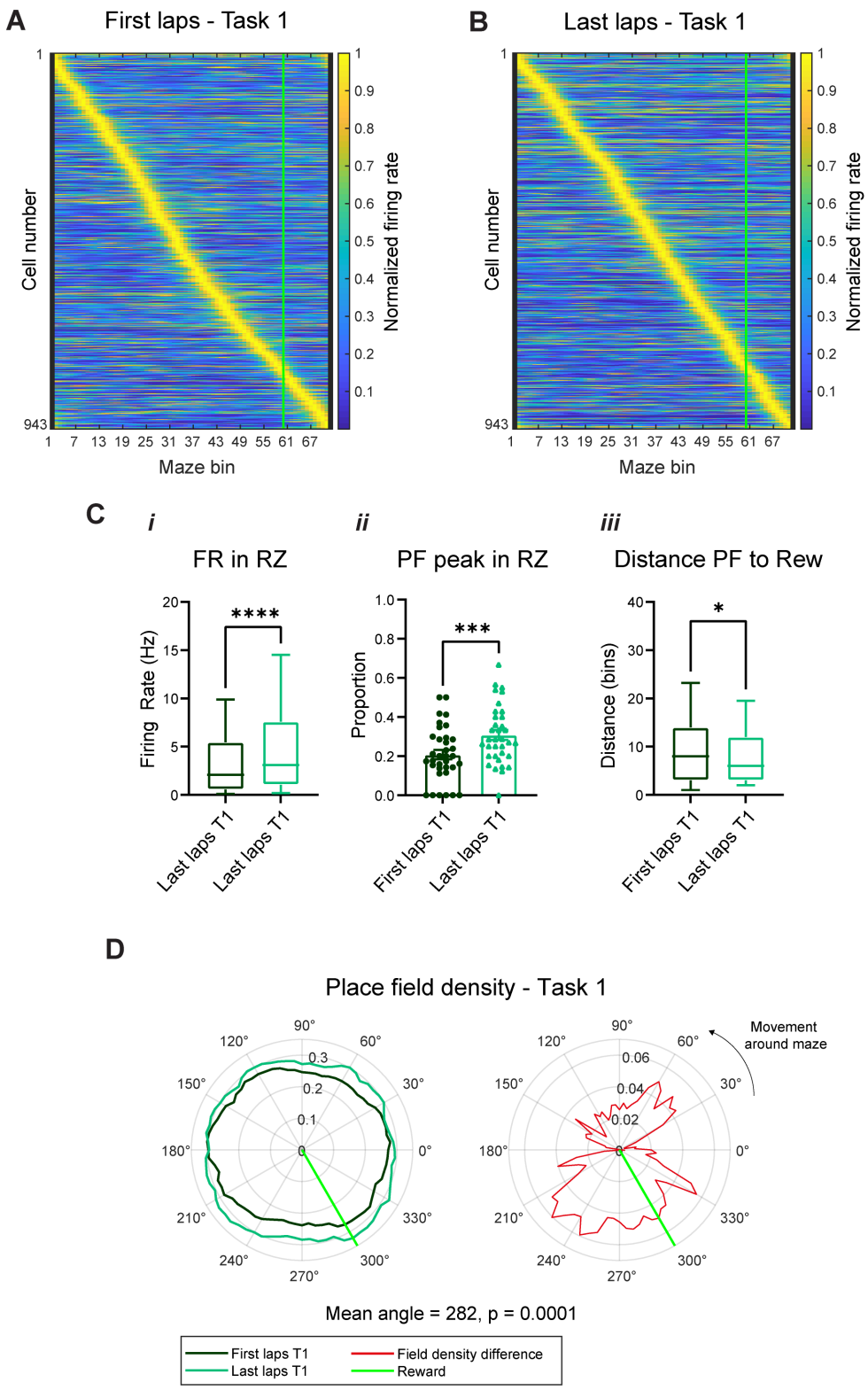
A
First laps - Task 1
B
Last laps - Task 1
Cell number
Maze bin
Normalized firing rate
C
i
FR in RZ
ii
PF peak in RZ
iii
Distance PF to Rew
Firing Rate (Hz)
Proportion
Distance (bins)
****
***
*
Last laps T1
First laps T1
D
Place field density - Task 1
Movement around maze
Mean angle = 282, p = 0.0001
First laps T1
Last laps T1
Field density difference
Reward

Figure 3.9: Change of CA2 putative pyramidal cells activity during the task.
(A) *Linearized rate maps of all CA2-PYR during the ten first laps of Task 1.* ***(B)*** *Same for the ten last laps.* ***(C) (i)*** *Comparison of the average firing rates in RZ in the first and last 10 laps of Task 1. n = 943 PYR. Boxplots represent median and 25-75 percentiles, whiskers represent 10-90 percentiles. Two-tailed Wilcoxon was performed to assess significance. **** p = 0.0001.* ***(ii)*** *Proportions of recorded CA2-PYR with a place field (PF) peak in reward zone (RZ) (defined as 6 spatial bins before and after the reward position) compared between the first and last 10 laps of Task 1. n= 35 sessions. Bar represents mean ± SEM. Two-tailed Wilcoxon test was performed to assess significance ***p = 0.0002.* ***(iii)*** *Distance between the reward and the closest place field calculated for the first and last 10 laps of Task 1. Boxplots represent median and 25-75 percentiles, whiskers represent 10-90 percentiles. *p = 0.0423 (Two-tailed Wilcoxon).* ***(D) Left:*** *Polar plots showing the proportion of PYR with place fields in each spatial bin during the first (dark green line) and last (lighter green line) laps of Task 1, along the circular maze. Reward position is indicated by the green line.* ***Right****: The difference between the two distributions is plotted in red. The preferred direction of the difference was computed as the resultant vector angle. Significance was assessed via a bootstrap test (10,000 iterations), yielding p < 0.0001. Similar observations were done for Task2 (not shown).*

Altogether, these results suggest that despite the general increase in CA2-PYR excitability and number of place fields, these place fields tend to accumulate during the course of the task within a relatively broad area that contains the reward location.

As for CA1, I next investigated residual CA2-PYR activity at the previous reward location.

2.7.CA2 activity at the previous reward location.

To assess whether CA2-PYR maintain spatial representations of the previously rewarded location after the goal shift, as for CA1, I analyzed activity during the first ten laps of Task 2, which began after a 90-minute rest period and featured a new reward location on the same circular maze.

As previously for CA1 (**Figure 3.8A**), no obvious place field concentration was observed at the previously rewarded location as shown by the linearized rate map of all recorded CA2-PYR (**Figure 3.10A**). To quantify activity changes at the former reward, I compared the proportion of CA2-PYR with place field peaks in the previous reward zone across the last laps of Task 1 (in green) and the first laps of Task 2 (in grey). A significant decrease in this proportion was observed **(**n = 35 sessions; two-tailed Wilcoxon test; ***p = 0.0007, median = -0,13), (**Figure 3.10B-*i***). The average firing rate within the previous reward zone significantly decreased between the two epochs (n = 943 CA2-PYR; two-tailed Wilcoxon test; ***p < 0.0001, median = -0,4) (**Figure 3.10B-*ii***). In line with the reduced proportion of cells with place field peaks in the previous reward zone, the distance between the closest place field and the

previous reward location increased significantly from the end of Task 1 to the beginning of Task 2 (n = 703 CA2-PYRs with at least one place field in both conditions; two-tailed Wilcoxon test; ***$p < 0.0001$, median = +1 bin) (**Figure 3.10B-*iii***). This could potentially reflect a spatial drift away from the former goal.

To capture changes in spatial coding at the population level, I again computed the circular distribution of place field density across the spatial bins for the ten first and ten laps of Task 2 (**Figure 3.10D, Left**). Surprisingly, the difference between the distributions of these two epochs (**Figure 3.10D, Right**) revealed a significant directional bias towards the previous reward, as confirmed with a shuffled distribution (10,000 iterations; p =0.0004, median angle= 288°, previous reward at 300°). Combined with the reduction in the firing rates within the reward zone at the onset of Task 2 (**Figure 3.10B-*i***), this observation is consistent with a selective decrease in place field density near the old reward when Task 2 begins, followed by a return to a homogeneous distribution later on during Task 2 (**Figure 3.10C**).

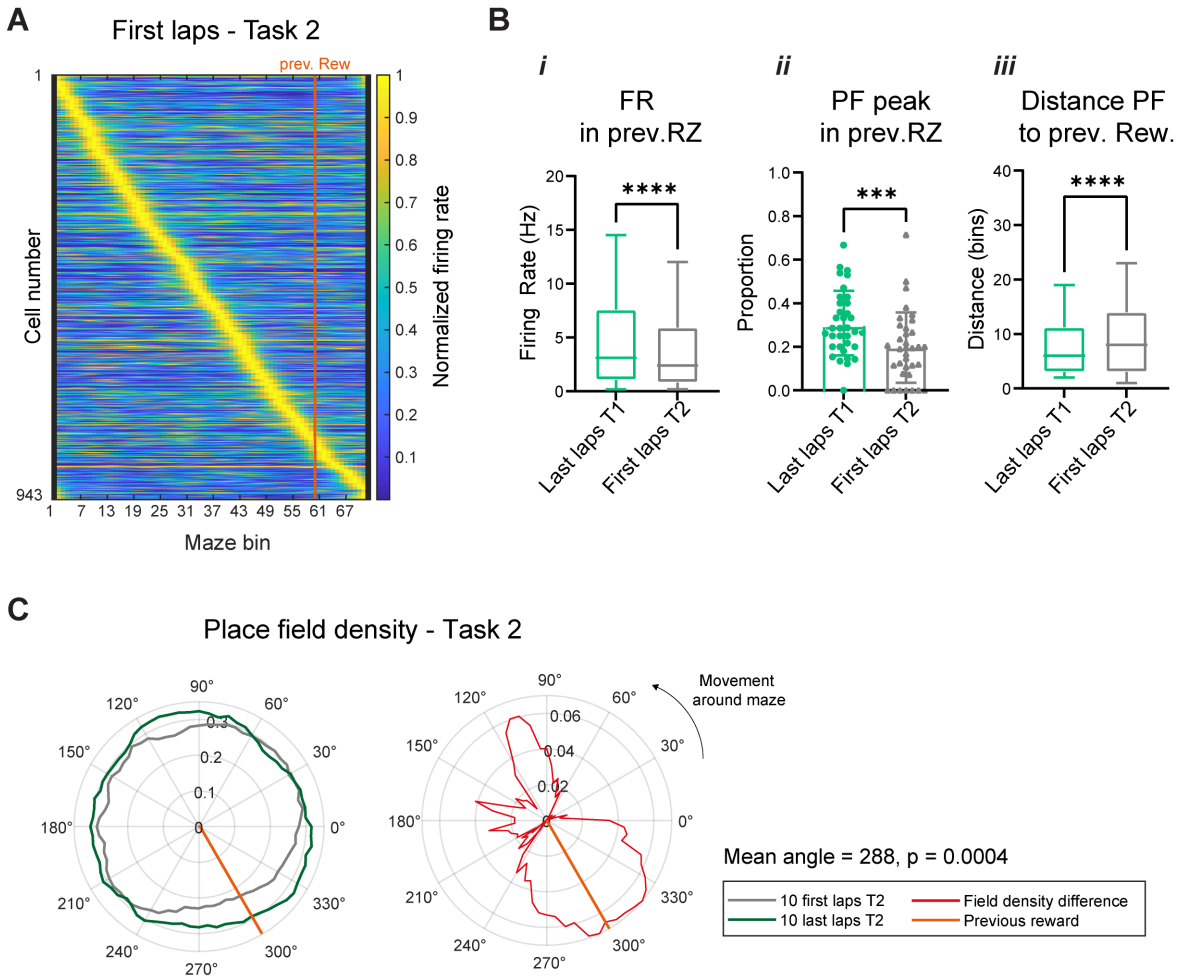

Figure 3.10: CA2 activity aligned on previous reward.
(A) *Linearized rate maps of all CA2 PYR during the ten first laps of Task 2, aligned on the previous Reward (prev. Rew, orange line).* ***(B) (i)*** *Proportions of recorded CA2 PYR with a place field (PF) peak in previous reward zone compared between the last ten laps of Trial 1 and the first ten laps of Task 2. n= 35 sessions. Bar represents mean ± SEM. ***p = 0.0007 (Two-tailed Wilcoxon).* ***(ii)*** *Comparison of average firing rates in previous reward zone (prev. RZ). n = 943 CA2-PYR. Boxplots represent median and 25-75 percentiles, whiskers represent 10-90 percentiles. **** p < 0.0001 (Two-tailed Wilcoxon).* ***(iii)*** *Distance between the previous reward and the closest PF calculated for last 10 laps of Trial 1 and first 10 laps of Trial 2. Boxplots represent median and 25-75 percentiles, whiskers represent 10-90 percentiles. ****p < 0.0001 (Two-tailed Wilcoxon).* ***(D) Left:*** *Polar plots showing the proportion of PYR with place fields in each spatial bin during the first (grey line) and last (green line) laps of Task 2, along the circular maze. Previous reward position is indicated by the orange line.* ***Right****: The difference between the two distributions is plotted in red. The preferred direction of the difference was computed as the resultant vector angle. Significance was assessed via a bootstrap test (10,000 iterations), yielding p = 0.0004*.

These findings show that during the course of Task 2 and unlike CA1-PYR, CA2-PYR modulate the density of their place fields near the location of a reward that was previously learned (in Task 1) but that has recently disappeared. Importantly, it shows that place field density shift is not only observed in the context of reward presence: it can also correlate with novel reward disappearance. As this feature was not seen in CA1-PYR, it could be a unique property of CA2-PYR related to their sensitivity to novelty.

2.8.Neuronal activity stability

A significant amount of work has assessed the stability of CA2 spatial representations across time in the same environment (Mankin *et al.*, 2015b; Alexander *et al.*, 2016b), when the environment is slightly modified (Lu *et al.*, 2015b), or when a novel object or a social stimulus is introduced (Alexander *et al.*, 2016b). Yet, so far, it remains unknown how the CA2 spatial code reacts to change in goal-location in a familiar environment, unlike CA1 (Dupret *et al.*, 2010b; Kaufman, Geiller and Losonczy, 2020b; Zemla *et al.*, 2022) and CA3 (Dupret *et al.*, 2010b; Jeong *et al.*, 2025).I therefore wanted to test how the CA2 spatial representation evolves in the Clock maze task and how it potentially differs from CA1.

First, rate maps were generated using non-overlapping blocks of 5 laps, and population vector (PVs) were computed separately for each block. The Pearson correlation coefficient (r) was then calculated between the PVs of all pairwise lap blocks across Task 1 and Task 2 (see Methods). Each matrix entry reflects the stability of the ensemble spatial representation

between two lap sets. High correlation values close to the diagonal indicate stable spatial coding across adjacent lap blocks, while lower off-diagonal values reflect remapping or reorganization (**Figure 3.11A** for CA1**, Figure 3.11B** for CA2). We can readily observe in these example sessions that the population correlation values were similar between CA1 and CA2, with strikingly lower correlation values obtained when comparing Task 1 and Task 2. I plan to perform a quantification of this qualitative observation by combining all recorded sessions in the future.

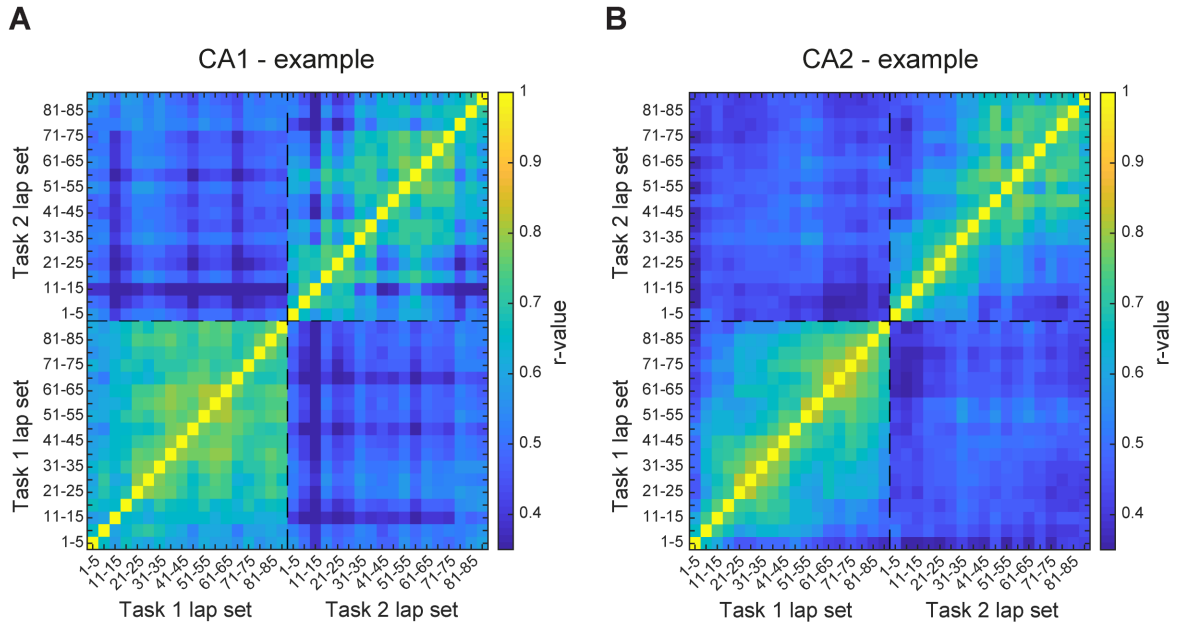

Figure 3.11: Population vector correlation
(A) *Example of population vector (PV) correlation matrix for CA1-PYR ensembles across the different sets of laps in Tasks 1 and 2. Each matrix entry reflects the stability of the ensemble spatial representation between two lap sets.* ***(B)*** *Same as in (A) but for CA2-PYR.*

Within-task stability:

For now, we turned to single cell analyses to investigate spatial representation remapping within a given task epoch. For each PYR, spatial stability was assessed as the Pearson's correlation coefficient (r) resulting from the comparison between the mean spatial rate maps obtained from the first ten and last ten laps (**intra-task stability**). To assess significance of the observed correlation value of each cell, it was compared to a null distribution resulting from a shuffling first ten and last ten labels, a null distribution that would reflect no difference between ten first and ten last laps (see Methods).

In CA1, the cumulative distribution of correlation values for all PYR rate maps from the first and last ten laps of Task 1 was significantly different from the shuffled control distribution (**Figure 3.12A-*i*, Left**; two-sample Kolmogorov–Smirnov test, **** $p < 0.001$), indicating a

global spatial remapping intra-task. A similar shift was observed in Task 2 (**Figure 3.12A-*ii*, Right,** **** $p < 0.001$). Despite this general trend, when considered individually, only a small proportion of cells significantly remapped (significantly negative correlations) from the beginning to the end of the task: 9% of CA1-PYR in Task 1 (**Figure 3.12A-*ii*, Left**) and 13% of CA1-PYR in Task 2 (**Figure 3.12A-*ii*, Right**). As a result, 81% (Task 1) and 77% (Task 2) of the PYR fell into the non-remapping category (i.e. non-different from shuffle or significantly correlated).

In contrast, CA2 showed a different profile (**Figure 3.12B**). While significant differences between observed and shuffled distributions were still present in both tasks (two-sample Kolmogorov–Smirnov test, **** $p < 0.001$) (**Figure 3.12B-*i***), only 3% CA2-PYR significantly remapped in both tasks. A higher proportion of cells fell into non-remapping category (Task 1: 87%, Task 2: 86%) (**Figure 12B-*iii***), a proportion significantly greater than in CA1 (two-sided chi-square test for both tasks, $p < 0.0001$). These results suggest that CA2 spatial representations are less variable or flexible across laps compared to CA1.

Inter-task stability:

Further, I wanted to quantify how much the spatial representations shift when the environment is kept identical except the reward position that is displaced (i.e. between Task 1 and Task 2). To evaluate inter-task remapping, for each cell, the correlations between rate maps during the last ten laps of Task 1 and the first ten laps of Task 2, were calculated. In CA1, the cumulative distributions again significantly deviated from the null distribution (**Figure 3.12C-*i*, Left**; two-sample Kolmogorov–Smirnov test, ****$p < 0.001$). 18% of CA-PYR cells showed significantly negative correlations, indicating spatial remapping (**Figure 12C-*ii*, Left**).

In CA2, inter-task correlation values were also significantly different from the null distribution (**Figure 12C-*i*, Right,** two-sample Kolmogorov–Smirnov test, **** $p < 0.001$). However, CA2-PYR showed a significantly smaller proportion of remapping units (5%) (**Figure 12C-*iii*, Right**) as compared to in CA1-PYR (two-sided chi-square test, $p < 0.0001$).

These results indicate that CA1-PYR exhibit greater spatial remapping across tasks than CA2-PYR, similar to the results obtained within-tasks where CA1 showed less stable units. CA1-PYR may therefore be more sensitive to small changes (like reward location) in a familiar environment.

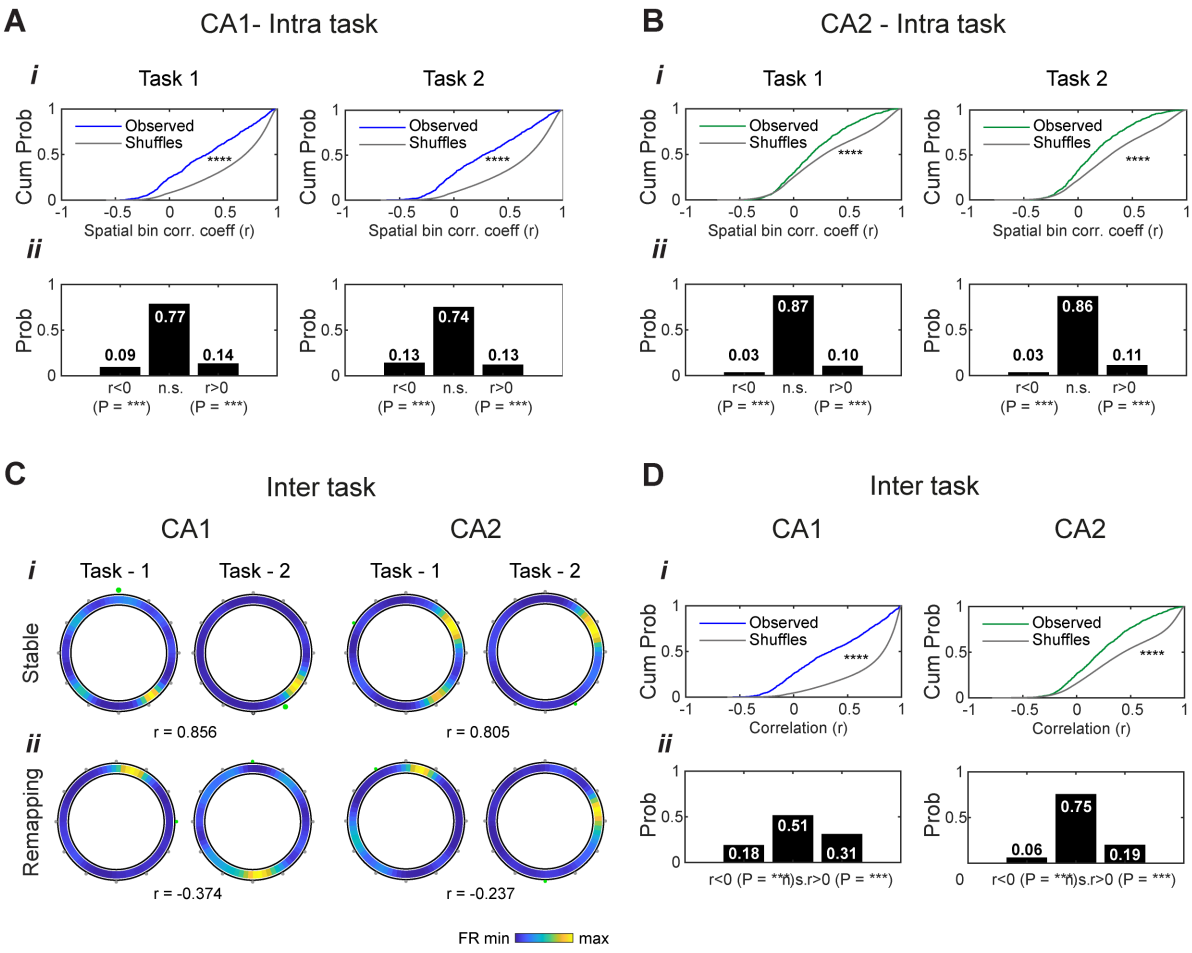

Figure 3.12: Spatial activity stability during the tasks compared between regions.
(A) Intra-task stability (i) *CA1-PYR cells cumulative distributions of spatial correlation coefficients (r) between first-10 vs last-10 laps (observed = blue, shuffles = grey, two-sample Kolmogorov-Smirnov, **** p<0.001) during Task-1 (left) and Task-2 (right).* ***(ii)*** *Proportion of cells classed as significantly positively correlated (r > 0), significantly negatively correlated (r < 0), or not significantly different (n.s.). For each cell, the p-value was assessed as the inverse percentile of the observed correlation coefficient relative to the shuffled distribution of the same cell (see Methods). To class significant cells, statistical threshold was arbitrarily set as (p < 0.001).* ***(B)*** *Same as in (A) but for CA2-PYR, with Task 1 on the left and Task2 on the right.* ***(C) Between-task cell-stability****. **(i)** Example of stable rate maps between first-10 laps of Task-1 and last-10 laps of Task-2, for CA1-PYR (left) and CA2-PYR (right).* ***(ii)*** *Example of remapping maps between the two tasks, for CA1-PYR (left) and CA2-PYR (right).* ***(D)(i) Left:*** *CA1-PYR cells cumulative distributions of spatial correlation coefficients (r) between last-10 of Task1 vs first-10 laps Task 2 (observed = blue, shuffles = grey, two-sample Kolmogorov-Smirnov, **** p<0.001).* ***Right:*** *same for CA2 (observed = green, shuffles = grey, two-sample Kolmogorov-Smirnov, **** p<0.001).* ***(ii) Left:*** *Proportion of cells classed as significantly positively correlated (r > 0), significantly negatively correlated (r < 0), or not significantly different than shuffle (n.s.).* ***Right:*** *same for CA2.*

2.9. Impact of omitted reward on spatial representations

Is spatial activity different after an omission trial?

To control for potential impact of reward omission on spatial coding, for each PYR, the Pearson correlation coefficient between pre-omission rate maps (**Figure 3.13A, left**) and post-omission rate maps (**Figure 3.13A, right**) was calculated. The cumulative distribution of correlation coefficient of CA2-PYR was no different from shuffle distribution (two sample Kolmogorov-Smirnov test, Task 1: p = 0.4222, Task 2, p = 0.5482) (**Figure 3.13B-*i***). The distribution of observed correlation and corresponding probability did not differ from shuffle (**Figure 3.13B, D-*ii***). Most of cells did not have a correlation different from the shuffle (**Figure 3.13B, D-*ii***), indicating that spatial activity of CA2-PYR cells was not affected by an immediately preceding reward omission, despite the decreased certainty about the next lap outcome.

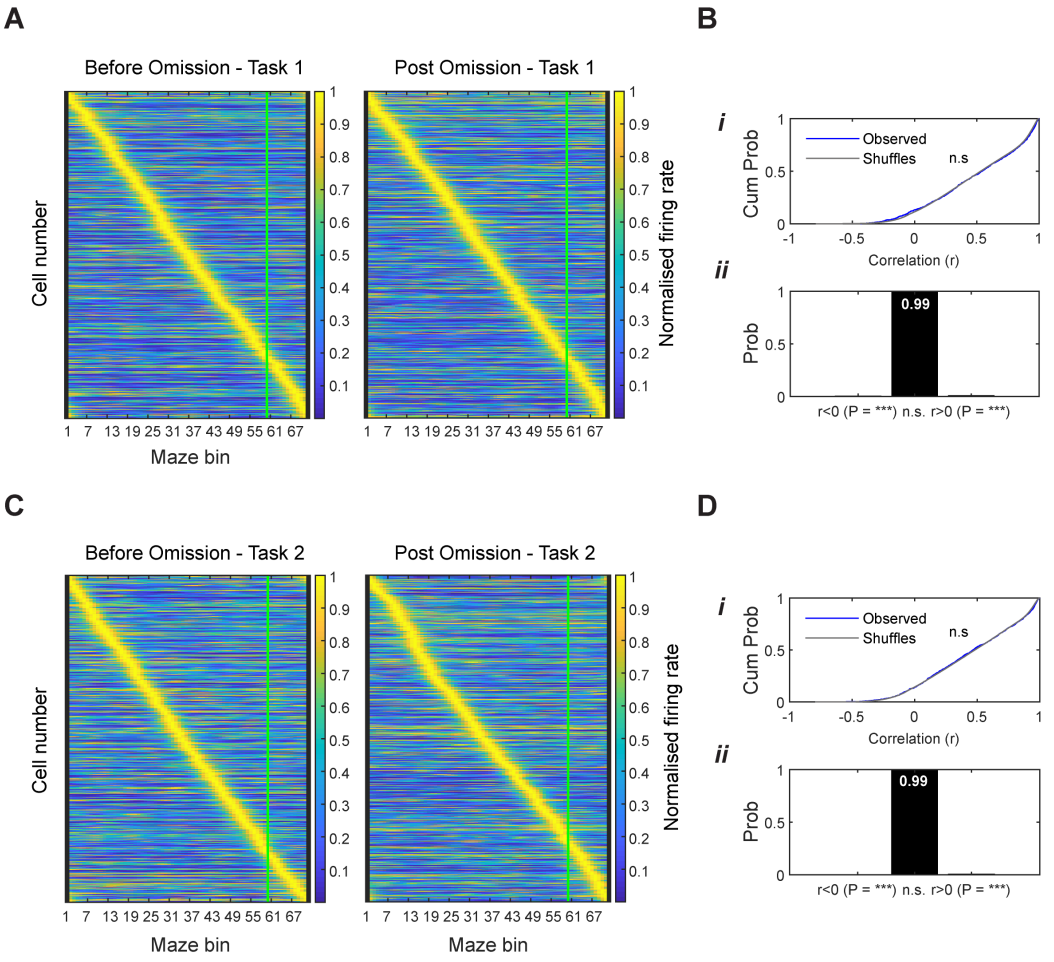

Figure 3.13: Spatial correlation between rewarded and post-omission laps in CA2. ***(A) Left:*** *Linearized rate maps of all CA2-PYR during the laps of Task 1 that precede reward omissions.* ***Right:*** *Same for the laps that follow reward omissions. (**B**) **(i)** Cumulative distribution of observed bin-by-bin correlation values (blue) for all CA2-PYR when comparing their respective rate maps before and after omissions (Task 1). Grey: distribution of the correlation values obtained for the shuffles (see Methods). **(iii)** Proportion of cells falling into three categories based on the comparison between their observed r values and their respective shuffled distributions (***p < 0.001): significantly positively correlated (r > 0), significantly negatively correlated (r < 0), or not significantly different than shuffle (n.s.).* ***(C) and (D)*** *Same as (A) and (B) but for Task 2.*

Following these observations during the movement periods and knowing the importance of CA2 in spatial encoding during immobility (Kay2014), I will next compare the activity of both hippocampal regions at port entry, moment of reward delivery and reduced speed.

3. CA1 and CA2 regions activity at reward

3.1. Activity of CA1 and CA2 around and during rewarded port nose-poke entry

To investigate if CA2-PYR encode reward during immobility, my next goal was to investigate their activity at the rewarded port and compare it to CA1-PYR which is known to be less active during immobility (Kay *et al.*, 2016). Port entry was detected by an infrared beam and, following a fixed one-second delay, a reward was delivered *via* the opening of a valve in rewarded trials. To control for possible neuronal responses to the auditory stimulus related to valve click, which could complicate our interpretation of reward-related responses, a mock valve was activated upon omission trials (see Methods).

Peri-Event-Histograms (PETHs) aligned on rewarded port entry and computed for all CA1-PYR (**Figure 3.14A**) and all CA2-PYR (**Figure 3.14B**) showed an accumulation of peaks of activity after the nose-poke, especially in CA2. A noticeable proportion of CA2-PYR also had a peak of activity after reward delivery (i.e. one second after entering the port) which was less pronounced for CA1-PYR. These differences in CA1-PYR and CA2-PYR profiles were also observable in the mean rate curves computed for the entire population of PYR in each region (**Figure 3.14A-*iii*** for CA1-PYR and **Figure 3.14B-*iii*** for CA2-PYR): a peak in population

activity was observed for CA2-PYR at port entry and reward delivery, while CA1-PYR showed a global activity decrease after port entry.

We then wondered whether individual units would maintain their activity profile when the reward was moved to a different port in Task 2. We therefore computed the PETHs for Task 2 but ordered the units using their peak activity in the PETHs from Task 1 (**Figure 3.14A-*ii*** for CA1-PYR, and **Figure 3.14B-*ii*** for CA2-PYR). By doing so, we observed that the activity profiles of individual units are different between the two tasks, although units seem to keep their preference for movement (before time zero) versus immobility in the port (after time zero). Importantly, when units were re-ordered according to their peak activity in Task 2 PETHs, a profile similar to Task 1 was observed (**Figure 3.14A-*iv*** for CA1, and **Figure 3.14B-*iv*** for CA2), meaning that as a population, units behaved similarly regardless of the reward location. Accordingly, the population mean rate curves showed no difference between Task 1 and 2 for both regions (**Figure 3.14A-*iii*** for CA1 and **Figure 3.14B-*iii*** for CA2). Together, these data suggest that different cells respond to port entry and reward in Task 1 and 2, consistent with the hippocampus coding for spatial information, including during immobility (Kay *et al.*, 2016).

To assess whether the population activity around nose-poke evolves during the course of a given task, the mean z-scored population activity was plotted for Task 1 and 2. No striking difference was observed between the beginning and end of the Task for CA1-PYR (**Figure 3.14C**), nor for CA2-PYR (**Figure 3.14D**). This indicates that the bumps of activity observed after port entry and valve opening were already present at the time of the first 10 laps and remained as prominent until the end of the task.

Secondly, I wondered if the responses were different between rewarded and omission laps. The mean z-scored population activity was plotted for both conditions and regions. Neither CA1-PYR (**Figure 3.14E**), nor CA2-PYR (**Figure 3.14F**) showed a distinct response upon omission of reward at population level. However, the population activity seems to be related to speed profile, indeed the increase in population activity after an omission seems to follow the acceleration of the animal that occurs more rapidly after an omission (**Figure 3.14E, F)**. This suggests that PYR cells can be tuned to changes in velocity and possibly omission of reward however, not at population level.

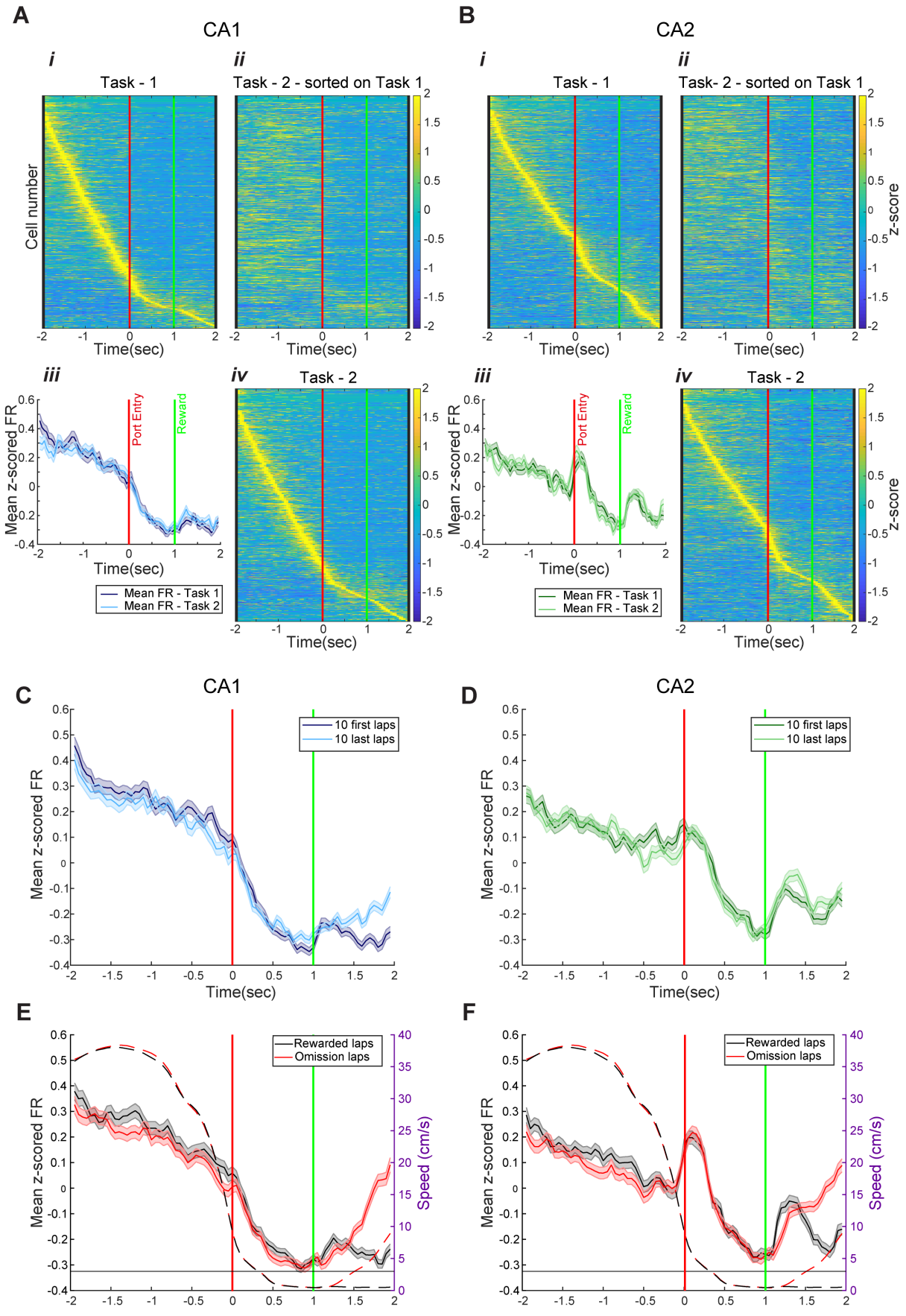
A
CA1
i
Task - 1
ii
Task - 2 - sorted on Task 1
Cell number
Time(sec)
z-score
iii
Mean z-scored FR
Port Entry
Reward
Mean FR - Task 1
Mean FR - Task 2
iv
Task - 2
B
CA2
Task- 2 - sorted on Task 1
C
CA1
10 first laps
10 last laps
D
CA2
E
Rewarded laps
Omission laps
Speed (cm/s)
F

Figure 3.14: CA1- and CA2-PYR activity around the rewarded port.
(A) (i) *Peri-event-histogram (PETH) centered on rewarded port entry (red vertical line) showing the z-scored firing rate of all CA1-PYR sorted by peak activity. Rates are averaged over all rewarded laps of Task 1. Green vertical line: reward valve opening.* ***(ii)*** *Same as (i) but for Task 2, with units sorted according to Task 1 (i.e. same order as in (i)).* ***(iv)*** *PETH for Task 2 sorted by peak activity during Task 2.* ***(iii)*** *Mean z-scored firing rate (FR) across all CA1-PYR (n = 883) for Task 1 (dark blue) and Task 2 (light blue), aligned on port entry.* ***(B)*** *Same as in (A) but for CA2-PYR (n = 943). For (iii): Task 1 in dark green, Task 2 in light green.* ***(C)*** *Mean z-scored FR across all CA1-PYR (n = 1766) computed for the first ten (dark blue) and last ten laps (light blue).* ***(D)*** *Same as in (A) but for CA2-PYR (n = 1886) for the first ten (dark green) and last ten laps (light green).* ***(E)*** *Mean z-scored FR across all CA1-PYR for rewarded laps (in black) and omission laps (in red), mean speed for rewarded laps (dashed black) and omission laps (dashed red).* ***(F)*** *Same for CA2.*

These results based on the entire population of recorded cells suggested differences between CA1 and CA2 activity profiles. However, they did not provide a fine-grained description of response diversity around nose port entry and reward delivery. We therefore aimed at exploiting the activity of individual units to identify groups of PYR with similar activity profile. PETHs of all cells from both region and both sessions were pooled and we perform k-means clustering to extract the 5 main clusters (or groups) of PYR. Z-scored PETHs aligned on port entry for each identified group were represented separately (**Figure 3.15C-*i***), as well as the mean z-scored activity curves of all PYR in each group (**Figure 3.15C-*ii***).

By examining the activity patterns, we identified distinct temporal dynamics across the five groups. **Group 1** showed two bumps of activity riding on an overall reduced activity within the nose port: one after nose port entry and one after reward valve opening. **Group 2** displayed an increased excitation shortly before entering the nose port, with a rapid return to baseline, suggesting a transient activation preceding port entry. In contrast, **Group 3 and 4** showed mobility-selective profiles undergoing a strong and gradual reduction in activity levels beginning before port entry and persisting into the nose-poke period. Finally, **Group 5** showed a drastic increase in activity level after the animal stops and enters the port, corresponding to an immobility-selective profile. These temporally distinct activity dynamics underscore the functional diversity of neuronal responses aligned to behavioral events in the task.

The five different groups were differentially represented within PYR of CA1 (**Figure 3.15E**) and CA2 (**Figure 3.15F**) (two-sided chi-square test, $p < 0.0001$). In particular, CA2 proportionally showed twice more units belonging to the immobility-selective **Group 5** as

compared to CA1 (26% *vs* 13% for CA2 and CA1, respectively; chi-square test, $p < 0.0001$, followed by Bonferroni correction. Conversely, CA1 showed nearly twice as many units belonging to **Group 3** with anticipatory decrease in activity before nose port entry compared to CA2 (28% *vs* 17% for CA1 and CA2, respectively chi-square test, $p < 0.0001$, followed by Bonferroni correction). A more similar repartition was observed for Group 2 (19% *vs* 14% for CA1 and CA2, respectively chi-square test, $p = 0.0002$, followed by Bonferroni correction). Other groups were equally represented in both hippocampal subfields (Chi square tests followed by Bonferroni corrections, $p > 0.05$). We next wondered whether units would stay in the same group when comparing the two tasks from the same day. We found that most units change group from Task 1 to Task 2, with slightly higher proportions (70%) in CA1-PYR (**Figure 3.14E**) than in CA2-PYR (62%) (**Figure 3.14F**) (two-tailed chi-square test, $p = 0.0765$). This result indicates that for most units, the activity profile around rewarded port entry is not fixed and can change over time or task contingency. Nonetheless, a noticeable part of the units (~30%) remained in the same group regardless of the task identity. Interestingly, the PYR that did not change groups across tasks where mostly in Group 3 in CA1 and Group 5 in CA2, the two groups that were selectively over-represented in each of these subregions (**Figure 3.15 E, F**).

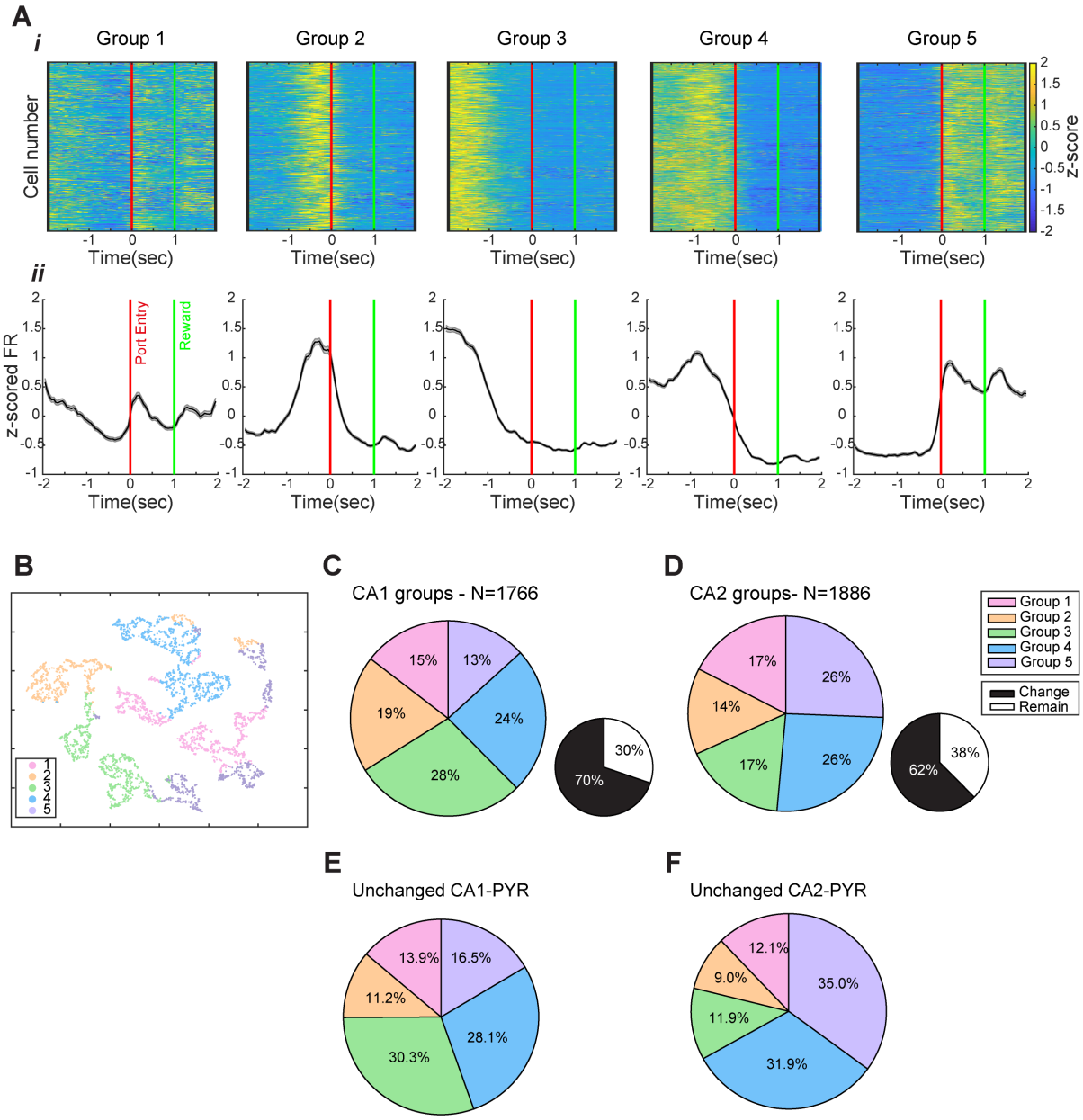

Figure 3.15: Clustering of CA1- and CA2-PYR based on their activity around the rewarded port.
*(**A**) (**i**) PETH obtained for the 5 groups resulting from k-means clustering of the z-scored activity of all PYR cells (CA1 and CA2) in both Tasks 1 and 2 around port-entry. (**ii**) Mean z-scored firing rate across all units of each group. (**B**) T-SNE representation of the 5 groups. (**C**) Pie chart representing the proportions of PYR in each group in CA1. (**C**) same as in (E) but in CA2. Insets: pie charts representing the proportions of units changing groups from Task 1 to Task 2. (**E**) Pie charts representing the proportions of CA1-PYR of each group that do not change groups across tasks. (**F**) same for CA2.*

Next, I wanted to quantify the activity dynamics of the five identified clusters within CA2-PYR. The firing rates of individual PYR in each group were analyzed at two different stages, centered on port entry:

- **Around port entry**: the mean firing rates within the second that surrounds port entry ([-0.5: +0.5] sec) was compared to the mean firing rate before (from [-1.5: -0.5] sec)
- **Around reward valve opening**: the mean firing rates 300 msec after reward valve opening was compared to the mean firing rates 300ms before valve opening. Mice did not leave the port (including in omission trials) before 300 msec post-valve opening (**Figure 3C**). The interval of 300 msec therefore insured that the animal was immobile during the analyzed window.

At port entry, CA2-PYR of Groups 2 and 5 showed an increased firing rate (two-tailed Wilcoxon test; ****$p < 0.0001$; Group 2, n = 270, difference of median = 0.9593; Group 5, n = 483, difference of median = 1.513). In contrast, the mean firing rate of Groups 3 and 4 CA2-PYR diminished (two-tailed Wilcoxon test; ****$p < 0.0001$; Group 3, n = 317, difference of median = -1.763; Group 4, n = 487, difference of median = -1,939).

At reward delivery, four group out of five showed a significant increase in firing rate when compare to the preceding 300 msec time interval (two-tailed Wilcoxon test; Group 1: **$p = 0.0014$, difference of median = 0.0034; Group 3, ****$p < 0.0001$, difference of median = 0.04463; Group 4, ****$p < 0.0001$, difference of median = 0.08333; Group 5, ***$p = 0.0001$, difference of median = 0.1392). Only Group 2 showed no significant change in activity ($p = 0.4814$).

Since several groups showed an increase in their firing rates following reward valve opening, I next wondered if this was due to the reward presence. I therefore used units' activity during the omission trials and compared their mean firing rates in rewarded trials versus in omission trials, during the 300 msec time-window that follows valve opening.

Group 1 and 4, that showed an increase activity following reward delivery, showed a decreased activity after an omission compared to reward (two-tailed Wilcoxon test; Group 1: *$p = 0.0427$, difference of median = -0.0238; Group 4: *$p = 0.0313$, difference of median = - 0,0476). I was not the case for the other groups.

Interestingly, in the Group 5 CA2-PYR - that showed an increased firing rate immediately after arrival at port and after valve opening in rewarded trials, no difference was revealed by comparing rewarded trials with omission trials (two-tailed Wilcoxon test; $p = 0.1445$, difference

of medians = -0.1754). These results suggest that cells that respond at reward delivery are not sensitive to the reward *per se*, but maybe to the action of licking or expectation of reward. Indeed, mice presumably lick in both reward and omission trials since the click of a valve happens in both cases.

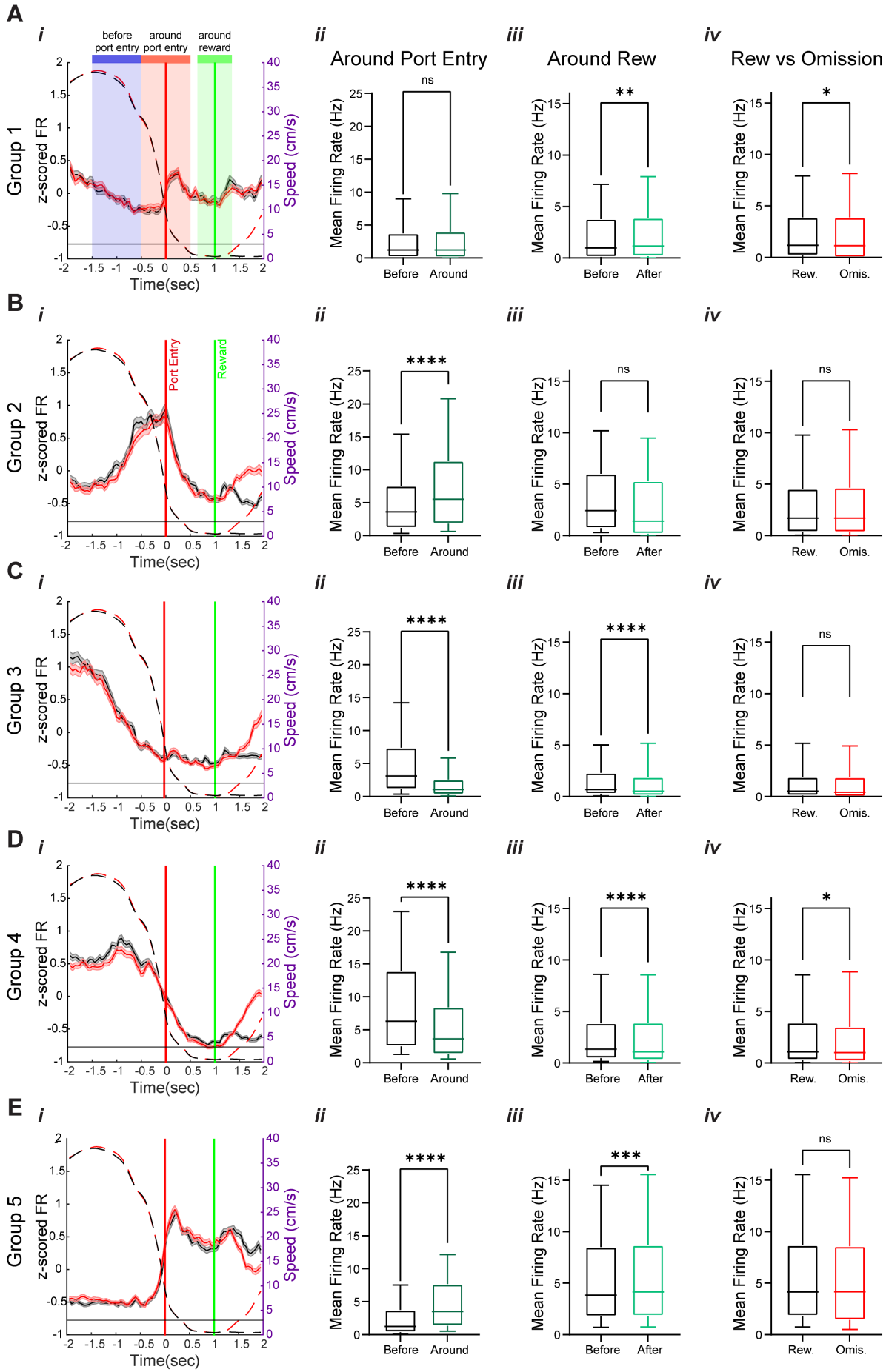
A
B
C
D
E
i
ii
iii
iv
Group 1
Group 2
Group 3
Group 4
Group 5
before port entry
around port entry
around reward
Port Entry
Reward
z-scored FR
Speed (cm/s)
Time(sec)
Around Port Entry
Around Rew
Rew vs Omission
Mean Firing Rate (Hz)
Before
Around
After
Rew.
Omis.
ns
**
*
****
***

Figure 3.16: Quantification of the activity of CA2-PYR groups around rewarded port and effect of omissions.
(A) (i) *Mean z-scored firing rate (FR) of Group 1 CA2-PYR in rewarded laps (black), and omission laps (red). Mean speed (cm/s) is shown with a dashed black line for rewarded laps and a dashed red line for omission laps. Red vertical line: nose port entry. Green vertical line: reward or mock valve opening (see Methods).* ***(ii)*** *Comparison of the mean FR before (blue rectangle (i), [-1.5; -0.5] sec) and after (red rectangle in (i), [-0.5; 0.5] sec) nose port entry. Wilcoxon signed-rank test, p = 0.4721, n = 329 CA2-PYR.* ***(iii)*** *Comparison of the mean FR before ([-0,7;1] sec) and after ([1;1.3] sec, green rectangle) reward delivery. Wilcoxon signed-rank test, **p = 0.0014.* ***(iv)*** *Comparison of the mean FR in the 300 ms following reward delivery (black) versus its omission (red). Wilcoxon signed-rank test, *p = 0.0427.* ***(B)*** *Same for Group 2 CA2-PYR, n = 270.* ***(ii)*** *Around port entry, Wilcoxon signed-rank test, p < 0.0001.* ***(iii)*** *Around reward, p = 0.4814.* ***(iv)*** *Reward vs Omission, p = 0.7914.* ***(C)*** *Same for Group 3 CA2-PYR, n = 317.* ***(ii)*** *Around port entry, Wilcoxon signed-rank test, p < 0.0001.* ***(iii)*** *Around reward, p = 0.3761.* ***(iv)*** *Reward vs Omission, p = 0.1134.* ***(D)*** *Same for Group 4 CA2-PYR, n = 487.* ***(ii)*** *Around port entry, Wilcoxon signed-rank test, p < 0.0001.* ***(iii)*** *Around reward, p < 0.0001.* ***(iv)*** *Reward vs Omission, * p = 0.0313.* ***(E)*** *Same for Group 5 CA2-PYR, n = 483.* ***(ii)*** *Around port entry, Wilcoxon signed-rank test, p < 0.0001.* ***(iii)*** *Around reward, p < 0.0001.* ***(iv)*** *Reward vs Omission, p = 0.1445.*

3.2. Interneurons activity during immobility at rewarded port.

Z-scored PETHs computed for all INs of CA2 (**Figure 3.17B-*i***) and CA1 (**Figure 3.16A-*i***) showed striking differences between the two regions: CA2-INs showed an accumulation of activity peaks before port entry which was not the case for CA1-INs. Interestingly, as a population, CA2-INs also showed a large increase in activity following reward delivery (**Figure 3.17B-*ii***) which seemed lower for CA1-INs (**Figure 3.17A-*ii***). Like for PYR, the mean INs-population firing rate qualitatively did not show any difference between Task 1 and Task2 and between the first and last ten laps in CA1 (**Figure 3.17A-*ii, iii***), nor in CA2 (**Figure 3.17B-*ii, iii***). When comparing rewarded with omission trials, the activity of CA2-INs seemed to be reduced following omissions (**Figure 3.17B-*iv***) and that was less the case for CA1-INs (**Figure 3.17A-*iv***). To assess the significance of these observations, a linear mixed models were applied to the mean firing rates of both IN populations, for the same time-window conditions as for PYR (**Figure 3.16**):

- **Around port entry (Figure 3.17C):** a significant decrease in INs firing rates was found for both regions (task phase factor: $p < 0.0001$, region factor: $p < 0.0001$, no significant phase of the task x region interaction: $p = 0.2962$).
- **Around reward valve opening (Figure 3.17D):** a significant increase after reward delivery was observed for both IN populations with a larger increase in CA2 as

compared to CA1 (task phase factor: $p < 0.0001$, region factor: $p < 0.0001$, phase of the task x region interaction: $p = 0.0139$)

- **Reward vs Omission (Figure 3.17E):** shortly after valve opening and before the animal speed starts rising again, a decreased firing was observed following omission compared to reward delivery, to a greater extent in CA2 compared to CA1 (condition: $p < 0.0001$, region factor: $p < 0.0001$, condition x region interaction: $p = 0.0013$).

These results suggest that CA2-INs, unlike CA1 and CA2-PYR, may play an important role in the reward response. These observations rose the question of what happens during movement for INs activity, since we know they also play a role in spatial coding (Marshall *et al.*, 2002b; Maurer *et al.*, 2006b; Turi *et al.*, 2019b; Geiller *et al.*, 2020b, 2022; Rolotti *et al.*, 2022b; Jeong *et al.*, 2025). Are they capable or goal-oriented remapping in our task?

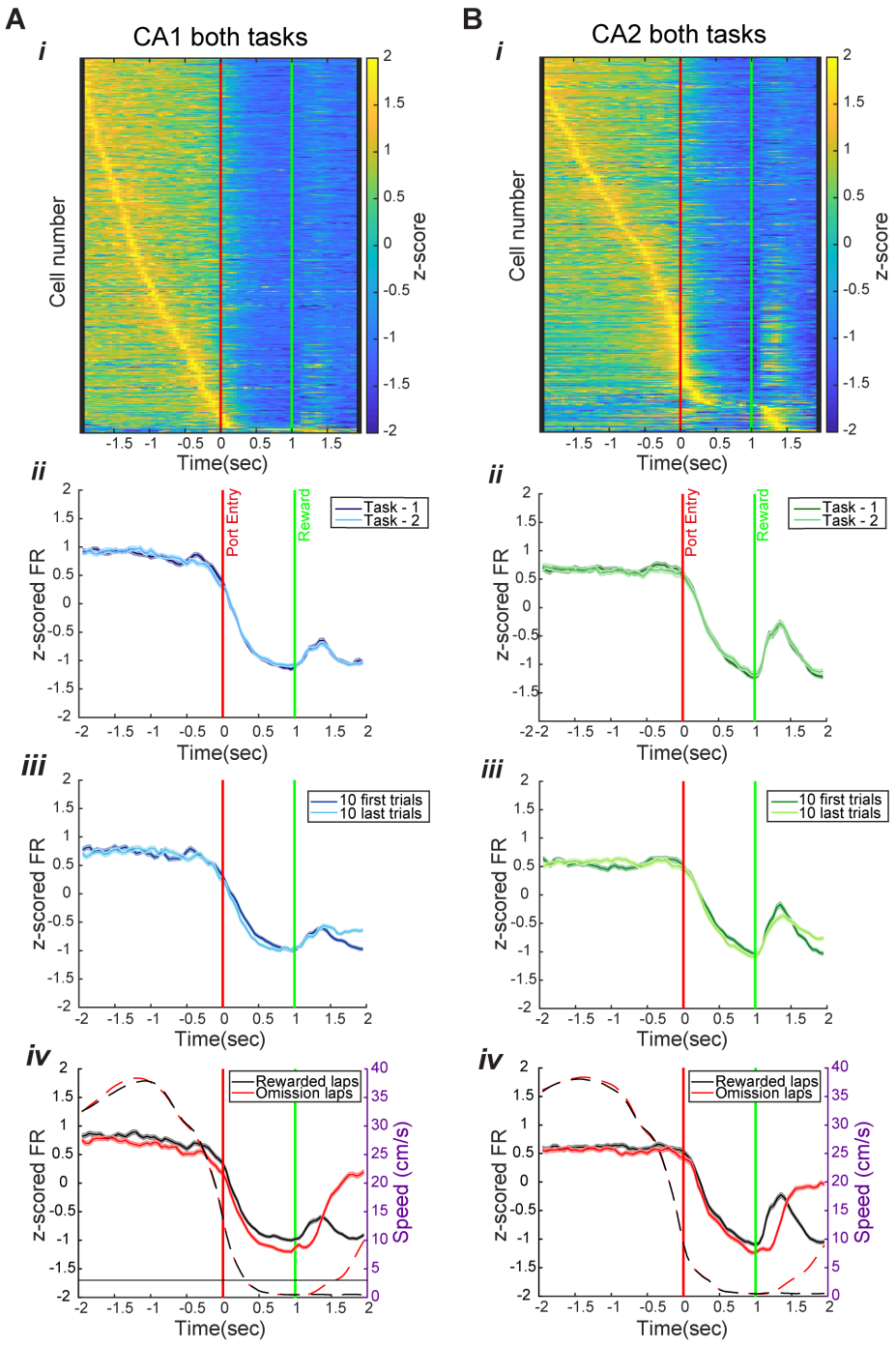
A
CA1 both tasks
B
CA2 both tasks
i
Cell number
z-score
Time(sec)
ii
z-scored FR
Port Entry
Reward
Task - 1
Task - 2
iii
10 first trials
10 last trials
iv
Rewarded laps
Omission laps
Speed (cm/s)

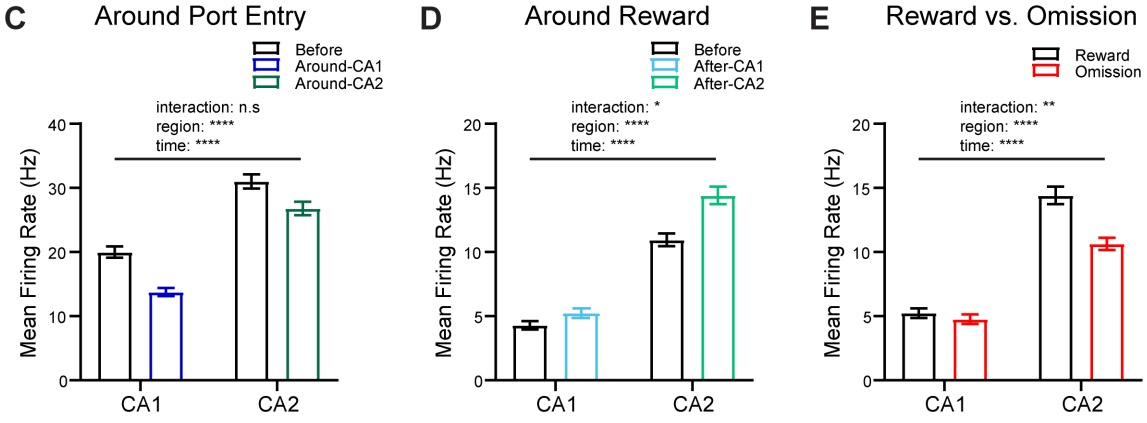
C
Around Port Entry
Before
Around-CA1
Around-CA2
interaction: n.s
region: ****
time: ****
D
Around Reward
Before
After-CA1
After-CA2
interaction: *
region: ****
time: ****
E
Reward vs. Omission
Reward
Omission
interaction: **
region: ****
time: ****
Mean Firing Rate (Hz)
CA1
CA2

Figure 3.17: Activity of putative CA1 and CA2 interneurons at the rewarded port.
(A)(i) *Peri-event-histogram (PETH) centered on rewarded port entry (red vertical line) showing the z-scored firing rate of all CA1 interneurons (INs) sorted by peak activity. Rates are averaged over all rewarded laps of both tasks. Green vertical line: reward valve opening.* ***(ii)*** *Mean z-scored firing rate (FR) across all CA1-INs (n = 215) for Task 1 (dark blue) and Task 2 (light blue), aligned on port entry. Line shadow indicates SEM.* ***(iii)*** *Mean z-scored FR across all CA1-INs (n = 215) for first 10 laps (dark blue) and last 10 laps (light blue), both tasked pooled together, aligned on port entry.* ***(iv)*** *Mean z-scored FR across all CA1-INs for rewarded laps (in black) and omission laps (in red), mean speed for rewarded laps (dashed black) and omission laps (dashed red).* ***(B)*** *Same as in (A) but for CA2-PYR (n = 252). For* ***(ii)****: Task 1 in dark green, Task 2 in light green,* ***(iii)*** *first 10 laps in dark green, last 10 laps in light green. (****C****) Comparison of their mean FR before ([-1.5; -0.5] sec) and after ([-0.5; 0.5] sec) nose port entry. Data are shown as bar plots ± SEM. A linear mixed-effects model revealed significant effects of hippocampal region (****p < 0.0001) and time condition (****p < 0.0001), no significant interaction between mouse and time condition (p = 0.2962). (****D****) Comparison of the mean FR before ([-0,7;1] sec) and after ([1;1.3] sec) reward delivery. A linear mixed-effects model revealed significant effects of hippocampal region (****p < 0.0001), time condition (****p < 0.0001), and a significant interaction between mouse and time condition (*p = 0.0139). (****E****) Comparison of the mean FR in the 300ms following reward delivery (black) versus its omission (red). A linear mixed-effects model revealed significant effects of hippocampal region (****p < 0.0001), time condition (****p < 0.0001), and a significant interaction between mouse and time condition (**p = 0.0013).*

To address this question, we computed the linearized rate maps for all INs aligned on the rewarded location as we did previously for PYR (**Figure 3.7A, B**). When sorting CA1-INs based on the location of their maximal peak firing rate on the maze, no apparent accumulation of place field peaks was observed at the reward (green line), neither in the first 10 laps (**Figure 3.18A-*i*)**, nor in the last ones (**Figure 3.18A-*ii*)**, nor for the all laps of Task 1 combined (**Figure 3.18A-*iii*)**. They rather showed a global inhibition at rewarded port, observation in line with our previous results at the port location (**Figure 3.17A**). In contrast, CA2-INs linearized rate maps showed a clear accumulation of peaks of activity before the rewarded port. This was already present during the first 10 laps (**Figure 3.18B-*i*)**, still there during the last 10 laps (**Figure 3.18B-*ii*)**, and was very prominent when pooling all the laps of Task 1 (Figure **3.18B-*iii*)**. Similar observations were made during Task 2 (**Figure 3.19**). Further analysis will be performed to characterize and explore CA2-INs role in goal-oriented remapping.

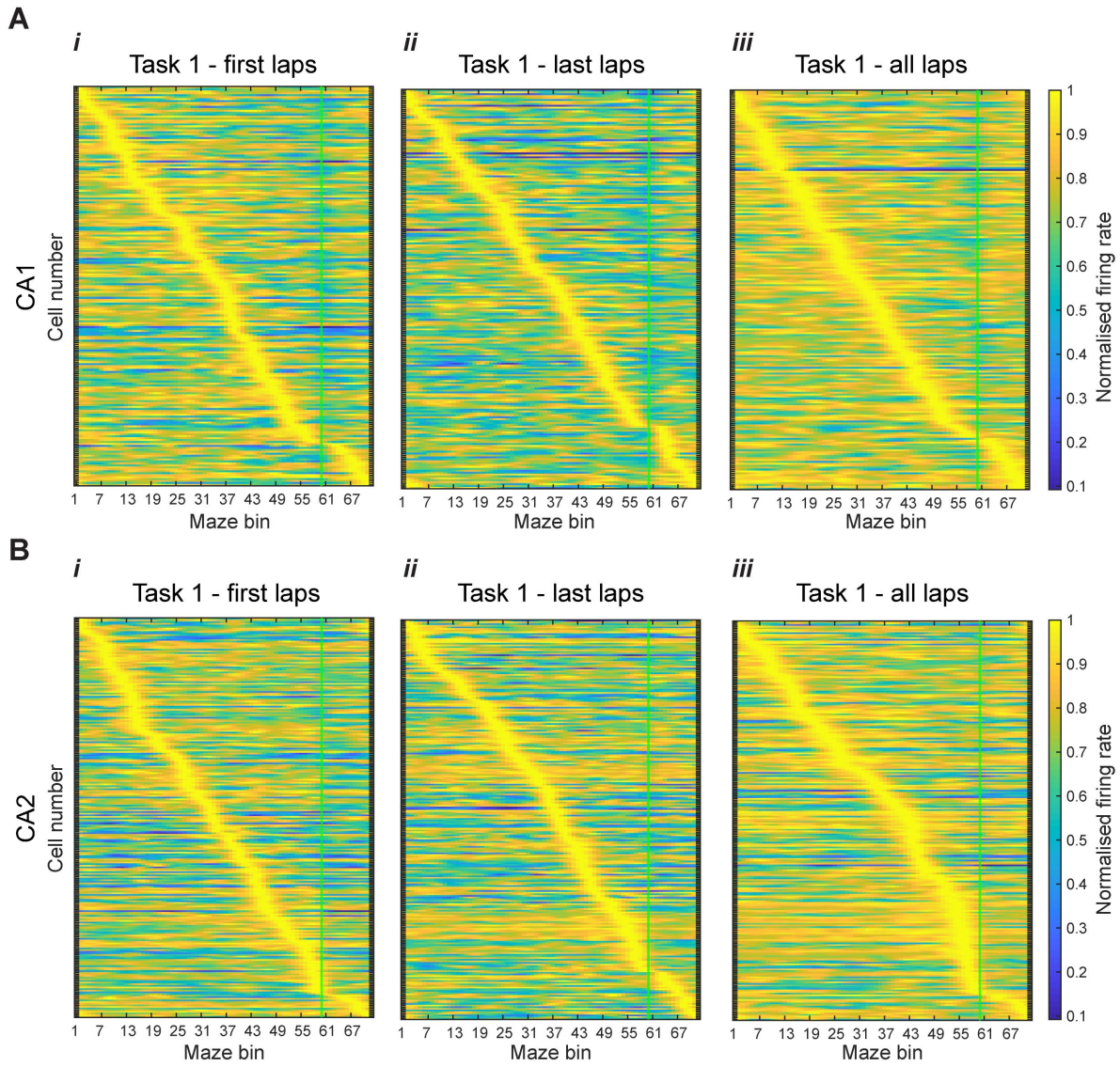

Figure 3.18: Interneurons activity during movement, Task 1
(A) *Linearized rate maps of all CA1-INs* ***(i)*** *during the first ten laps of Task 1* ***(ii)*** *during the last ten laps and,* ***(iii)*** *for all laps.* ***(B)*** *Same for CA2-INs.*

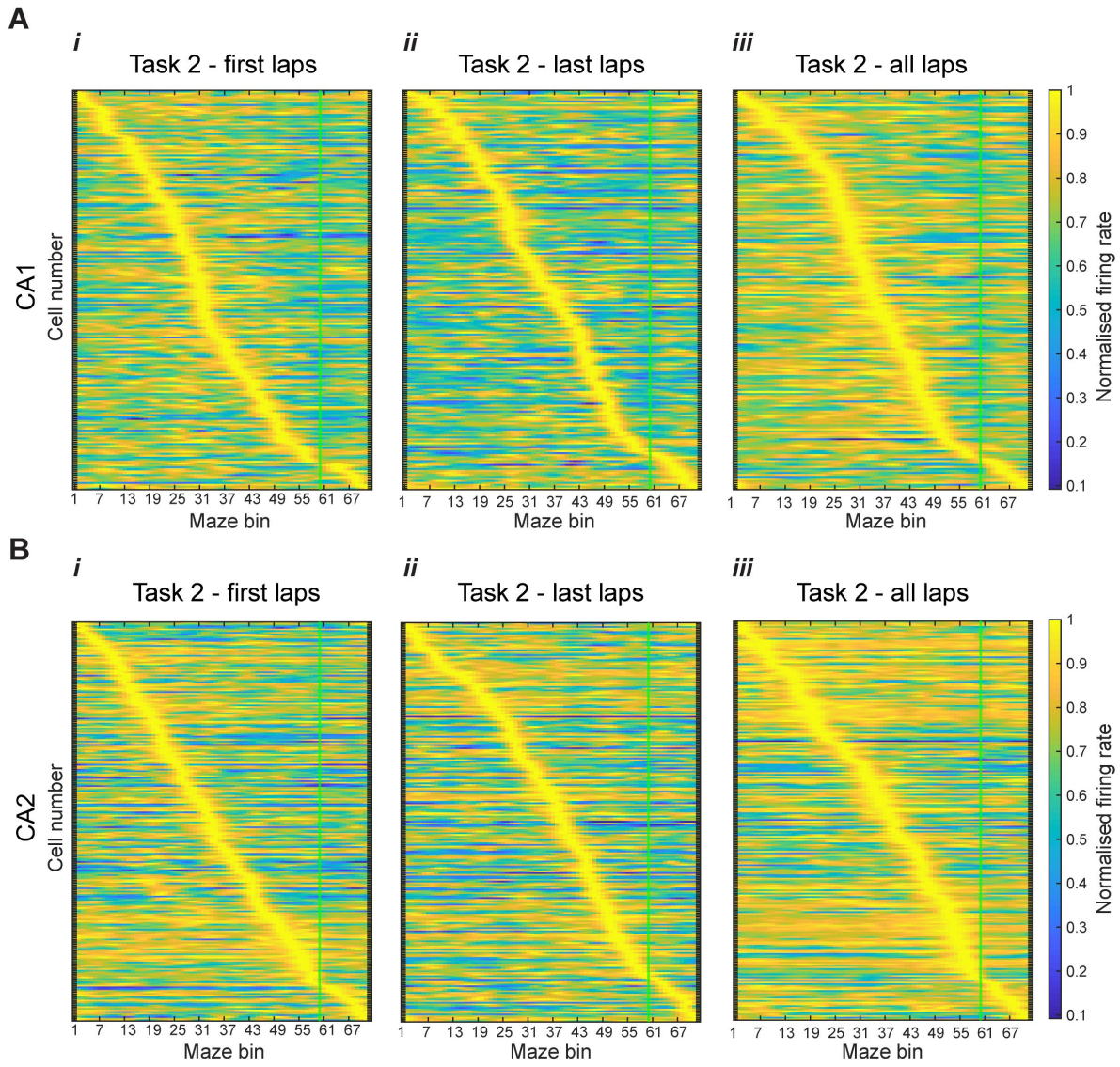

Figure 3.19: Interneurons activity during movement, Task 2
(A) *Linearized rate maps of all CA1-INs* ***(i)*** *during the first ten laps of Task 2* ***(ii)*** *during the last ten laps and,* ***(iii)*** *for all laps.* ***(B)*** *Same for CA2-INs.*

Chapter 4: Discussion and perspectives

The purpose of this PhD project was to study CA2 activity in a goal-oriented spatial navigation task, as well as during reward approach and consumption, taking advantage of a new spatial learning task in the Clock-maze. This project also allowed us to assess the differences between CA2 and CA1, the spatial properties of which are well established. First, I focused on the activity of these two regions through a classical place cells analysis during movement. In the second part of my work, the activity of CA2 and CA1 were studied during immobility at reward location.

In the following sections, I summarize the main findings, discuss their validity and their significance, and put them into perspective with previous research works. I also propose new experiments or analyses that could further consolidate our main findings.

1. Learning in the Clock-maze: a new behavioral task to study goal-directed behavior and reward responses

I developed a goal-oriented spatial-navigation task in an automated maze that we called the Clock-maze, where animals were able to learn two reward positions per day. Mice completed a high number of rewarded and omission laps, which was necessary for statistical comparison in the framework of my project. Most importantly, the Clock-maze enabled us to study neuronal activity of freely behaving animals during running, immobility and reward consumption in multiple locations. Beyond this specific project, I believe Clock-maze could be used to address other questions in future works and potentially other interested labs. Indeed, we can for instance easily adapt the number of rewarded ports per lap, alternate between goal-oriented tasks and foraging, or vary the duration of the delay between nose port entry and reward delivery. During the course of my PhD work, I had the opportunity to run a number of foraging sessions as a control (the rewarded port was changed at every lap) and intend to analyze those in the future. At this stage, it is difficult to say whether mice use and allocentric, cue-guided or egocentric strategy to navigate towards the rewarded port. This led us to use the generic term “goal-oriented learning”. It is also likely that depending on the mouse, the type of strategy differs. Based on the work of Dupret *et al. (2010*) that showed that goal-oriented remapping of place cells in CA1 is absent in a cue-guided version of the cheeseboard task, it could be that our effect

on place cell remapping remains relatively small because some mice may use local cues to reach the rewarded port. However, I tried to limit cue-guided behavior by cleaning systematically the maze from olfactory cues and display only distal visual cues. Alternatively, they could use egocentric signals, for instance count their steps, in order to accomplish their desired trajectory (a full turn). To start addressing this question, I am planning to run the task with slightly different conditions: at each task present two reward locations, non-symmetric in the circle, forcing the animal to stop at these different locations and therefore break the full turn in routes of different lengths and not like previously, a full turn. During the second task of the day, one of the rewards would be displaced, giving the possibility to compare cells' activity around the changed and remained reward positions.

2. Remapping differs between CA1 and CA2 subfields

During the course of this project, I first focused on describing the activity of CA1- and CA2-PYR during goal-directed navigation in the Clock-maze since it had not been explored yet in CA2.

Goal-oriented remapping in the clock maze

The recorded CA2-PYR exhibited similar spatial properties as previously describe: reduced spatial information content, larger place fields than CA1-PYR and an overall higher firing rate (Lu *et al.*, 2015b; Mankin *et al.*, 2015b; Oliva, Fernández-Ruiz, *et al.*, 2016). Upon learning, PYR from both regions displayed an increase in their firing rate (which was larger in CA2) and number of place fields per cell, as well as a decrease in the distance between place field peak and reward (**Figure 3.6**). These observations could be unspecific to the reward zone, as a general increase in PYR activity was observed when comparing the beginning and the end of the task. Nevertheless, an increase in place field density around the reward zone was significant when comparing the beginning and the end of the task in both regions, consistent with a goal-directed remapping (**Figure 3.7D, 3.9D**). Although, no apparent accumulation of place field peaks near reward was observed in population rate-maps (**Figure 3.7A, B and 3.9A, B**). This apparent discrepancy can be explained by the fact that, even if a cell's maximal firing peak lies outside the reward location, the spatial extent of its place field still encompasses the reward zone. As a result, these overlapping place fields together robustly encode the reward area, even though their individual firing peaks may not align precisely with the reward location.

It should however be noted that the effect remains relatively small. I will discuss below some limits of our study which could explain this reduced effect.

One of the limits of this work is that all PYR were included in the analysis and not only place cells. Indeed, we have not made any selection in our analysis based – for instance - on spatial information or on the presence of a place field, contrary to previous studies focused on goal-oriented remapping. Therefore, it would be interesting to look at the activity of only defined place cells populations. This selection could yield clearer results (for instance a stronger increase in place field density around the reward zone), as CA2-PYR with at least one place represent only a low proportion of all PYR (section 2 of Results, 40% of CA2-PYR against 72% of CA1-PYR). In other words, the effect could be in part dilute because of the inclusion of PYR with low spatial content.

A second limit of this study is the fact that we compared the ten first laps and ten last laps of each task to assess learning induced changes in spatial representations. However, we know mice can learn the reward location after only ~15 laps and they might exhibit demotivation at the end of the task. Such lack of engagement could influence spatial representations and reduce our ability to detect learning-induced changes. We propose, in future work, to determine the first laps when mice reach plateau performance and use those first laps for the comparison with the very first laps.

A third limitation of this study is the number of recorded neurons within the same task. Indeed, place cells do not represent all PYR-population and, in this spatially -modulated population, only a certain percentage will remap. Therefore, the size of CA2 region – even in its anterior part - and electrophysiological recordings make it a challenging task. Studies that showed clearer place fields concentration at the goal, in mice, were performed with large population recordings, using imaging technics (Zaremba *et al.*, 2017b; Kaufman, Geiller and Losonczy, 2020b; Zemla *et al.*, 2022; Qian, Li and Magee, 2025).

A forth limitation is the variability in behaviour observed across mice. Some animals displayed rapid, stereotyped navigation towards the goal, while others were slower or showed demotivation towards the end of the task (**Figure 3.2**). As it was shown that spatial map stability is linked to the level of engagement in memory tasks (Kentros *et al.*, 2004b; Krishnan *et al.*, 2022; Pettit, Yuan and Harvey, 2022), such behavioural variability could have partly contaminated our results. To address this issue, we plan to categorize the animals based on their performance and assess potential differences in spatial representations and place cell stability between these groups. Additional experiments may be required to have sufficient statistical power.

Spatial map stability in the Clock-maze upon reward-position changes in CA1 and CA2

The spatial correlation analysis made during mobility periods revealed distinct dynamics in hippocampal spatial representations across CA1 and CA2. While CA1-PYR exhibit flexible spatial coding with significant remapping both within and between tasks, CA2-PYR maintain more stable representations, showing minimal spatial reorganization despite changes in goal locations, suggesting that CA2 place coding is less sensitive to shifts in reward location compared to CA1. These results are in line with previous observations that showed that CA2 is less sensitive to small contextual changes (Lu *et al.*, 2015b; Mankin *et al.*, 2015b) and more sensitive to larger changes, such as changes in social context (Alexander *et al.*, 2016b; Chen *et al.*, 2020b; Oliva *et al.*, 2020; Bhasin and Nair, 2022b).

Future analyses could refine the current observation by investigating whether this relative rigidity in CA2 arises from specific cell populations by restricting correlation analyses to place cells alone. Moreover, examining correlation around reward zones might reveal subtle local plasticity masked by global stability, particularly when comparing CA1 and CA2. It would be interesting for instance to compare the dynamics of remapping and non-remapping cells: within the same task, are the cells in reward zone more stable (as it was demonstrated previously after learning Mizuta 2021, Sato 2020) and do the place fields of the remapping cells get closer to the reward zone? Are the cells that remap between tasks the ones which were previously in the reward zone? Is the place field accumulation in the reward zone due to the emergence of newly recruited place cells as it was shown before(Sato *et al.*, 2020b; Mizuta *et al.*, 2021b).

A stable spatial code enables the possibility to predict the animal position based on neuronal activity. Interestingly, there has already been some attempts aiming at decoding animals' position based on CA2 activity. The study of Donegan *et al.* (2021) for instance did so, although this was done in a social context rather than a spatial navigation task (this could make a difference). While CA1 activity could reliably predict the animals' position in these conditions, CA2 activity instead encoded contextual changes within the environment. A decoder trained on CA2 activity accurately identified different behavioral sessions in a social three-chamber task, outperforming decoding based on CA1 activity. Moreover, Hassan *et al. (*2023) demonstrated that CA2-PYR represent the social odors extracted from different conspecifics, with these representations being refined during associative learning. Specifically, CA2 discrimination capacity improved between rewarded and unrewarded odors during the course of learning Decoding accuracy of odor identities improved for rewarded stimulus *vs* unrewarded ones.

Spatial map stability is linked to engagement in the task

Previous studies have demonstrated that behavioural engagement strongly influences learning outcomes and spatial cognitive maps(Muzzio *et al.*, 2009; Taxidis *et al.*, 2020; Krishnan *et al.*, 2022; Pettit, Yuan and Harvey, 2022). More precisely in goal-directed navigation, Dupret *et al*. (2010) found that the accumulation of place fields at goal locations was predictive of task performance. Furthermore, spatial map stability over several hours was linked to the level of engagement in memory tasks (Kentros *et al.*, 2004b).Notably, animals that failed to learn the location of a safe zone exhibited unstable cognitive maps compared to those that succeeded, suggesting that engagement influences the fidelity of spatial representations. Similarly, in tasks that did not require spatial learning—such as cue-guided navigation towards goals or foraging—no accumulation of place fields at reward locations was observed (Kentros *et al.*, 2004b; Dupret *et al.*, 2010b; Krishnan *et al.*, 2022).

Additionally, Krishnan et al., identified "disengaged" laps, as less engaged in the task, by measuring pupil area of mice and approaching behaviour (deceleration at reward zone). They found a significant reduction in decoding performance of reward location when using only those laps. Consistent with this, Zaremba et al. 2017 reported that in a mouse model of schizophrenia, impaired spatial learning was associated with the absence of accumulation at the reward zone and unstable rate maps.

Based on these studies, it seems that in the absence of structured attention or memory demands, spatial representations do not stabilize. This likely explains why performance can be correlated with the strength and reliability of neuronal representations (Kentros *et al.*, 2004b; Dupret *et al.*, 2010b; Krishnan *et al.*, 2022; Pettit, Yuan and Harvey, 2022). Therefore, as for goal-oriented remapping, classifying animals based on their task performance might reveal some differences in encoded spatial information and its stability. Zelma *et al.* further demonstrated that, using neuronal decoders (Brown *et al.*, 1998; Ziv *et al.*, 2013b; Rubin *et al.*, 2015), task performance was strongly correlated with the accuracy of hippocampal spatial maps in predicting position and trial context. Implementing a similar decoder in our dataset could help reveal differences in map stability and decoding efficiency between behaviorally distinct groups and across hippocampal regions.

Exploring further learning-induced changes in CA2 spatial representations

An additional question we are planning to address with this dataset is: how does place cell information content evolve over the course of the task. In parallel, it would be valuable to assess how spatial representations progressively stabilize as learning occurs. One promising approach

for this would be lap-by-lap correlation analyses throughout the task (**Figure 3.11**), which could reveal a gradual increase in spatial map stability and spatial information as animals gain experience and improve performance and more particularly around the goal. Such dynamic changes in spatial coding—where field stability and information content increase across trials—have been reported in previous studies (Roux *et al.*, 2017a; Zemla *et al.*, 2022) but it remains to be addressed in CA2. I would not expect to see this change in the foraging version of the task, where the memory load is minimal.

Reward displacement in a familiar environment: does CA2 respond to a novelty signal?

Detecting novelty is an essential ability that enables the brain to prioritize and encode information that deviates from past experience. Accordingly, novelty signals powerfully drive attention, perception, and enhance memory formation.

An intriguing observation we made while analysing spatial representations in the Clock-maze task, is the drop of CA2 PYR place field density at the previous reward location during Task 2 during the ten first laps compared to the ten last (**Figure 3.10C**). This drop was not observed for CA1 PYR (**Figure 3.8C**). One possible interpretation is that CA2-PYR might respond to reward displacement by a decreased activity that translates into a lower place field density at the previous reward location. At end of Task 2, after learning, place field density around the previous reward zone recovers and match neighbouring regions in the maze (except reward 2 zone which shows an increased place field density), which reads out as an increase at previous reward location compared to the ten first trials. The decrease in place field density at the previous reward location aligns with findings by Krishnan et al. (2022), who showed that removing an expected reward leads to a reorganization of CA1 spatial maps, even as the animal continues performing the task. This reorganization coincides with the decline of anticipatory licking at the former reward site. It could be that in our task, this reorganization is slower in CA1 than CA2, leading to an effect in CA2 only. Additionally, Krishnan *et al.* (2022) found that dopaminergic axons from the VTA increase their activity as the animal approaches the reward, and inhibiting these axons mimics the effect of diminished reward expectation on the spatial maps. Based on this work, we could hypothesize that VTA sends expectation signals at rewarded port approach in our task and that reward displacement (or omissions) triggers a reward prediction error signal corresponding to a suppression of dopaminergic inputs from VTA on hippocampal circuits.

We could address this hypothesis by performing supplementary experiments where the reward is not displaced at the second Task. If CA2-PYR are sensitive to reward displacement,

we would not observe a decrease in place field density in this case. However, one could argue, that change in specific behaviour — licking — could be responsible of these changes, this could be addressed by changing the reward value: replacing the condensate milk by water. Additional experiments could include the characterization of the dynamics of dopaminergic projections from VTA (or LC) onto CA2 in our task, using fiber photometry.

This hypothesis is particularly interesting to explore since CA2 was previously reported to be sensitive to change upon social, time or contextual novelty(Wintzer *et al.*, 2014b; Mankin *et al.*, 2015b; Alexander *et al.*, 2016b; Bhasin and Nair, 2022b) .

3. Activity of CA1- and CA2 PYR during immobility

Does CA2 code for immobility-related states?

Our observations reveal different patterns of PYR activity in CA1 and CA2 during behaviorally relevant events: nose port approach and reward consumption (**Figure 3.13**). In particular, CA2-PYR showed a large proportion of units active during immobility with clear peaks after port entry and reward delivery. We identified five distinct groups of PYR, each displaying characteristic activity changes around port entry and reward delivery. Notably, Group 5 PYR in CA2 exhibited a significant increase in firing rate immediately after port entry— suggesting an immobility-selective profile—while other groups (e.g., Group 3 and 4) showed a decrease in firing rate, reflecting mobility-selective profiles (**Figure 3.15**). In fact, we found that the immobility-related activity profile (Group 5) was overrepresented in CA2 compared to CA1 (26% vs. 13%) (**Figure 3.14C, D**), supporting the idea that CA2 contributes more prominently to immobility-related coding than CA1.

These findings resonate with the work of Kay *et al.* (2016), who characterized a unique firing pattern of a subpopulation of CA2-PYR during immobility and sharp-wave ripples (SWRs). The so-called “N-units”, showed increased firing specifically during immobility in certain places and decreased firing during sharp-wave ripples (SWRs) (N for negatively modulated), contrasting with typical SWR-related increased firing seen in CA1 and CA3 neurons as ramping cells observed by Oliva et *al. 2016*. However, careful examination of neuronal activity during immobility periods uncovered new information about what CA2 could code for during immobility. Indeed, we found that Group 5 CA2-PYR exhibit an increased activity after port entry—when the animal is immobile— but also at reward delivery. Omissions events revealed that CA2-PYR may not be sensitive to reward consumption *per se* but rather

be related to licking behavior as activity levels were similar after omissions as compared to after rewards (**Figure 13.5E**). These results overall suggest that CA2 play a role in encoding contextually relevant events and potentially actions during immobility, such as nose-poke or collecting the reward. **CA2 neurons may therefore also represent immobility-related states beyond immobility alone**. In future analyses, it would be interesting to use decoding methods to assess whether the activity of identified subpopulations can predict the different behavioral states (post-nose-poke or post-valve-opening).

Importantly, we showed that this code is not static and largely evolves with time, reward displacement, or spatial location. Indeed, not the same neurons are activated after port entry or valve opening when the rewarded port is moved to a different location in Task 2 (**Figure 3.13B**). Yet, the majority of neurons that maintained a consistent activity profile across the two different tasks also belonged to Group 5 in CA2 (**Figure 3.14F**), hinting at a more stable code for these neurons during immobility at different locations. Additional analysis on immobility periods at other locations than the rewarded port will help us complementing this work.

Spatial properties of immobility-selective neurons

Furthermore, it would be valuable to investigate the spatial properties of the different groups, notably, whether the immobility-sensitive units correspond to a stable CA2 population when it comes to place fields along the maze, or if they do not carry much spatial information when the animal runs. One hypothesis could be that different subgroups of CA2 neurons are coding for either space during run or state during immobility. In this case, we would expect low information content for the immobility-selective groups.

Altogether, these findings extend the immobility-related coding function of CA2 neurons identified by Kay *et al.* (2016) to a goal-directed task framework. They suggest that while CA2's contribution to navigation *per se* (i.e. directed movement) may be limited, its role in encoding behavioral states during immobility—and potentially integrating these states with goal-directed actions—may be a fundamental feature of this hippocampal subregion.

4. Activity of Interneurons during immobility and running

CA2 network activity is highly regulated by inhibition, and plays a critical role in excitability control within the hippocampus (Piskorowski *et al.*, 2016; Boehringer *et al.*, 2017b). Accumulating evidence underscores the importance of interneurons (INs) in spatial

navigation and memory encoding, e.g. for hippocampal theta oscillations (Buzsáki, 2002; Stark *et al.*, 2014), for the so-called phase precession (Marshall *et al.*, 2002b; Maurer *et al.*, 2006b) for stabilizing place fields (Ego-Stengel and Wilson, 2007b; Turi *et al.*, 2019b; Dudok, Klein, *et al.*, 2021; Geiller *et al.*, 2022; Rolotti *et al.*, 2022b; Jeong *et al.*, 2025) and selecting active cell assemblies at any moment in time *via* lateral inhibition of competing assemblies (Trouche *et al.*, 2016) . They are also central during the consolidation processes for instance *via* their role in sharp-wave ripple (SWR) generation (Roux *et al.*, 2017b; Vancura *et al.*, 2023; Karaba *et al.*, 2024b). Therefore, I was curious to explore the INs activity in the Clock-maze task.

Observed results reveal a distinct profile of CA2-INs activity during reward-related immobility periods when compared to their CA1 counterparts. While both CA1 and CA2 INs were suppressed following immobilization at the port (consistent with their known speed modulation), CA2-INs also showed a robust increase in firing after reward delivery — a pattern that was less prominent in CA1-INs (**Figure 3.16**). Interestingly, this activity was significantly attenuated during omission trials, suggesting a sensitivity of CA2-INs to reward consumption. These results suggest that CA2-INs may provide a unique contribution to reward-context integration, complementing the activity of PYR which, in contrast, remained relatively unaffected by reward omission.

Further insights from the population rate maps extracted from locomotion epochs (speed > 3 cm/sec) indicate that CA2-INs show an accumulation of activity peaks near the goal location, unlike CA1-INs that were generally suppressed (**Figure 3.18, 3.19**). This increased activity of CA2-INs was also apparent in PETHs aligned on rewarded port entries: a large proportion of CA2-INs increased their firing during port approach (**Figure 3.16B**). While the apparent anchoring of CA2-IN activity to the reward location is compelling, further quantification is required to determine the statistical robustness and functional relevance of this pattern and how it might participate in spatial representations establishment around behaviorally salient locations, such as the reward site. Importantly, the contribution of the animal's speed to the modulation of INs activity must be addressed in future analyses.

These results raise many important questions. First, it will be important to determine whether the observed post-reward excitation in CA2-INs reflects true reward processing or is confounded by sharp-wave ripple (SWR) events, which frequently occur during immobility and are known to modulate INs firing (Csicsvari *et al.*, 1999; Roux *et al.*, 2017b). Ongoing work

incorporating SWR detection will help clarifying this issue. It is important to note that SWR-detection in CA2 is quite challenging, and not all the recorded animals presented SWR features suitable for a robust automated SWR detection approach. This could in part be due to the thickness of the pyramidal cell layer that prevents from sampling simultaneously from the pyramidal cell layer and the stratum radiatum. However, in our last recordings, we used a Janus double-sided probe (*Diagnostic Biochips*) which should help disentangling these possibilities. Indeed, this type of probe has more recording sites and spans a larger tissue depth (300µm, with 16 channels per shank per side), enabling us to record from both the pyramidal cell layer and the stratum radiatum where the sharp wave typically occurs (i.e. LFP reversal during SWR events was observed). Overall, these recordings showed very promising SWR-detection results.

Second, these findings confirm the fact that INs participate in encoding behaviourally relevant locations. Notably, our results align with growing evidence showing that INs are not merely modulators of excitatory activity, but actively participate in learning-dependent changes critical for goal-directed behaviour. For instance, Dupret *et al.* (2013) demonstrated that during the learning of new goal locations, pyramidal cell (PYR) assemblies strengthen their connections to INs that preferentially fire in the context of the new goal map, while weakening connections to those active in the old map. Importantly, this synaptic reorganization was more likely to occur at the rewarded locations, highlighting the spatial specificity of the observed changes (Turi *et al.*, 2019b; Prince *et al.*, 2021).

In a complementary and recent work, Jeong *et al.* (2025) observed a decrease of paravalbumin positive (PV+) CA3 IN activity preceding goal-related PYR increase in activity within the reward zone. This specific dynamic was established rapidly in the new environment and correlated with improved task performance. Further, they demonstrated, by optogenetic manipulations, that PV+ INs suppression in the reward zone is necessary for learning of new goal locations. Interestingly, the decrease in activity observed before the reward was not observed at the salient cue, in another decision making task, where the cue indicated a rewarded corridor. In line with this observation, Turi *et al.* (2019) emphasized that learning-dependent changes in IN firing are only evident during tasks requiring goal-directed learning and not during random foraging, underscoring the dependence of these inhibitory circuit on behavioural contingency. Building on these promising observations, it will be valuable to probe how the strength of PYR-IN monosynaptic connections dynamically evolves during task performance in our dataset. Such analyses could reveal whether CA2-INs help gating the incorporation of

reward information into local ensembles supporting goal-oriented behaviour (Dupret, O'Neill and Csicsvari, 2013; Turi *et al.*, 2019b; Jeong *et al.*, 2025).

Recent works highlighted the importance of maintaining an adequate excitation/inhibition balance in CA2: Boehringer *et al.* (2017) showed that CA2 inhibition increases HPC excitability and destabilize HPC spatial maps. Complementarily, CA2 inhibition was shown to slow down learning (Hitti and Siegelbaum, 2014b). In another form of episodic memory, CA2 impairments in mouse model of schizophrenia induced social memory deficits (Donegan *et al.*, 2020b). Based on these results, one possibility could be that the increased inhibition observed at nose port approach and during reward consumption unlock the necessary mechanisms for spatial map changes in the downstream CA1 region, potentially *via* a disinhibition of CA3 (Boehringer *et al.*, 2017b).

Interestingly, in the same mouse model, deletion syndrome 22q11.2, another study reported impaired goal-oriented remapping (Zaremba *et al.*, 2017b). Importantly, this mouse model was shown to specifically have a decreased PV population in CA2 (Piskorowski *et al.*, 2016).

By extending our current work to include connectivity analyses and incorporating finer behavioural classification (learners *vs* non-learners), we hope to elucidate whether CA2-INs participate in a broader, circuit-level mechanism by which interneurons shape and refine hippocampal maps in support of motivated spatial navigation behaviours.

Furthermore, in another extension of this work, we would like **to identify what are the inputs responsible for CA2-INs activation at reward approach and during reward consumption**. Viral tracing strategies targeting LC, VTA and the SuM as well as a functional characterization of the activity profiles of these inputs in the Clock-maze *via* a fiber photometry approach should provide valuable information to start addressing this question.

Finally, given their sustained and localized activation patterns, CA2-INs could potentially mediate reward-context integration, shaping hippocampal representations of salient behavioural contexts. In summary, these findings open up a novel perspective on CA2 role in memory processing.

5. CA2 in pathology

Interneurons are pivotal in maintaining the excitatory/inhibitory (E/I) balance across brain regions, a balance crucial for proper cognitive functions, including memory. The hippocampal area CA2 is characterized by a high density of interneurons, and its activity is heavily reliant on inhibitory transmission, establishing a finely tuned E/I equilibrium. Disruption of this balance in CA2 has been linked to hippocampal network hyperexcitability and impaired spatial coding precision (Boehringer *et al.*, 2017b; He *et al.*, 2021). Notably, alterations in CA2 inhibitory transmission have been implicated in various neurological and psychiatric disorders as schizophrenia (Piskorowski *et al.*, 2016; Donegan *et al.*, 2020b), Alzheimer disease (Cattaud *et al.*, 2018; Rey *et al.*, 2022a), autism spectrum disorders (Modi *et al.*, 2019) or epilepsy (Whitebirch *et al.*, 2022). The implication of CA2 inhibitory transmission in pathologies has recently been very nicely reviewed in (Piskorowski and Chevaleyre, 2023).

For instance, in the Df(16)A+/− mouse model of the 22q11.2 microdeletion—a genetic risk factor for schizophrenia—there is a significant reduction in PV+ INs density within CA2, but not in CA1 or CA3, leading to decreased feedforward inhibition from CA3 inputs and altered pyramidal neuron excitability (hyperpolarization, due to TREK leak channels over expression)(Piskorowski *et al.*, 2016). These mice exhibit deficits in social memory encoding (Donegan *et al.*, 2020b). Interestingly the same mice used in another study displayed impairments in learning and goal-oriented remapping (Zaremba *et al.*, 2017b). Unfortunately, both of these studies looked solely at PYR activity. It would be very interesting to explore how the modulation of inhibitory transmission in CA2 is impacted in this mouse model *in vivo*, using a task like the Clock-maze task where activity during immobility and reward consumption at specific locations can be characterized. More generally, it would be interesting to study the impact of a perturbation of inhibitory transmission on CA2 on hippocampal spatial coding, given CA2's role in initiating SWRs, notably during wake(Oliva, Fernández-Ruiz, *et al.*, 2016), and the importance of SWR in stabilizing acquired spatial maps (Roux *et al.*, 2017b). I would predict an impairment in spatial cognition following CA2 INs perturbation.

In summary, past findings highlighted the central role of CA2 interneurons in maintaining hippocampal network stability and their involvement in the pathophysiology of numerous disorders. Future research focusing on the modulation of inhibitory transmission within CA2 may offer novel therapeutic possibilities for these conditions.

References

A

Alexander, G.M. *et al.* (2016a) 'Social and novel contexts modify hippocampal CA2 representations of space', *Nature Communications*, 7(1), p. 10300. Available at: https://doi.org/10.1038/ncomms10300.

Alexander, G.M. *et al.* (2016b) 'Social and novel contexts modify hippocampal CA2 representations of space', *Nature Communications*, 7(1), p. 10300. Available at: https://doi.org/10.1038/ncomms10300.

Alvarez, P. and Squire, L.R. (1994) 'Memory consolidation and the medial temporal lobe: a simple network model.', *Proceedings of the National Academy of Sciences*, 91(15), pp. 7041–7045. Available at: https://doi.org/10.1073/pnas.91.15.7041.

Amaral, D.G. and Dent, J.A. (1981) 'Development of the mossy fibers of the dentate gyrus: I. A light and electron microscopic study of the mossy fibers and their expansions', *Journal of Comparative Neurology*, 195(1), pp. 51–86. Available at: https://doi.org/10.1002/cne.901950106.

Amaral, D.G. and Witter, M.P. (1989) 'The three-dimensional organization of the hippocampal formation: A review of anatomical data', *Neuroscience*, 31(3), pp. 571–591. Available at: https://doi.org/10.1016/0306-4522(89)90424-7.

Anderson, M.I. and Jeffery, K.J. (2003) 'Heterogeneous Modulation of Place Cell Firing by Changes in Context', *The Journal of Neuroscience*, 23(26), pp. 8827–8835. Available at: https://doi.org/10.1523/JNEUROSCI.23-26-08827.2003.

Annese, J. *et al.* (2014) 'Postmortem examination of patient H.M.'s brain based on histological sectioning and digital 3D reconstruction', *Nature Communications*, 5(1), p. 3122. Available at: https://doi.org/10.1038/ncomms4122.

Ascoli, G.A. *et al.* (2009) 'Quantitative morphometry of electrophysiologically identified CA3b interneurons reveals robust local geometry and distinct cell classes', *Journal of Comparative Neurology*, 515(6), pp. 677–695. Available at: https://doi.org/10.1002/cne.22082.

Atkinson, R.C. and Shiffrin, R.M. (1968) 'Human Memory: A Proposed System and its Control Processes', in *Psychology of Learning and Motivation*. Elsevier, pp. 89–195. Available at: https://doi.org/10.1016/S0079-7421(08)60422-3.

B

Bach, M.E. *et al.* (1999) 'Age-related defects in spatial memory are correlated with defects in the late phase of hippocampal long-term potentiation *in vitro* and are attenuated by drugs that enhance the cAMP signaling pathway', *Proceedings of the National Academy of Sciences*, 96(9), pp. 5280–5285. Available at: https://doi.org/10.1073/pnas.96.9.5280.

Baddeley, A.D. and Hitch, G. (1974) 'Working Memory', in *Psychology of Learning and Motivation*. Elsevier, pp. 47–89. Available at: https://doi.org/10.1016/S0079-7421(08)60452-1.

Baddeley, A.D. and Warrington, E.K. (1970) 'Amnesia and the distinction between long- and short-term memory', *Journal of Verbal Learning and Verbal Behavior*, 9(2), pp. 176–189. Available at: https://doi.org/10.1016/S0022-5371(70)80048-2.

Baimbridge, K.G. and Miller, J.J. (1982) 'Immunohistochemical localization of calcium-binding protein in the cerebellum, hippocampal formation and olfactory bulb of the rat', *Brain Research*, 245(2), pp. 223–229. Available at: https://doi.org/10.1016/0006-8993(82)90804-6.

Bannister, N.J. and Larkman, A.U. (1995) 'Dendritic morphology of CA1 pyramidal neurones from the rat hippocampus: I. Branching patterns', *Journal of Comparative Neurology*, 360(1), pp. 150–160. Available at: https://doi.org/10.1002/cne.903600111.

Barnstedt, O., Mocellin, P. and Remy, S. (2024) 'A hippocampus-accumbens code guides goal-directed appetitive behavior', *Nature Communications*, 15(1), p. 3196. Available at: https://doi.org/10.1038/s41467-024-47361-x.

Bartesaghi, R. and Gessi, T. (2004) 'Parallel activation of field CA2 and dentate gyrus by synaptically elicited perforant path volleys', *Hippocampus*, 14(8), pp. 948–963. Available at: https://doi.org/10.1002/hipo.20011.

Bartesaghi, R., Migliore, M. and Gessi, T. (2006) 'Input–output relations in the entorhinal cortex–dentate–hippocampal system: Evidence for a non-linear transfer of signals', *Neuroscience*, 142(1), pp. 247–265. Available at: https://doi.org/10.1016/j.neuroscience.2006.06.001.

Basu, J. *et al.* (2013) 'A Cortico-Hippocampal Learning Rule Shapes Inhibitory Microcircuit Activity to Enhance Hippocampal Information Flow', *Neuron*, 79(6), pp. 1208–1221. Available at: https://doi.org/10.1016/j.neuron.2013.07.001.

Beier, K.T. *et al.* (2015) 'Circuit Architecture of VTA Dopamine Neurons Revealed by Systematic Input-Output Mapping', *Cell*, 162(3), pp. 622–634. Available at: https://doi.org/10.1016/j.cell.2015.07.015.

Benes, F.M. *et al.* (2008) 'Circuitry-based gene expression profiles in GABA cells of the trisynaptic pathway in schizophrenics versus bipolars', *Proceedings of the National Academy of Sciences*, 105(52), pp. 20935–20940. Available at: https://doi.org/10.1073/pnas.0810153105.

Benoy, A., Dasgupta, A. and Sajikumar, S. (2018) 'Hippocampal area CA2: an emerging modulatory gateway in the hippocampal circuit', *Experimental Brain Research*, 236(4), pp. 919–931. Available at: https://doi.org/10.1007/s00221-018-5187-5.

Berke, J.D. (2018) 'What does dopamine mean?', *Nature Neuroscience*, 21(6), pp. 787–793. Available at: https://doi.org/10.1038/s41593-018-0152-y.

Bhasin, G. and Nair, I.R. (2022a) 'Dynamic Hippocampal CA2 Responses to Contextual Spatial Novelty', *Frontiers in Systems Neuroscience*, 16, p. 923911. Available at: https://doi.org/10.3389/fnsys.2022.923911.

Bhasin, G. and Nair, I.R. (2022b) 'Dynamic Hippocampal CA2 Responses to Contextual Spatial Novelty', *Frontiers in Systems Neuroscience*, 16, p. 923911. Available at: https://doi.org/10.3389/fnsys.2022.923911.

Bienkowski, M.S. (2023) 'Further refining the boundaries of the hippocampus CA2 with gene expression and connectivity: Potential subregions and heterogeneous cell types', *Hippocampus*, 33(3), pp. 150–160. Available at: https://doi.org/10.1002/hipo.23508.

Boehringer, R. *et al.* (2017a) 'Chronic Loss of CA2 Transmission Leads to Hippocampal Hyperexcitability', *Neuron*, 94(3), pp. 642-655.e9. Available at: https://doi.org/10.1016/j.neuron.2017.04.014.

Boehringer, R. *et al.* (2017b) 'Chronic Loss of CA2 Transmission Leads to Hippocampal Hyperexcitability', *Neuron*, 94(3), pp. 642-655.e9. Available at: https://doi.org/10.1016/j.neuron.2017.04.014.

Bostock, E., Muller, R.U. and Kubie, J.L. (1991) 'Experience-dependent modifications of hippocampal place cell firing', *Hippocampus*, 1(2), pp. 193–205. Available at: https://doi.org/10.1002/hipo.450010207.

Botcher, N.A. *et al.* (2014a) 'Distribution of interneurons in the CA2 region of the rat hippocampus', *Frontiers in Neuroanatomy*, 8. Available at: https://doi.org/10.3389/fnana.2014.00104.

Botcher, N.A. *et al.* (2014b) 'Distribution of interneurons in the CA2 region of the rat hippocampus', *Frontiers in Neuroanatomy*, 8. Available at: https://doi.org/10.3389/fnana.2014.00104.

Boulanger, L. *et al.* (1995) 'Cellular and molecular characterization of a brain-enriched protein tyrosine phosphatase', *The Journal of Neuroscience*, 15(2), pp. 1532–1544. Available at: https://doi.org/10.1523/JNEUROSCI.15-02-01532.1995.

Broussard, J.I. *et al.* (2016) 'Dopamine Regulates Aversive Contextual Learning and Associated In Vivo Synaptic Plasticity in the Hippocampus', *Cell Reports*, 14(8), pp. 1930–1939. Available at: https://doi.org/10.1016/j.celrep.2016.01.070.

Brown, E.N. *et al.* (1998) 'A Statistical Paradigm for Neural Spike Train Decoding Applied to Position Prediction from Ensemble Firing Patterns of Rat Hippocampal Place Cells', *The Journal of Neuroscience*, 18(18), pp. 7411–7425. Available at: https://doi.org/10.1523/JNEUROSCI.18-18-07411.1998.

Buhl, E.H. *et al.* (1996) 'Physiological properties of anatomically identified basket and bistratified cells in the CA1 area of the rat hippocampus in vitro', *Hippocampus*, 6(3), pp. 294–305. Available at: https://doi.org/10.1002/(SICI)1098-1063(1996)6:3<294::AID-HIPO7>3.0.CO;2-N.

Burke, S.N. *et al.* (2011) 'The influence of objects on place field expression and size in distal hippocampal CA1', *Hippocampus*, 21(7), pp. 783–801. Available at: https://doi.org/10.1002/hipo.20929.

Buzsaki, G. (1984) 'Feed-forward inhibition in the hippocampal formation', *Progress in Neurobiology*, 22(2), pp. 131–153. Available at: https://doi.org/10.1016/0301-0082(84)90023-6.

Buzsáki, G. (1989) 'Two-stage model of memory trace formation: A role for "noisy" brain states', *Neuroscience*, 31(3), pp. 551–570. Available at: https://doi.org/10.1016/0306-4522(89)90423-5.

Buzsáki, G. (2002) 'Theta Oscillations in the Hippocampus', *Neuron*, 33(3), pp. 325–340. Available at: https://doi.org/10.1016/S0896-6273(02)00586-X.

Buzsáki, G. (2015a) 'Hippocampal sharp wave-ripple: A cognitive biomarker for episodic memory and planning', *Hippocampus*, 25(10), pp. 1073–1188. Available at: https://doi.org/10.1002/hipo.22488.

Buzsáki, G. (2015b) 'Hippocampal sharp wave-ripple: A cognitive biomarker for episodic memory and planning', *Hippocampus*, 25(10), pp. 1073–1188. Available at: https://doi.org/10.1002/hipo.22488.

Buzsáki, G. and Moser, E.I. (2013) 'Memory, navigation and theta rhythm in the hippocampal-entorhinal system', *Nature Neuroscience*, 16(2), pp. 130–138. Available at: https://doi.org/10.1038/nn.3304.

C

Cacucci, F. *et al.* (2007) 'Experience-Dependent Increase in CA1 Place Cell Spatial Information, But Not Spatial Reproducibility, Is Dependent on the Autophosphorylation of the α-Isoform of the Calcium/Calmodulin-Dependent Protein Kinase II', *The Journal of Neuroscience*, 27(29), pp. 7854–7859. Available at: https://doi.org/10.1523/JNEUROSCI.1704-07.2007.

Cattaud, V. *et al.* (2018) 'Early disruption of parvalbumin expression and perineuronal nets in the hippocampus of the Tg2576 mouse model of Alzheimer's disease can be rescued by enriched environment', *Neurobiology of Aging*, 72, pp. 147–158. Available at: https://doi.org/10.1016/j.neurobiolaging.2018.08.024.

Caviness, V.S. (1973) 'Time of neuron origin in the hippocampus and dentate gyrus of normal and reeler mutant mice: An autoradiographic analysis', *Journal of Comparative Neurology*, 151(2), pp. 113–119. Available at: https://doi.org/10.1002/cne.901510203.

Cembrowski, M.S. *et al.* (2016) 'Hipposeq: a comprehensive RNA-seq database of gene expression in hippocampal principal neurons', *eLife*, 5, p. e14997. Available at: https://doi.org/10.7554/eLife.14997.

Chafai, M. *et al.* (2012) 'Vasopressin Inhibits LTP in the CA2 Mouse Hippocampal Area', *PLoS ONE*. Edited by T. Amédée, 7(12), p. e49708. Available at: https://doi.org/10.1371/journal.pone.0049708.

Chen, S. *et al.* (2020a) 'A hypothalamic novelty signal modulates hippocampal memory', *Nature*, 586(7828), pp. 270–274. Available at: https://doi.org/10.1038/s41586-020-2771-1.

Chen, S. *et al.* (2020b) 'A hypothalamic novelty signal modulates hippocampal memory', *Nature*, 586(7828), pp. 270–274. Available at: https://doi.org/10.1038/s41586-020-2771-1.

Chevaleyre, V. and Piskorowski, R. (2023) 'New hues for CA2', *Hippocampus*, 33(3), pp. 161–165. Available at: https://doi.org/10.1002/hipo.23496.

Chevaleyre, V. and Piskorowski, R.A. (2016) 'Hippocampal Area CA2: An Overlooked but Promising Therapeutic Target', *Trends in Molecular Medicine*, 22(8), pp. 645–655. Available at: https://doi.org/10.1016/j.molmed.2016.06.007.

Chevaleyre, V. and Siegelbaum, S.A. (2010) 'Strong CA2 Pyramidal Neuron Synapses Define a Powerful Disynaptic Cortico-Hippocampal Loop', *Neuron*, 66(4), pp. 560–572. Available at: https://doi.org/10.1016/j.neuron.2010.04.013.

Chiang, M.-C. *et al.* (2018) 'A role for CA3 in social recognition memory', *Behavioural Brain Research*, 354, pp. 22–30. Available at: https://doi.org/10.1016/j.bbr.2018.01.019.

Chockanathan, U. and Padmanabhan, K. (2021) 'Divergence in Population Coding for Space between Dorsal and Ventral CA1', *eNeuro*, 8(5), p. ENEURO.0211-21.2021. Available at: https://doi.org/10.1523/ENEURO.0211-21.2021.

Ciocchi, S. *et al.* (2015) 'Selective information routing by ventral hippocampal CA1 projection neurons', *Science*, 348(6234), pp. 560–563. Available at: https://doi.org/10.1126/science.aaa3245.

Cobb, S.R. *et al.* (1997) 'Synaptic effects of identified interneurons innervating both interneurons and pyramidal cells in the rat hippocampus', *Neuroscience*, 79(3), pp. 629–648. Available at: https://doi.org/10.1016/S0306-4522(97)00055-9.

Cohen, N.J. and Eichenbaum, H. (1994) *Memory, amnesia, and the hippocampal system*. 2. print. Cambridge, Mass.: MIT Press (A Bradford book).

Colgin, L.L. (2013) 'Mechanisms and Functions of Theta Rhythms', *Annual Review of Neuroscience*, 36(1), pp. 295–312. Available at: https://doi.org/10.1146/annurev-neuro-062012-170330.

Csicsvari, J. *et al.* (1999) 'Oscillatory Coupling of Hippocampal Pyramidal Cells and Interneurons in the Behaving Rat', *The Journal of Neuroscience*, 19(1), pp. 274–287. Available at: https://doi.org/10.1523/JNEUROSCI.19-01-00274.1999.

Cui, Z., Gerfen, C.R. and Young, W.S. (2013) 'Hypothalamic and other connections with dorsal CA2 area of the mouse hippocampus', *Journal of Comparative Neurology*, 521(8), pp. 1844–1866. Available at: https://doi.org/10.1002/cne.23263.

D

Danielson, N.B. *et al.* (2016a) 'Distinct Contribution of Adult-Born Hippocampal Granule Cells to Context Encoding', *Neuron*, 90(1), pp. 101–112. Available at: https://doi.org/10.1016/j.neuron.2016.02.019.

Danielson, N.B. *et al.* (2016b) 'Distinct Contribution of Adult-Born Hippocampal Granule Cells to Context Encoding', *Neuron*, 90(1), pp. 101–112. Available at: https://doi.org/10.1016/j.neuron.2016.02.019.

Dasgupta, A. *et al.* (2020) 'Group III metabotropic glutamate receptors gate long-term potentiation and synaptic tagging/capture in rat hippocampal area CA2', *eLife*, 9, p. e55344. Available at: https://doi.org/10.7554/eLife.55344.

De Lavilléon, G. *et al.* (2015) 'Explicit memory creation during sleep demonstrates a causal role of place cells in navigation', *Nature Neuroscience*, 18(4), pp. 493–495. Available at: https://doi.org/10.1038/nn.3970.

DeVito, L.M. *et al.* (2009) 'Vasopressin 1b Receptor Knock-Out Impairs Memory for Temporal Order', *The Journal of Neuroscience*, 29(9), pp. 2676–2683. Available at: https://doi.org/10.1523/JNEUROSCI.5488-08.2009.

Devoto, P. *et al.* (2001) 'Evidence for co-release of noradrenaline and dopamine from noradrenergic neurons in the cerebral cortex', *Molecular Psychiatry*, 6(6), pp. 657–664. Available at: https://doi.org/10.1038/sj.mp.4000904.

Donegan, M.L. *et al.* (2020a) 'Coding of social novelty in the hippocampal CA2 region and its disruption and rescue in a 22q11.2 microdeletion mouse model', *Nature Neuroscience*, 23(11), pp. 1365–1375. Available at: https://doi.org/10.1038/s41593-020-00720-5.

Donegan, M.L. *et al.* (2020b) 'Coding of social novelty in the hippocampal CA2 region and its disruption and rescue in a 22q11.2 microdeletion mouse model', *Nature Neuroscience*, 23(11), pp. 1365–1375. Available at: https://doi.org/10.1038/s41593-020-00720-5.

Dong, H.-W. *et al.* (2009) 'Genomic–anatomic evidence for distinct functional domains in hippocampal field CA1', *Proceedings of the National Academy of Sciences*, 106(28), pp. 11794–11799. Available at: https://doi.org/10.1073/pnas.0812608106.

Dubovyk, V. and Manahan-Vaughan, D. (2019) 'Gradient of Expression of Dopamine D2 Receptors Along the Dorso-Ventral Axis of the Hippocampus', *Frontiers in Synaptic Neuroscience*, 11, p. 28. Available at: https://doi.org/10.3389/fnsyn.2019.00028.

Dudok, B., Klein, P.M., *et al.* (2021) 'Alternating sources of perisomatic inhibition during behavior', *Neuron*, 109(6), pp. 997-1012.e9. Available at: https://doi.org/10.1016/j.neuron.2021.01.003.

Dudok, B., Szoboszlay, M., *et al.* (2021) 'Recruitment and inhibitory action of hippocampal axo-axonic cells during behavior', *Neuron*, 109(23), pp. 3838-3850.e8. Available at: https://doi.org/10.1016/j.neuron.2021.09.033.

Dupret, D. *et al.* (2010a) 'The reorganization and reactivation of hippocampal maps predict spatial memory performance', *Nature Neuroscience*, 13(8), pp. 995–1002. Available at: https://doi.org/10.1038/nn.2599.

Dupret, D. *et al.* (2010b) 'The reorganization and reactivation of hippocampal maps predict spatial memory performance', *Nature Neuroscience*, 13(8), pp. 995–1002. Available at: https://doi.org/10.1038/nn.2599.

Dupret, D., O'Neill, J. and Csicsvari, J. (2013) 'Dynamic Reconfiguration of Hippocampal Interneuron Circuits during Spatial Learning', *Neuron*, 78(1), pp. 166–180. Available at: https://doi.org/10.1016/j.neuron.2013.01.033.

Duszkiewicz, A.J. *et al.* (2019) 'Novelty and Dopaminergic Modulation of Memory Persistence: A Tale of Two Systems', *Trends in Neurosciences*, 42(2), pp. 102–114. Available at: https://doi.org/10.1016/j.tins.2018.10.002.

Duvelle, É. *et al.* (2019) 'Insensitivity of place cells to the value of spatial goals in a two-choice flexible navigation task', *The Journal of Neuroscience*, pp. 1578–18. Available at: https://doi.org/10.1523/JNEUROSCI.1578-18.2018.

E

Edelmann, E. and Lessmann, V. (2018) 'Dopaminergic innervation and modulation of hippocampal networks', *Cell and Tissue Research*, 373(3), pp. 711–727. Available at: https://doi.org/10.1007/s00441-018-2800-7.

Ego-Stengel, V. and Wilson, M.A. (2007a) 'Spatial selectivity and theta phase precession in CA1 interneurons', *Hippocampus*, 17(2), pp. 161–174. Available at: https://doi.org/10.1002/hipo.20253.

Ego-Stengel, V. and Wilson, M.A. (2007b) 'Spatial selectivity and theta phase precession in CA1 interneurons', *Hippocampus*, 17(2), pp. 161–174. Available at: https://doi.org/10.1002/hipo.20253.

El-Ghundi, M. *et al.* (1999) 'Spatial learning deficit in dopamine D1 receptor knockout mice', *European Journal of Pharmacology*, 383(2), pp. 95–106. Available at: https://doi.org/10.1016/S0014-2999(99)00573-7.

F

Fanselow, M.S. and Dong, H.-W. (2010) 'Are the Dorsal and Ventral Hippocampus Functionally Distinct Structures?', *Neuron*, 65(1), pp. 7–19. Available at: https://doi.org/10.1016/j.neuron.2009.11.031.

Fernandez-Lamo, I. *et al.* (2019) 'Proximodistal Organization of the CA2 Hippocampal Area', *Cell Reports*, 26(7), pp. 1734-1746.e6. Available at: https://doi.org/10.1016/j.celrep.2019.01.060.

Fernández-Ruiz, A. *et al.* (2019) 'Long-duration hippocampal sharp wave ripples improve memory', *Science*, 364(6445), pp. 1082–1086. Available at: https://doi.org/10.1126/science.aax0758.

Frank, L.M., Stanley, G.B. and Brown, E.N. (2004) 'Hippocampal Plasticity across Multiple Days of Exposure to Novel Environments', *The Journal of Neuroscience*, 24(35), pp. 7681–7689. Available at: https://doi.org/10.1523/JNEUROSCI.1958-04.2004.

Freund, T.F. and Buzsáki, G. (1998) 'Interneurons of the hippocampus', *Hippocampus*, 6(4), pp. 347–470. Available at: https://doi.org/10.1002/(SICI)1098-1063(1996)6:4<347::AID-HIPO1>3.0.CO;2-I.

Fuentealba, P. *et al.* (2008) 'Ivy Cells: A Population of Nitric-Oxide-Producing, Slow-Spiking GABAergic Neurons and Their Involvement in Hippocampal Network Activity', *Neuron*, 57(6), pp. 917–929. Available at: https://doi.org/10.1016/j.neuron.2008.01.034.

Fukaya, M. *et al.* (2005) 'Spatial diversity in gene expression for VDCCγ subunit family in developing and adult mouse brains', *Neuroscience Research*, 53(4), pp. 376–383. Available at: https://doi.org/10.1016/j.neures.2005.08.009.

Fyhn, M. *et al.* (2007) 'Hippocampal remapping and grid realignment in entorhinal cortex', *Nature*, 446(7132), pp. 190–194. Available at: https://doi.org/10.1038/nature05601.

G

Gangarossa, G. *et al.* (2012) 'Characterization of dopamine D1 and D2 receptor-expressing neurons in the mouse hippocampus', *Hippocampus*, 22(12), pp. 2199–2207. Available at: https://doi.org/10.1002/hipo.22044.

Gasbarri, A., Sulli, A. and Packard, M.G. (1997) 'The dopaminergic mesencephalic projections to the hippocampal formation in the rat', *Progress in Neuro-Psychopharmacology and Biological Psychiatry*, 21(1), pp. 1–22. Available at: https://doi.org/10.1016/S0278-5846(96)00157-1.

Gauthier, J.L. and Tank, D.W. (2018) 'A Dedicated Population for Reward Coding in the Hippocampus', *Neuron*, 99(1), pp. 179-193.e7. Available at: https://doi.org/10.1016/j.neuron.2018.06.008.

Geiller, T. *et al.* (2020a) 'Large-Scale 3D Two-Photon Imaging of Molecularly Identified CA1 Interneuron Dynamics in Behaving Mice', *Neuron*, 108(5), pp. 968-983.e9. Available at: https://doi.org/10.1016/j.neuron.2020.09.013.

Geiller, T. *et al.* (2020b) 'Large-Scale 3D Two-Photon Imaging of Molecularly Identified CA1 Interneuron Dynamics in Behaving Mice', *Neuron*, 108(5), pp. 968-983.e9. Available at: https://doi.org/10.1016/j.neuron.2020.09.013.

Geiller, T. *et al.* (2022) 'Local circuit amplification of spatial selectivity in the hippocampus', *Nature*, 601(7891), pp. 105–109. Available at: https://doi.org/10.1038/s41586-021-04169-9.

Girardeau, G. *et al.* (2009) 'Selective suppression of hippocampal ripples impairs spatial memory', *Nature Neuroscience*, 12(10), pp. 1222–1223. Available at: https://doi.org/10.1038/nn.2384.

Gómez-Pinilla, F., Lee, J.W.-K. and Cotman, C.W. (1994) 'Distribution of basic fibroblast growth factor in the developing rat brain', *Neuroscience*, 61(4), pp. 911–923. Available at: https://doi.org/10.1016/0306-4522(94)90412-X.

Granado, N. *et al.* (2008) 'D1 but not D5 Dopamine Receptors Are Critical for LTP, Spatial Learning, and LTP-Induced arc and zif268 Expression in the Hippocampus', *Cerebral Cortex*, 18(1), pp. 1–12. Available at: https://doi.org/10.1093/cercor/bhm026.

Gupta, A.S. *et al.* (2012) 'Segmentation of spatial experience by hippocampal theta sequences', *Nature Neuroscience*, 15(7), pp. 1032–1039. Available at: https://doi.org/10.1038/nn.3138.

H

Haglund, L., Swanson, L.W. and Köhler, C. (1984) 'The projection of the supramammillary nucleus to the hippocampal formation: An immunohistochemical and anterograde transport study with the lectin PHA-L in the rat', *Journal of Comparative Neurology*, 229(2), pp. 171–185. Available at: https://doi.org/10.1002/cne.902290204.

Han, Z.-S. (1994) 'Electrophysiological and morphological differentiation of chandelier and basket cells in the rat hippocampal formation: a study combining intracellular recording and intracellular staining with biocytin', *Neuroscience Research*, 19(1), pp. 101–110. Available at: https://doi.org/10.1016/0168-0102(94)90013-2.

Hassan, S.I., Bigler, S. and Siegelbaum, S.A. (2023) 'Social odor discrimination and its enhancement by associative learning in the hippocampal CA2 region', *Neuron*, 111(14), pp. 2232-2246.e5. Available at: https://doi.org/10.1016/j.neuron.2023.04.026.

Hayashi, Y., Sawa, A. and Hikida, T. (2016) 'Impaired hippocampal activity at the goal zone on the place preference task in a DISC1 mouse model', *Neuroscience Research*, 106, pp. 70–73. Available at: https://doi.org/10.1016/j.neures.2015.10.005.

He, H. *et al.* (2021) 'CA2 inhibition reduces the precision of hippocampal assembly reactivation', *Neuron*, 109(22), pp. 3674-3687.e7. Available at: https://doi.org/10.1016/j.neuron.2021.08.034.

Helton, T.D. *et al.* (2019) 'Diversity of dendritic morphology and entorhinal cortex synaptic effectiveness in mouse CA2 pyramidal neurons', *Hippocampus*, 29(2), pp. 78–92. Available at: https://doi.org/10.1002/hipo.23012.

Henke, P.G. (1990) 'Hippocampal pathway to the amygdala and stress ulcer development', *Brain Research Bulletin*, 25(5), pp. 691–695. Available at: https://doi.org/10.1016/0361-9230(90)90044-Z.

Henriksen, E.J. *et al.* (2010) 'Spatial Representation along the Proximodistal Axis of CA1', *Neuron*, 68(1), pp. 127–137. Available at: https://doi.org/10.1016/j.neuron.2010.08.042.

Hill, A.J. (1978) 'First occurrence of hippocampal spatial firing in a new environment', *Experimental Neurology*, 62(2), pp. 282–297. Available at: https://doi.org/10.1016/0014-4886(78)90058-4.

Hitti, F.L. and Siegelbaum, S.A. (2014a) 'The hippocampal CA2 region is essential for social memory', *Nature*, 508(7494), pp. 88–92. Available at: https://doi.org/10.1038/nature13028.

Hitti, F.L. and Siegelbaum, S.A. (2014b) 'The hippocampal CA2 region is essential for social memory', *Nature*, 508(7494), pp. 88–92. Available at: https://doi.org/10.1038/nature13028.

Hok, V. *et al.* (2007) 'Goal-Related Activity in Hippocampal Place Cells', *The Journal of Neuroscience*, 27(3), pp. 472–482. Available at: https://doi.org/10.1523/JNEUROSCI.2864-06.2007.

Hollup, S.A. *et al.* (2001a) 'Accumulation of Hippocampal Place Fields at the Goal Location in an Annular Watermaze Task', *The Journal of Neuroscience*, 21(5), pp. 1635–1644. Available at: https://doi.org/10.1523/JNEUROSCI.21-05-01635.2001.

Hollup, S.A. *et al.* (2001b) 'Accumulation of Hippocampal Place Fields at the Goal Location in an Annular Watermaze Task', *The Journal of Neuroscience*, 21(5), pp. 1635–1644. Available at: https://doi.org/10.1523/JNEUROSCI.21-05-01635.2001.

I

Igarashi, K.M. *et al.* (2014) 'Coordination of entorhinal–hippocampal ensemble activity during associative learning', *Nature*, 510(7503), pp. 143–147. Available at: https://doi.org/10.1038/nature13162.

Ishizuka, N., Cowan, W.M. and Amaral, D.G. (1995) 'A quantitative analysis of the dendritic organization of pyramidal cells in the rat hippocampus', *Journal of Comparative Neurology*, 362(1), pp. 17–45. Available at: https://doi.org/10.1002/cne.903620103.

J

Jarzebowski, P. *et al.* (2021) 'Impaired spatial learning and suppression of sharp wave ripples by cholinergic activation at the goal location', *eLife*, 10, p. e65998. Available at: https://doi.org/10.7554/eLife.65998.

Jarzebowski, P. *et al.* (2022a) 'Different encoding of reward location in dorsal and intermediate hippocampus', *Current Biology*, 32(4), pp. 834-841.e5. Available at: https://doi.org/10.1016/j.cub.2021.12.024.

Jarzebowski, P. *et al.* (2022b) 'Different encoding of reward location in dorsal and intermediate hippocampus', *Current Biology*, 32(4), pp. 834-841.e5. Available at: https://doi.org/10.1016/j.cub.2021.12.024.

Jeffery, K.J. *et al.* (2003) 'Preserved performance in a hippocampal-dependent spatial task despite complete place cell remapping', *Hippocampus*, 13(2), pp. 175–189. Available at: https://doi.org/10.1002/hipo.10047.

Jeong, N. *et al.* (2025) 'Goal-specific hippocampal inhibition gates learning', *Nature* [Preprint]. Available at: https://doi.org/10.1038/s41586-025-08868-5.

Jones, M.W. and McHugh, T.J. (2011) 'Updating hippocampal representations: CA2 joins the circuit', *Trends in Neurosciences*, 34(10), pp. 526–535. Available at: https://doi.org/10.1016/j.tins.2011.07.007.

Jung, M.W. and McNaughton, B.L. (1993) 'Spatial selectivity of unit activity in the hippocampal granular layer', *Hippocampus*, 3(2), pp. 165–182. Available at: https://doi.org/10.1002/hipo.450030209.

K

Karaba, L.A. *et al.* (2024a) 'A hippocampal circuit mechanism to balance memory reactivation during sleep', *Science*, 385(6710), pp. 738–743. Available at: https://doi.org/10.1126/science.ado5708.

Karaba, L.A. *et al.* (2024b) 'A hippocampal circuit mechanism to balance memory reactivation during sleep', *Science*, 385(6710), pp. 738–743. Available at: https://doi.org/10.1126/science.ado5708.

Kaufman, A.M., Geiller, T. and Losonczy, A. (2020a) 'A Role for the Locus Coeruleus in Hippocampal CA1 Place Cell Reorganization during Spatial Reward Learning', *Neuron*, 105(6), pp. 1018-1026.e4. Available at: https://doi.org/10.1016/j.neuron.2019.12.029.

Kaufman, A.M., Geiller, T. and Losonczy, A. (2020b) 'A Role for the Locus Coeruleus in Hippocampal CA1 Place Cell Reorganization during Spatial Reward Learning', *Neuron*, 105(6), pp. 1018-1026.e4. Available at: https://doi.org/10.1016/j.neuron.2019.12.029.

Kay, K. *et al.* (2016) 'A hippocampal network for spatial coding during immobility and sleep', *Nature*, 531(7593), pp. 185–190. Available at: https://doi.org/10.1038/nature17144.

Kempadoo, K.A. *et al.* (2016) 'Dopamine release from the locus coeruleus to the dorsal hippocampus promotes spatial learning and memory', *Proceedings of the National Academy of Sciences*, 113(51), pp. 14835–14840. Available at: https://doi.org/10.1073/pnas.1616515114.

Kentros, C.G. *et al.* (2004a) 'Increased Attention to Spatial Context Increases Both Place Field Stability and Spatial Memory', *Neuron*, 42(2), pp. 283–295. Available at: https://doi.org/10.1016/S0896-6273(04)00192-8.

Kentros, C.G. *et al.* (2004b) 'Increased Attention to Spatial Context Increases Both Place Field Stability and Spatial Memory', *Neuron*, 42(2), pp. 283–295. Available at: https://doi.org/10.1016/S0896-6273(04)00192-8.

Kern, A. *et al.* (2015) 'Hippocampal Dopamine/DRD1 Signaling Dependent on the Ghrelin Receptor', *Cell*, 163(5), pp. 1176–1190. Available at: https://doi.org/10.1016/j.cell.2015.10.062.

Kim, S.M. and Frank, L.M. (2009) 'Hippocampal Lesions Impair Rapid Learning of a Continuous Spatial Alternation Task', *PLoS ONE*. Edited by H. Tanimoto, 4(5), p. e5494. Available at: https://doi.org/10.1371/journal.pone.0005494.

Klausberger, T. (2009) 'GABAergic interneurons targeting dendrites of pyramidal cells in the CA1 area of the hippocampus', *European Journal of Neuroscience*, 30(6), pp. 947–957. Available at: https://doi.org/10.1111/j.1460-9568.2009.06913.x.

Klausberger, T. and Somogyi, P. (2008) 'Neuronal Diversity and Temporal Dynamics: The Unity of Hippocampal Circuit Operations', *Science*, 321(5885), pp. 53–57. Available at: https://doi.org/10.1126/science.1149381.

Kobayashi, T. *et al.* (1997) 'Task-Dependent Representations in Rat Hippocampal Place Neurons', *Journal of Neurophysiology*, 78(2), pp. 597–613. Available at: https://doi.org/10.1152/jn.1997.78.2.597.

Kobayashi, T. *et al.* (2003) 'Contribution of hippocampal place cell activity to learning and formation of goal-directed navigation in rats', *Neuroscience*, 117(4), pp. 1025–1035. Available at: https://doi.org/10.1016/S0306-4522(02)00700-5.

Kohara, K. *et al.* (2014a) 'Cell type–specific genetic and optogenetic tools reveal hippocampal CA2 circuits', *Nature Neuroscience*, 17(2), pp. 269–279. Available at: https://doi.org/10.1038/nn.3614.

Kohara, K. *et al.* (2014b) 'Cell type–specific genetic and optogenetic tools reveal hippocampal CA2 circuits', *Nature Neuroscience*, 17(2), pp. 269–279. Available at: https://doi.org/10.1038/nn.3614.

Kramis, R., Vanderwolf, C.H. and Bland, B.H. (1975) 'Two types of hippocampal rhythmical slow activity in both the rabbit and the rat: Relations to behavior and effects of atropine, diethyl ether, urethane, and pentobarbital', *Experimental Neurology*, 49(1), pp. 58–85. Available at: https://doi.org/10.1016/0014-4886(75)90195-8.

Krishnan, S. *et al.* (2022) 'Reward expectation extinction restructures and degrades CA1 spatial maps through loss of a dopaminergic reward proximity signal', *Nature Communications*, 13(1), p. 6662. Available at: https://doi.org/10.1038/s41467-022-34465-5.

L

Laham, B.J. *et al.* (2024) 'Adult-born granule cells modulate CA2 network activity during retrieval of developmental memories of the mother', *eLife*, 12, p. RP90600. Available at: https://doi.org/10.7554/eLife.90600.

Lee, H. *et al.* (2015) 'Neural Population Evidence of Functional Heterogeneity along the CA3 Transverse Axis: Pattern Completion versus Pattern Separation', *Neuron*, 87(5), pp. 1093–1105. Available at: https://doi.org/10.1016/j.neuron.2015.07.012.

Lee, J.S. *et al.* (2020) 'The Statistical Structure of the Hippocampal Code for Space as a Function of Time, Context, and Value', *Cell*, 183(3), pp. 620-635.e22. Available at: https://doi.org/10.1016/j.cell.2020.09.024.

Lee, S.E. *et al.* (2010) 'RGS14 is a natural suppressor of both synaptic plasticity in CA2 neurons and hippocampal-based learning and memory', *Proceedings of the National Academy of Sciences*, 107(39), pp. 16994–16998. Available at: https://doi.org/10.1073/pnas.1005362107.

Lee, S.-H. *et al.* (2014) 'Parvalbumin-Positive Basket Cells Differentiate among Hippocampal Pyramidal Cells', *Neuron*, 82(5), pp. 1129–1144. Available at: https://doi.org/10.1016/j.neuron.2014.03.034.

Lehr, A.B. *et al.* (2021) 'CA2 beyond social memory: Evidence for a fundamental role in hippocampal information processing', *Neuroscience & Biobehavioral Reviews*, 126, pp. 398–412. Available at: https://doi.org/10.1016/j.neubiorev.2021.03.020.

Lehr, A.B. *et al.* (2023) 'Silencing hippocampal CA2 reduces behavioral flexibility in spatial learning', *Hippocampus*, 33(6), pp. 759–768. Available at: https://doi.org/10.1002/hipo.23521.

Lein, E.S. *et al.* (2005) 'Redefining the boundaries of the hippocampal CA2 subfield in the mouse using gene expression and 3-dimensional reconstruction', *Journal of Comparative Neurology*, 485(1), pp. 1–10. Available at: https://doi.org/10.1002/cne.20426.

Lein, E.S., Zhao, X. and Gage, F.H. (2004) 'Defining a Molecular Atlas of the Hippocampus Using DNA Microarrays and High-Throughput *In Situ* Hybridization', *The Journal of Neuroscience*, 24(15), pp. 3879–3889. Available at: https://doi.org/10.1523/JNEUROSCI.4710-03.2004.

Lemon, N. *et al.* (2009) 'Locus Coeruleus Activation Facilitates Memory Encoding and Induces Hippocampal LTD that Depends on -Adrenergic Receptor Activation', *Cerebral Cortex*, 19(12), pp. 2827–2837. Available at: https://doi.org/10.1093/cercor/bhp065.

Leranth, C. and Ribak, C.E. (1991) 'Calcium-binding proteins are concentrated in the CA2 field of the monkey hippocampus: a possible key to this region's resistance to epileptic damage', *Experimental Brain Research*, 85(1). Available at: https://doi.org/10.1007/BF00229993.

Leroy, F. *et al.* (2017) 'Input-Timing-Dependent Plasticity in the Hippocampal CA2 Region and Its Potential Role in Social Memory', *Neuron*, 95(5), pp. 1089-1102.e5. Available at: https://doi.org/10.1016/j.neuron.2017.07.036.

Leroy, F. *et al.* (2018) 'A circuit from hippocampal CA2 to lateral septum disinhibits social aggression', *Nature*, 564(7735), pp. 213–218. Available at: https://doi.org/10.1038/s41586-018-0772-0.

Leutgeb, J.K. *et al.* (2005) 'Progressive Transformation of Hippocampal Neuronal Representations in "Morphed" Environments', *Neuron*, 48(2), pp. 345–358. Available at: https://doi.org/10.1016/j.neuron.2005.09.007.

Leutgeb, J.K. *et al.* (2007) 'Pattern Separation in the Dentate Gyrus and CA3 of the Hippocampus', *Science*, 315(5814), pp. 961–966. Available at: https://doi.org/10.1126/science.1135801.

Li, X. -G. *et al.* (1994) 'The hippocampal CA3 network: An in vivo intracellular labeling study', *Journal of Comparative Neurology*, 339(2), pp. 181–208. Available at: https://doi.org/10.1002/cne.903390204.

Llorens-Martín, M. *et al.* (2015) 'Novel connection between newborn granule neurons and the hippocampal CA2 field', *Experimental Neurology*, 263, pp. 285–292. Available at: https://doi.org/10.1016/j.expneurol.2014.10.021.

Loisy, M. *et al.* (2022) 'Sequential inhibitory plasticities in hippocampal area CA2 and social memory formation', *Neuron*, 110(17), pp. 2854-2866.e4. Available at: https://doi.org/10.1016/j.neuron.2022.06.013.

Lopez-Rojas, J. *et al.* (2022) 'A direct lateral entorhinal cortex to hippocampal CA2 circuit conveys social information required for social memory', *Neuron*, 110(9), pp. 1559-1572.e4. Available at: https://doi.org/10.1016/j.neuron.2022.01.028.

Lorente De Nó, R. (1934) 'Studies on the structure of the cerebral cortex. II. Continuation of the study of the ammonic system.', *Journal für Psychologie und Neurologie*, 46, pp. 113–177.

Lovett-Barron, M. *et al.* (2012) 'Regulation of neuronal input transformations by tunable dendritic inhibition', *Nature Neuroscience*, 15(3), pp. 423–430. Available at: https://doi.org/10.1038/nn.3024.

Lu, L. *et al.* (2015a) 'Topography of Place Maps along the CA3-to-CA2 Axis of the Hippocampus', *Neuron*, 87(5), pp. 1078–1092. Available at: https://doi.org/10.1016/j.neuron.2015.07.007.

Lu, L. *et al.* (2015b) 'Topography of Place Maps along the CA3-to-CA2 Axis of the Hippocampus', *Neuron*, 87(5), pp. 1078–1092. Available at: https://doi.org/10.1016/j.neuron.2015.07.007.

M

MacDonald, C.J. and Tonegawa, S. (2021) 'Crucial role for CA2 inputs in the sequential organization of CA1 time cells supporting memory', *Proceedings of the National Academy of Sciences*, 118(3), p. e2020698118. Available at: https://doi.org/10.1073/pnas.2020698118.

Maglóczky, Z., Acsády, L. and Freund, T.F. (1994) 'Principal cells are the postsynaptic targets of supramammillary afferents in the hippocampus of the rat', *Hippocampus*, 4(3), pp. 322–334. Available at: https://doi.org/10.1002/hipo.450040316.

Mamad, O. *et al.* (2017a) 'Place field assembly distribution encodes preferred locations', *PLOS Biology*. Edited by J. Csicsvari, 15(9), p. e2002365. Available at: https://doi.org/10.1371/journal.pbio.2002365.

Mamad, O. *et al.* (2017b) 'Place field assembly distribution encodes preferred locations', *PLOS Biology*. Edited by J. Csicsvari, 15(9), p. e2002365. Available at: https://doi.org/10.1371/journal.pbio.2002365.

Mankin, E.A. *et al.* (2012) 'Neuronal code for extended time in the hippocampus', *Proceedings of the National Academy of Sciences*, 109(47), pp. 19462–19467. Available at: https://doi.org/10.1073/pnas.1214107109.

Mankin, E.A. *et al.* (2015a) 'Hippocampal CA2 Activity Patterns Change over Time to a Larger Extent than between Spatial Contexts', *Neuron*, 85(1), pp. 190–201. Available at: https://doi.org/10.1016/j.neuron.2014.12.001.

Mankin, E.A. *et al.* (2015b) 'Hippocampal CA2 Activity Patterns Change over Time to a Larger Extent than between Spatial Contexts', *Neuron*, 85(1), pp. 190–201. Available at: https://doi.org/10.1016/j.neuron.2014.12.001.

Markram, H. *et al.* (1997) 'Regulation of Synaptic Efficacy by Coincidence of Postsynaptic APs and EPSPs', *Science*, 275(5297), pp. 213–215. Available at: https://doi.org/10.1126/science.275.5297.213.

Marshall, L. *et al.* (2002a) 'Hippocampal Pyramidal Cell–Interneuron Spike Transmission Is Frequency Dependent and Responsible for Place Modulation of Interneuron Discharge', *The Journal of Neuroscience*, 22(2), pp. RC197–RC197. Available at: https://doi.org/10.1523/JNEUROSCI.22-02-j0001.2002.

Marshall, L. *et al.* (2002b) 'Hippocampal Pyramidal Cell–Interneuron Spike Transmission Is Frequency Dependent and Responsible for Place Modulation of Interneuron Discharge', *The Journal of Neuroscience*, 22(2), pp. RC197–RC197. Available at: https://doi.org/10.1523/JNEUROSCI.22-02-j0001.2002.

Masurkar, A.V. *et al.* (2017) 'Medial and Lateral Entorhinal Cortex Differentially Excite Deep versus Superficial CA1 Pyramidal Neurons', *Cell Reports*, 18(1), pp. 148–160. Available at: https://doi.org/10.1016/j.celrep.2016.12.012.

Maurer, A.P. *et al.* (2006a) 'Phase precession in hippocampal interneurons showing strong functional coupling to individual pyramidal cells', *The Journal of Neuroscience: The Official Journal of the Society for Neuroscience*, 26(52), pp. 13485–13492. Available at: https://doi.org/10.1523/JNEUROSCI.2882-06.2006.

Maurer, A.P. *et al.* (2006b) 'Phase precession in hippocampal interneurons showing strong functional coupling to individual pyramidal cells', *The Journal of Neuroscience: The Official Journal of the Society for Neuroscience*, 26(52), pp. 13485–13492. Available at: https://doi.org/10.1523/JNEUROSCI.2882-06.2006.

McNamara, C.G. *et al.* (2014) 'Dopaminergic neurons promote hippocampal reactivation and spatial memory persistence', *Nature Neuroscience*, 17(12), pp. 1658–1660. Available at: https://doi.org/10.1038/nn.3843.

Meira, T. *et al.* (2018) 'A hippocampal circuit linking dorsal CA2 to ventral CA1 critical for social memory dynamics', *Nature Communications*, 9(1), p. 4163. Available at: https://doi.org/10.1038/s41467-018-06501-w.

Mercer, A., Eastlake, K., *et al.* (2012) 'Local circuitry involving parvalbumin-positive basket cells in the CA2 region of the hippocampus', *Hippocampus*, 22(1), pp. 43–56. Available at: https://doi.org/10.1002/hipo.20841.

Mercer, A., Botcher, N.A., *et al.* (2012) 'SP–SR interneurones: A novel class of neurones of the CA2 region of the hippocampus', *Hippocampus*, 22(8), pp. 1758–1769. Available at: https://doi.org/10.1002/hipo.22010.

Miles, R. (1990) 'Synaptic excitation of inhibitory cells by single CA3 hippocampal pyramidal cells of the guinea-pig in vitro.', *The Journal of Physiology*, 428(1), pp. 61–77. Available at: https://doi.org/10.1113/jphysiol.1990.sp018200.

Milner, B., Corkin, S. and Teuber, H.-L. (1968) 'Further analysis of the hippocampal amnesic syndrome: 14-year follow-up study of H.M.', *Neuropsychologia*, 6(3), pp. 215–234. Available at: https://doi.org/10.1016/0028-3932(68)90021-3.

Milner, B., Squire, L.R. and Kandel, E.R. (1998) 'Cognitive Neuroscience and the Study of Memory', *Neuron*, 20(3), pp. 445–468. Available at: https://doi.org/10.1016/S0896-6273(00)80987-3.

Mizuseki, K. *et al.* (2009) 'Theta Oscillations Provide Temporal Windows for Local Circuit Computation in the Entorhinal-Hippocampal Loop', *Neuron*, 64(2), pp. 267–280. Available at: https://doi.org/10.1016/j.neuron.2009.08.037.

Mizuseki, K. *et al.* (2011) 'Hippocampal CA1 pyramidal cells form functionally distinct sublayers', *Nature Neuroscience*, 14(9), pp. 1174–1181. Available at: https://doi.org/10.1038/nn.2894.

Mizuta, K. *et al.* (2021a) 'Multiple coordinated cellular dynamics mediate CA1 map plasticity', *Hippocampus*, 31(3), pp. 235–243. Available at: https://doi.org/10.1002/hipo.23300.

Mizuta, K. *et al.* (2021b) 'Multiple coordinated cellular dynamics mediate CA1 map plasticity', *Hippocampus*, 31(3), pp. 235–243. Available at: https://doi.org/10.1002/hipo.23300.

Modi, B. *et al.* (2019) 'Possible Implication of the CA2 Hippocampal Circuit in Social Cognition Deficits Observed in the Neuroligin 3 Knock-Out Mouse, a Non-Syndromic Animal Model of Autism', *Frontiers in Psychiatry*, 10, p. 513. Available at: https://doi.org/10.3389/fpsyt.2019.00513.

Montague, P., Dayan, P. and Sejnowski, T. (1996) 'A framework for mesencephalic dopamine systems based on predictive Hebbian learning', *The Journal of Neuroscience*, 16(5), pp. 1936–1947. Available at: https://doi.org/10.1523/JNEUROSCI.16-05-01936.1996.

Morris, R.G.M. *et al.* (1982) 'Place navigation impaired in rats with hippocampal lesions', *Nature*, 297(5868), pp. 681–683. Available at: https://doi.org/10.1038/297681a0.

Moser, M.B. *et al.* (1995) 'Spatial learning with a minislab in the dorsal hippocampus.', *Proceedings of the National Academy of Sciences*, 92(21), pp. 9697–9701. Available at: https://doi.org/10.1073/pnas.92.21.9697.

Moser, M.-B. and Moser, E.I. (1998) 'Functional differentiation in the hippocampus', *Hippocampus*, 8(6), pp. 608–619. Available at: https://doi.org/10.1002/(SICI)1098-1063(1998)8:6<608::AID-HIPO3>3.0.CO;2-7.

Muller, R. and Kubie, J. (1987) 'The effects of changes in the environment on the spatial firing of hippocampal complex-spike cells', *The Journal of Neuroscience*, 7(7), pp. 1951–1968. Available at: https://doi.org/10.1523/JNEUROSCI.07-07-01951.1987.

Muzzio, I.A. *et al.* (2009) 'Attention Enhances the Retrieval and Stability of Visuospatial and Olfactory Representations in the Dorsal Hippocampus', *PLoS Biology*. Edited by L. Ungerleider, 7(6), p. e1000140. Available at: https://doi.org/10.1371/journal.pbio.1000140.

N

Naber, P.A., Lopes Da Silva, F.H. and Witter, M.P. (2001) 'Reciprocal connections between the entorhinal cortex and hippocampal fields CA1 and the subiculum are in register with the projections from CA1 to the subiculum', *Hippocampus*, 11(2), pp. 99–104. Available at: https://doi.org/10.1002/hipo.1028.

Nadel, L. and Moscovitch, M. (1997) 'Memory consolidation, retrograde amnesia and the hippocampal complex', *Current Opinion in Neurobiology*, 7(2), pp. 217–227. Available at: https://doi.org/10.1016/S0959-4388(97)80010-4.

Nakamura, N.H. *et al.* (2013) 'Proximodistal Segregation of Nonspatial Information in CA3: Preferential Recruitment of a Proximal CA3-Distal CA1 Network in Nonspatial Recognition Memory', *Journal of Neuroscience*, 33(28), pp. 11506–11514. Available at: https://doi.org/10.1523/JNEUROSCI.4480-12.2013.

Nasrallah, K. *et al.* (2019) 'Routing Hippocampal Information Flow through Parvalbumin Interneuron Plasticity in Area CA2', *Cell Reports*, 27(1), pp. 86-98.e3. Available at: https://doi.org/10.1016/j.celrep.2019.03.014.

Nasrallah, K., Piskorowski, R.A. and Chevaleyre, V. (2015a) 'Inhibitory Plasticity Permits the Recruitment of CA2 Pyramidal Neurons by CA3', *eneuro*, 2(4), p. ENEURO.0049-15.2015. Available at: https://doi.org/10.1523/ENEURO.0049-15.2015.

Nasrallah, K., Piskorowski, R.A. and Chevaleyre, V. (2015b) 'Inhibitory Plasticity Permits the Recruitment of CA2 Pyramidal Neurons by CA3', *eneuro*, 2(4), p. ENEURO.0049-15.2015. Available at: https://doi.org/10.1523/ENEURO.0049-15.2015.

Nasrallah, K., Piskorowski, R.A. and Chevaleyre, V. (2017) 'Bi-directional interplay between proximal and distal inputs to CA2 pyramidal neurons', *Neurobiology of Learning and Memory*, 138, pp. 173–181. Available at: https://doi.org/10.1016/j.nlm.2016.06.024.

Nguyen, C.L. *et al.* (2014) 'Hippocampal place cell responses to distal and proximal cue manipulations in dopamine D2 receptor-knockout mice', *Brain Research*, 1567, pp. 13–27. Available at: https://doi.org/10.1016/j.brainres.2014.04.023.

Ntamati, N.R. and Lüscher, C. (2016) 'VTA Projection Neurons Releasing GABA and Glutamate in the Dentate Gyrus', *eneuro*, 3(4), p. ENEURO.0137-16.2016. Available at: https://doi.org/10.1523/ENEURO.0137-16.2016.

Nyberg, N. *et al.* (2022) 'Spatial goal coding in the hippocampal formation', *Neuron*, 110(3), pp. 394–422. Available at: https://doi.org/10.1016/j.neuron.2021.12.012.

O

O'Carroll, C.M. *et al.* (2006) 'Dopaminergic modulation of the persistence of one-trial hippocampus-dependent memory', *Learning & Memory*, 13(6), pp. 760–769. Available at: https://doi.org/10.1101/lm.321006.

Ochiishi, T. *et al.* (1999) 'High level of adenosine A1 receptor-like immunoreactivity in the CA2/CA3a region of the adult rat hippocampus', *Neuroscience*, 93(3), pp. 955–967. Available at: https://doi.org/10.1016/S0306-4522(99)00179-7.

Okamoto, K. and Ikegaya, Y. (2019) 'Recurrent connections between CA2 pyramidal cells', *Hippocampus*, 29(4), pp. 305–312. Available at: https://doi.org/10.1002/hipo.23064.

O'Keefe, J. and Dostrovsky, J. (1971) 'The hippocampus as a spatial map. Preliminary evidence from unit activity in the freely-moving rat', *Brain Research*, 34(1), pp. 171–175. Available at: https://doi.org/10.1016/0006-8993(71)90358-1.

O'Keefe, J. and Nadel, L. (1978) *The hippocampus as a cognitive map*. Oxford : New York: Clarendon Press ; Oxford University Press.

Okuyama, T. *et al.* (2016) 'Ventral CA1 neurons store social memory', *Science*, 353(6307), pp. 1536–1541. Available at: https://doi.org/10.1126/science.aaf7003.

Oliva, A., Fernández-Ruiz, A., *et al.* (2016) 'Role of Hippocampal CA2 Region in Triggering Sharp-Wave Ripples', *Neuron*, 91(6), pp. 1342–1355. Available at: https://doi.org/10.1016/j.neuron.2016.08.008.

Oliva, A., Fernández-Ruiz, A., *et al.* (2016) 'Spatial coding and physiological properties of hippocampal neurons in the Cornu Ammonis subregions', *Hippocampus*, 26(12), pp. 1593–1607. Available at: https://doi.org/10.1002/hipo.22659.

Oliva, A. *et al.* (2020) 'Hippocampal CA2 sharp-wave ripples reactivate and promote social memory', *Nature*, 587(7833), pp. 264–269. Available at: https://doi.org/10.1038/s41586-020-2758-y.

Oliva, A., Fernandez-Ruiz, A. and Karaba, L.A. (2023) 'CA2 orchestrates hippocampal network dynamics', *Hippocampus*, 33(3), pp. 241–251. Available at: https://doi.org/10.1002/hipo.23495.

P

Pastalkova, E. *et al.* (2008) 'Internally Generated Cell Assembly Sequences in the Rat Hippocampus', *Science*, 321(5894), pp. 1322–1327. Available at: https://doi.org/10.1126/science.1159775.

Pettit, N.L., Yuan, X.C. and Harvey, C.D. (2022) 'Hippocampal place codes are gated by behavioral engagement', *Nature Neuroscience*, 25(5), pp. 561–566. Available at: https://doi.org/10.1038/s41593-022-01050-4.

Pfeiffer, B.E. and Foster, D.J. (2013) 'Hippocampal place-cell sequences depict future paths to remembered goals', *Nature*, 497(7447), pp. 74–79. Available at: https://doi.org/10.1038/nature12112.

Phillips, H.S. *et al.* (1990) 'Widespread Expression of BDNF But Not NT3 by Target Areas of Basal Forebrain Cholinergic Neurons', *Science*, 250(4978), pp. 290–294. Available at: https://doi.org/10.1126/science.1688328.

Piskorowski, R.A. *et al.* (2016) 'Age-Dependent Specific Changes in Area CA2 of the Hippocampus and Social Memory Deficit in a Mouse Model of the 22q11.2 Deletion Syndrome', *Neuron*, 89(1), pp. 163–176. Available at: https://doi.org/10.1016/j.neuron.2015.11.036.

Piskorowski, R.A. and Chevaleyre, V. (2012) 'Synaptic integration by different dendritic compartments of hippocampal CA1 and CA2 pyramidal neurons', *Cellular and Molecular Life Sciences*, 69(1), pp. 75–88. Available at: https://doi.org/10.1007/s00018-011-0769-4.

Piskorowski, R.A. and Chevaleyre, V. (2013) 'Delta-Opioid Receptors Mediate Unique Plasticity onto Parvalbumin-Expressing Interneurons in Area CA2 of the Hippocampus', *The Journal of Neuroscience*, 33(36), pp. 14567–14578. Available at: https://doi.org/10.1523/JNEUROSCI.0649-13.2013.

Piskorowski, R.A. and Chevaleyre, V. (2018) 'Memory circuits: CA2', *Current Opinion in Neurobiology*, 52, pp. 54–59. Available at: https://doi.org/10.1016/j.conb.2018.04.015.

Piskorowski, R.A. and Chevaleyre, V. (2023) 'Hippocampal area CA2: interneuron disfunction during pathological states', *Frontiers in Neural Circuits*, 17, p. 1181032. Available at: https://doi.org/10.3389/fncir.2023.1181032.

Prince, S.M. *et al.* (2021) 'Alzheimer's pathology causes impaired inhibitory connections and reactivation of spatial codes during spatial navigation', *Cell Reports*, 35(3), p. 109008. Available at: https://doi.org/10.1016/j.celrep.2021.109008.

Puighermanal, E. *et al.* (2015) '*drd2-cre:ribotag* mouse line unravels the possible diversity of dopamine d2 receptor-expressing cells of the dorsal mouse hippocampus', *Hippocampus*, 25(7), pp. 858–875. Available at: https://doi.org/10.1002/hipo.22408.

Puighermanal, E. *et al.* (2017) 'Anatomical and molecular characterization of dopamine D1 receptor-expressing neurons of the mouse CA1 dorsal hippocampus', *Brain Structure and Function*, 222(4), pp. 1897–1911. Available at: https://doi.org/10.1007/s00429-016-1314-x.

Q

Qian, F.K., Li, Y. and Magee, J.C. (2025) 'Mechanisms of experience-dependent place-cell referencing in hippocampal area CA1', *Nature Neuroscience* [Preprint]. Available at: https://doi.org/10.1038/s41593-025-01930-5.

R

Radzicki, D., Chong, S. and Dudek, S.M. (2023) 'Morphological and molecular markers of mouse area CA2 along the proximodistal and dorsoventral hippocampal axes', *Hippocampus*, 33(3), pp. 133–149. Available at: https://doi.org/10.1002/hipo.23509.

Retailleau, A. and Morris, G. (2018) 'Spatial Rule Learning and Corresponding CA1 Place Cell Reorientation Depend on Local Dopamine Release', *Current Biology*, 28(6), pp. 836-846.e4. Available at: https://doi.org/10.1016/j.cub.2018.01.081.

Rey, C.C. *et al.* (2022a) 'Altered inhibitory function in hippocampal CA2 contributes in social memory deficits in Alzheimer's mouse model', *iScience*, 25(3), p. 103895. Available at: https://doi.org/10.1016/j.isci.2022.103895.

Rey, C.C. *et al.* (2022b) 'Altered inhibitory function in hippocampal CA2 contributes in social memory deficits in Alzheimer's mouse model', *iScience*, 25(3), p. 103895. Available at: https://doi.org/10.1016/j.isci.2022.103895.

Robinson, N.T.M. *et al.* (2020) 'Targeted Activation of Hippocampal Place Cells Drives Memory-Guided Spatial Behavior', *Cell*, 183(6), pp. 1586-1599.e10. Available at: https://doi.org/10.1016/j.cell.2020.09.061.

Rollenhagen, A. *et al.* (2007) 'Structural Determinants of Transmission at Large Hippocampal Mossy Fiber Synapses', *The Journal of Neuroscience*, 27(39), pp. 10434–10444. Available at: https://doi.org/10.1523/JNEUROSCI.1946-07.2007.

Rolotti, S.V. *et al.* (2022a) 'Local feedback inhibition tightly controls rapid formation of hippocampal place fields', *Neuron*, 110(5), pp. 783-794.e6. Available at: https://doi.org/10.1016/j.neuron.2021.12.003.

Rolotti, S.V. *et al.* (2022b) 'Local feedback inhibition tightly controls rapid formation of hippocampal place fields', *Neuron*, 110(5), pp. 783-794.e6. Available at: https://doi.org/10.1016/j.neuron.2021.12.003.

Roux, L. *et al.* (2017a) 'Sharp wave ripples during learning stabilize the hippocampal spatial map', *Nature Neuroscience*, 20(6), pp. 845–853. Available at: https://doi.org/10.1038/nn.4543.

Roux, L. *et al.* (2017b) 'Sharp wave ripples during learning stabilize the hippocampal spatial map', *Nature Neuroscience*, 20(6), pp. 845–853. Available at: https://doi.org/10.1038/nn.4543.

Roux, L. and Buzsáki, G. (2015) 'Tasks for inhibitory interneurons in intact brain circuits', *Neuropharmacology*, 88, pp. 10–23. Available at: https://doi.org/10.1016/j.neuropharm.2014.09.011.

Rowland, D.C. *et al.* (2013) 'Transgenically Targeted Rabies Virus Demonstrates a Major Monosynaptic Projection from Hippocampal Area CA2 to Medial Entorhinal Layer II Neurons', *The Journal of Neuroscience*, 33(37), pp. 14889–14898. Available at: https://doi.org/10.1523/JNEUROSCI.1046-13.2013.

Royer, S. *et al.* (2012) 'Control of timing, rate and bursts of hippocampal place cells by dendritic and somatic inhibition', *Nature Neuroscience*, 15(5), pp. 769–775. Available at: https://doi.org/10.1038/nn.3077.

Rubin, A. *et al.* (2015) 'Hippocampal ensemble dynamics timestamp events in long-term memory', *eLife*, 4, p. e12247. Available at: https://doi.org/10.7554/eLife.12247.

Rudy, J.W. and Sutherland, R.J. (1995) 'Configural association theory and the hippocampal formation: An appraisal and reconfiguration', *Hippocampus*, 5(5), pp. 375–389. Available at: https://doi.org/10.1002/hipo.450050502.

S

Sarel, A. *et al.* (2017) 'Vectorial representation of spatial goals in the hippocampus of bats', *Science*, 355(6321), pp. 176–180. Available at: https://doi.org/10.1126/science.aak9589.

Sato, M. *et al.* (2020a) 'Distinct Mechanisms of Over-Representation of Landmarks and Rewards in the Hippocampus', *Cell Reports*, 32(1), p. 107864. Available at: https://doi.org/10.1016/j.celrep.2020.107864.

Sato, M. *et al.* (2020b) 'Distinct Mechanisms of Over-Representation of Landmarks and Rewards in the Hippocampus', *Cell Reports*, 32(1), p. 107864. Available at: https://doi.org/10.1016/j.celrep.2020.107864.

Savasta, M., Dubois, A. and Scatton, B. (1986) 'Autoradiographic localization of D1 dopamine receptors in the rat brain with [3H]SCH 23390', *Brain Research*, 375(2), pp. 291–301. Available at: https://doi.org/10.1016/0006-8993(86)90749-3.

Schultz, W., Dayan, P. and Montague, P.R. (1997) 'A Neural Substrate of Prediction and Reward', *Science*, 275(5306), pp. 1593–1599. Available at: https://doi.org/10.1126/science.275.5306.1593.

Scoville, W.B. and Milner, B. (1957) 'LOSS OF RECENT MEMORY AFTER BILATERAL HIPPOCAMPAL LESIONS', *Journal of Neurology, Neurosurgery & Psychiatry*, 20(1), pp. 11–21. Available at: https://doi.org/10.1136/jnnp.20.1.11.

Shinohara, Y. *et al.* (2012a) 'Hippocampal CA3 and CA2 have distinct bilateral innervation patterns to CA1 in rodents', *European Journal of Neuroscience*, 35(5), pp. 702–710. Available at: https://doi.org/10.1111/j.1460-9568.2012.07993.x.

Shinohara, Y. *et al.* (2012b) 'Hippocampal CA3 and CA2 have distinct bilateral innervation patterns to CA1 in rodents', *European Journal of Neuroscience*, 35(5), pp. 702–710. Available at: https://doi.org/10.1111/j.1460-9568.2012.07993.x.

Sik, A. *et al.* (1995) 'Hippocampal CA1 interneurons: an in vivo intracellular labeling study', *The Journal of Neuroscience*, 15(10), pp. 6651–6665. Available at: https://doi.org/10.1523/JNEUROSCI.15-10-06651.1995.

Silva, W.C.N.D. *et al.* (2012) 'D1/D5 dopamine receptors modulate spatial memory formation', *Neurobiology of Learning and Memory*, 97(2), pp. 271–275. Available at: https://doi.org/10.1016/j.nlm.2012.01.005.

Simons, S.B. *et al.* (2009) 'Regional differences in hippocampal calcium handling provide a cellular mechanism for limiting plasticity', *Proceedings of the National Academy of Sciences*, 106(33), pp. 14080–14084. Available at: https://doi.org/10.1073/pnas.0904775106.

Skaggs, W.E., McNaughton, B.L. and Gothard, K.M. (1993) 'An information-theoretic approach to deciphering the hippocampal code', in *Advances in Neural Information Processing Systems 5*. Hanson, S.; Cowan, J.; Giles, C. Morgan-Kaufmann, pp. 1030–1037.

Slomianka, L. *et al.* (2011) 'Hippocampal pyramidal cells: the reemergence of cortical lamination', *Brain Structure and Function*, 216(4), pp. 301–317. Available at: https://doi.org/10.1007/s00429-011-0322-0.

Sloviter, R.S. (1989) 'Calcium-binding protein (calbindin-D_{28k}) and parvalbumin immunocytochemistry: Localization in the rat hippocampus with specific reference to the selective vulnerability of hippocampal neurons to seizure activity', *Journal of Comparative Neurology*, 280(2), pp. 183–196. Available at: https://doi.org/10.1002/cne.902800203.

Smith, A.S. *et al.* (2016) 'Targeted activation of the hippocampal CA2 area strongly enhances social memory', *Molecular Psychiatry*, 21(8), pp. 1137–1144. Available at: https://doi.org/10.1038/mp.2015.189.

Soltesz, I. and Losonczy, A. (2018a) 'CA1 pyramidal cell diversity enabling parallel information processing in the hippocampus', *Nature Neuroscience*, 21(4), pp. 484–493. Available at: https://doi.org/10.1038/s41593-018-0118-0.

Soltesz, I. and Losonczy, A. (2018b) 'CA1 pyramidal cell diversity enabling parallel information processing in the hippocampus', *Nature Neuroscience*, 21(4), pp. 484–493. Available at: https://doi.org/10.1038/s41593-018-0118-0.

Somogyi, P. and Klausberger, T. (2005) 'Defined types of cortical interneurone structure space and spike timing in the hippocampus', *The Journal of Physiology*, 562(1), pp. 9–26. Available at: https://doi.org/10.1113/jphysiol.2004.078915.

Sosa, M. and Giocomo, L.M. (2021) 'Navigating for reward', *Nature Reviews Neuroscience*, 22(8), pp. 472–487. Available at: https://doi.org/10.1038/s41583-021-00479-z.

Sosa, M., Plitt, M.H. and Giocomo, L.M. (2023) 'Hippocampal sequences span experience relative to rewards'. Available at: https://doi.org/10.1101/2023.12.27.573490.

Spiers, H.J., Olafsdottir, H.F. and Lever, C. (2018) 'Hippocampal CA1 activity correlated with the distance to the goal and navigation performance', *Hippocampus*, 28(9), pp. 644–658. Available at: https://doi.org/10.1002/hipo.22813.

Squire, L.R. (1982) 'The Neuropsychology of Human Memory', *Annual Review of Neuroscience*, 5(1), pp. 241–273. Available at: https://doi.org/10.1146/annurev.ne.05.030182.001325.

Squire, L.R. (2004) 'Memory systems of the brain: A brief history and current perspective', *Neurobiology of Learning and Memory*, 82(3), pp. 171–177. Available at: https://doi.org/10.1016/j.nlm.2004.06.005.

Squire, L.R. and Zola, S.M. (1996a) 'Structure and function of declarative and nondeclarative memory systems', *Proceedings of the National Academy of Sciences*, 93(24), pp. 13515–13522. Available at: https://doi.org/10.1073/pnas.93.24.13515.

Squire, L.R. and Zola, S.M. (1996b) 'Structure and function of declarative and nondeclarative memory systems', *Proceedings of the National Academy of Sciences*, 93(24), pp. 13515–13522. Available at: https://doi.org/10.1073/pnas.93.24.13515.

Srinivas, K.V. *et al.* (2017) 'The Dendrites of CA2 and CA1 Pyramidal Neurons Differentially Regulate Information Flow in the Cortico-Hippocampal Circuit', *The Journal of Neuroscience*, 37(12), pp. 3276–3293. Available at: https://doi.org/10.1523/JNEUROSCI.2219-16.2017.

Stanfield, B.B. and Cowan, W.M. (1979) 'The development of the hippocampus and dentate gyrus in normal and reeler mice', *Journal of Comparative Neurology*, 185(3), pp. 423–459. Available at: https://doi.org/10.1002/cne.901850303.

Stark, E. *et al.* (2013) 'Inhibition-Induced Theta Resonance in Cortical Circuits', *Neuron*, 80(5), pp. 1263–1276. Available at: https://doi.org/10.1016/j.neuron.2013.09.033.

Stark, E. *et al.* (2014) 'Pyramidal Cell-Interneuron Interactions Underlie Hippocampal Ripple Oscillations', *Neuron*, 83(2), pp. 467–480. Available at: https://doi.org/10.1016/j.neuron.2014.06.023.

Stark, E. *et al.* (2015) 'Local generation of multineuronal spike sequences in the hippocampal CA1 region', *Proceedings of the National Academy of Sciences*, 112(33), pp. 10521–10526. Available at: https://doi.org/10.1073/pnas.1508785112.

Stevenson, E.L. and Caldwell, H.K. (2014) 'Lesions to the CA 2 region of the hippocampus impair social memory in mice', *European Journal of Neuroscience*, 40(9), pp. 3294–3301. Available at: https://doi.org/10.1111/ejn.12689.

Sun, Q. *et al.* (2014) 'Dendritic Na+ spikes enable cortical input to drive action potential output from hippocampal CA2 pyramidal neurons', *eLife*, 3, p. e04551. Available at: https://doi.org/10.7554/eLife.04551.

Sun, Q. *et al.* (2017) 'Proximodistal Heterogeneity of Hippocampal CA3 Pyramidal Neuron Intrinsic Properties, Connectivity, and Reactivation during Memory Recall', *Neuron*, 95(3), pp. 656-672.e3. Available at: https://doi.org/10.1016/j.neuron.2017.07.012.

Swanson, L.W. and Cowan, W.M. (1977) 'An autoradiographic study of the organization of the efferet connections of the hippocampal formation in the rat', *Journal of Comparative Neurology*, 172(1), pp. 49–84. Available at: https://doi.org/10.1002/cne.901720104.

T

Takeuchi, T. *et al.* (2016) 'Locus coeruleus and dopaminergic consolidation of everyday memory', *Nature*, 537(7620), pp. 357–362. Available at: https://doi.org/10.1038/nature19325.

Talley, E.M. *et al.* (2001) 'CNS Distribution of Members of the Two-Pore-Domain (KCNK) Potassium Channel Family', *The Journal of Neuroscience*, 21(19), pp. 7491–7505. Available at: https://doi.org/10.1523/JNEUROSCI.21-19-07491.2001.

Tamamaki, N., Abe, K. and Nojyo, Y. (1988) 'Three-dimensional analysis of the whole axonal arbors originating from single CA2 pyramidal neurons in the rat hippocampus with the aid of a computer graphic technique', *Brain Research*, 452(1–2), pp. 255–272. Available at: https://doi.org/10.1016/0006-8993(88)90030-3.

Tamatsu, Y. *et al.* (2023) 'Optogenetic activation of the ventral tegmental area-hippocampal pathway facilitates rapid adaptation to changes in spatial goals', *iScience*, 26(12), p. 108536. Available at: https://doi.org/10.1016/j.isci.2023.108536.

Tang, J. and Dani, J.A. (2009) 'Dopamine Enables In Vivo Synaptic Plasticity Associated with the Addictive Drug Nicotine', *Neuron*, 63(5), pp. 673–682. Available at: https://doi.org/10.1016/j.neuron.2009.07.025.

Taxidis, J. *et al.* (2020) 'Differential Emergence and Stability of Sensory and Temporal Representations in Context-Specific Hippocampal Sequences', *Neuron*, 108(5), pp. 984-998.e9. Available at: https://doi.org/10.1016/j.neuron.2020.08.028.

Tolman, E.C. (1948) 'Cognitive maps in rats and men.', *Psychological Review*, 55(4), pp. 189–208. Available at: https://doi.org/10.1037/h0061626.

Tran, A.H. *et al.* (2008) 'Dopamine D_1 Receptor Modulates Hippocampal Representation Plasticity to Spatial Novelty', *The Journal of Neuroscience*, 28(50), pp. 13390–13400. Available at: https://doi.org/10.1523/JNEUROSCI.2680-08.2008.

Trouche, S. *et al.* (2016) 'Recoding a cocaine-place memory engram to a neutral engram in the hippocampus', *Nature Neuroscience*, 19(4), pp. 564–567. Available at: https://doi.org/10.1038/nn.4250.

Trouche, S. *et al.* (2019) 'A Hippocampus-Accumbens Tripartite Neuronal Motif Guides Appetitive Memory in Space', *Cell*, 176(6), pp. 1393-1406.e16. Available at: https://doi.org/10.1016/j.cell.2018.12.037.

Tsai, H.-C. *et al.* (2009) 'Phasic Firing in Dopaminergic Neurons Is Sufficient for Behavioral Conditioning', *Science*, 324(5930), pp. 1080–1084. Available at: https://doi.org/10.1126/science.1168878.

Tsetsenis, T. *et al.* (2021) 'Midbrain dopaminergic innervation of the hippocampus is sufficient to modulate formation of aversive memories', *Proceedings of the National Academy of Sciences*, 118(40), p. e2111069118. Available at: https://doi.org/10.1073/pnas.2111069118.

Tsetsenis, T., Broussard, J.I. and Dani, J.A. (2023) 'Dopaminergic regulation of hippocampal plasticity, learning, and memory', *Frontiers in Behavioral Neuroscience*, 16, p. 1092420. Available at: https://doi.org/10.3389/fnbeh.2022.1092420.

Tulving, E. (1972) 'Episodic and semantic memory.', in *Organization of memory.* Oxford, England: Academic Press, pp. xiii, 423–xiii, 423.

Turi, G.F. *et al.* (2019a) 'Vasoactive Intestinal Polypeptide-Expressing Interneurons in the Hippocampus Support Goal-Oriented Spatial Learning', *Neuron*, 101(6), pp. 1150-1165.e8. Available at: https://doi.org/10.1016/j.neuron.2019.01.009.

Turi, G.F. *et al.* (2019b) 'Vasoactive Intestinal Polypeptide-Expressing Interneurons in the Hippocampus Support Goal-Oriented Spatial Learning', *Neuron*, 101(6), pp. 1150-1165.e8. Available at: https://doi.org/10.1016/j.neuron.2019.01.009.

V

Valero, M. *et al.* (2015a) 'Determinants of different deep and superficial CA1 pyramidal cell dynamics during sharp-wave ripples', *Nature Neuroscience*, 18(9), pp. 1281–1290. Available at: https://doi.org/10.1038/nn.4074.

Valero, M. *et al.* (2015b) 'Determinants of different deep and superficial CA1 pyramidal cell dynamics during sharp-wave ripples', *Nature Neuroscience*, 18(9), pp. 1281–1290. Available at: https://doi.org/10.1038/nn.4074.

Vancura, B. *et al.* (2023) 'Inhibitory control of sharp-wave ripple duration during learning in hippocampal recurrent networks', *Nature Neuroscience*, 26(5), pp. 788–797. Available at: https://doi.org/10.1038/s41593-023-01306-7.

Vanderwolf, C.H. (1969) 'Hippocampal electrical activity and voluntary movement in the rat', *Electroencephalography and Clinical Neurophysiology*, 26(4), pp. 407–418. Available at: https://doi.org/10.1016/0013-4694(69)90092-3.

Vertes, R.P. (1992) 'PHA-L analysis of projections from the supramammillary nucleus in the rat', *Journal of Comparative Neurology*, 326(4), pp. 595–622. Available at: https://doi.org/10.1002/cne.903260408.

W

Wamsley, J.K. *et al.* (1992) 'CNS distribution of D1 receptors: Use of a new specific D1 receptor antagonist, [3H]SCH39166', *Neurochemistry International*, 20, pp. 123–128. Available at: https://doi.org/10.1016/0197-0186(92)90224-F.

Wang, M., Foster, D.J. and Pfeiffer, B.E. (2020) 'Alternating sequences of future and past behavior encoded within hippocampal theta oscillations', *Science*, 370(6513), pp. 247–250. Available at: https://doi.org/10.1126/science.abb4151.

Watabe-Uchida, M., Eshel, N. and Uchida, N. (2017) 'Neural Circuitry of Reward Prediction Error', *Annual Review of Neuroscience*, 40(1), pp. 373–394. Available at: https://doi.org/10.1146/annurev-neuro-072116-031109.

Wersinger, S.R. *et al.* (2002) 'Vasopressin V1b receptor knockout reduces aggressive behavior in male mice', *Molecular Psychiatry*, 7(9), pp. 975–984. Available at: https://doi.org/10.1038/sj.mp.4001195.

Whitebirch, A.C. *et al.* (2022) 'Enhanced excitability of the hippocampal CA2 region and its contribution to seizure activity in a mouse model of temporal lobe epilepsy', *Neuron*, 110(19), pp. 3121-3138.e8. Available at: https://doi.org/10.1016/j.neuron.2022.07.020.

Wilson, M.A. and McNaughton, B.L. (1994) 'Reactivation of Hippocampal Ensemble Memories During Sleep', *Science*, 265(5172), pp. 676–679. Available at: https://doi.org/10.1126/science.8036517.

Wintzer, M.E. *et al.* (2014a) 'The Hippocampal CA2 Ensemble Is Sensitive to Contextual Change', *The Journal of Neuroscience*, 34(8), pp. 3056–3066. Available at: https://doi.org/10.1523/JNEUROSCI.2563-13.2014.

Wintzer, M.E. *et al.* (2014b) 'The Hippocampal CA2 Ensemble Is Sensitive to Contextual Change', *The Journal of Neuroscience*, 34(8), pp. 3056–3066. Available at: https://doi.org/10.1523/JNEUROSCI.2563-13.2014.

Witter, M.P. *et al.* (2000) 'Anatomical Organization of the Parahippocampal-Hippocampal Network', *Annals of the New York Academy of Sciences*, 911(1), pp. 1–24. Available at: https://doi.org/10.1111/j.1749-6632.2000.tb06716.x.

Wood, E.R. *et al.* (2000) 'Hippocampal Neurons Encode Information about Different Types of Memory Episodes Occurring in the Same Location', *Neuron*, 27(3), pp. 623–633. Available at: https://doi.org/10.1016/S0896-6273(00)00071-4.

Wood, E.R., Dudchenko, P.A. and Eichenbaum, H. (1999) 'The global record of memory in hippocampal neuronal activity', *Nature*, 397(6720), pp. 613–616. Available at: https://doi.org/10.1038/17605.

Woodward, W. *et al.* (1992) 'Nuclear and cytoplasmic localization of basic fibroblast growth factor in astrocytes and CA2 hippocampal neurons', *The Journal of Neuroscience*, 12(1), pp. 142–152. Available at: https://doi.org/10.1523/JNEUROSCI.12-01-00142.1992.

X

Xiao, Z., Lin, K. and Fellous, J.-M. (2020) 'Conjunctive reward–place coding properties of dorsal distal CA1 hippocampus cells', *Biological Cybernetics*, 114(2), pp. 285–301. Available at: https://doi.org/10.1007/s00422-020-00830-0.

Xing, B. *et al.* (2010) 'Dopamine D1 but not D3 receptor is critical for spatial learning and related signaling in the hippocampus', *Neuroscience*, 169(4), pp. 1511–1519. Available at: https://doi.org/10.1016/j.neuroscience.2010.06.034.

Xu, H. *et al.* (2013) 'Neocortical Somatostatin-Expressing GABAergic Interneurons Disinhibit the Thalamorecipient Layer 4', *Neuron*, 77(1), pp. 155–167. Available at: https://doi.org/10.1016/j.neuron.2012.11.004.

Xu, H. *et al.* (2019) 'Assembly Responses of Hippocampal CA1 Place Cells Predict Learned Behavior in Goal-Directed Spatial Tasks on the Radial Eight-Arm Maze', *Neuron*, 101(1), pp. 119-132.e4. Available at: https://doi.org/10.1016/j.neuron.2018.11.015.

Y

Yang, K. *et al.* (2017) 'Dopamine receptor activity participates in hippocampal synaptic plasticity associated with novel object recognition', *European Journal of Neuroscience*. Edited by P. Bolam, 45(1), pp. 138–146. Available at: https://doi.org/10.1111/ejn.13406.

Young, W.S. *et al.* (2006) 'The vasopressin 1b receptor is prominent in the hippocampal area CA2 where it is unaffected by restraint stress or adrenalectomy', *Neuroscience*, 143(4), pp. 1031–1039. Available at: https://doi.org/10.1016/j.neuroscience.2006.08.040.

Z

Zaremba, J.D. *et al.* (2017a) 'Impaired hippocampal place cell dynamics in a mouse model of the 22q11.2 deletion', *Nature Neuroscience*, 20(11), pp. 1612–1623. Available at: https://doi.org/10.1038/nn.4634.

Zaremba, J.D. *et al.* (2017b) 'Impaired hippocampal place cell dynamics in a mouse model of the 22q11.2 deletion', *Nature Neuroscience*, 20(11), pp. 1612–1623. Available at: https://doi.org/10.1038/nn.4634.

Zemla, R. *et al.* (2022) 'Task-selective place cells show behaviorally driven dynamics during learning and stability during memory recall', *Cell Reports*, 41(8), p. 111700. Available at: https://doi.org/10.1016/j.celrep.2022.111700.

Zhang, S.-J. *et al.* (2013) 'Optogenetic Dissection of Entorhinal-Hippocampal Functional Connectivity', *Science*, 340(6128), p. 1232627. Available at: https://doi.org/10.1126/science.1232627.

Zhang, Y. *et al.* (2021) 'Cholinergic suppression of hippocampal sharp-wave ripples impairs working memory', *Proceedings of the National Academy of Sciences*, 118(15), p. e2016432118. Available at: https://doi.org/10.1073/pnas.2016432118.

Zhang, Z.J. and Reynolds, G.P. (2002) 'A selective decrease in the relative density of parvalbumin-immunoreactive neurons in the hippocampus in schizophrenia', *Schizophrenia Research*, 55(1–2), pp. 1–10. Available at: https://doi.org/10.1016/S0920-9964(01)00188-8.

Zhao, M. *et al.* (2007) 'Synaptic Plasticity (and the Lack Thereof) in Hippocampal CA2 Neurons', *The Journal of Neuroscience*, 27(44), pp. 12025–12032. Available at: https://doi.org/10.1523/JNEUROSCI.4094-07.2007.

Ziv, Y. *et al.* (2013a) 'Long-term dynamics of CA1 hippocampal place codes', *Nature Neuroscience*, 16(3), pp. 264–266. Available at: https://doi.org/10.1038/nn.3329.

Ziv, Y. *et al.* (2013b) 'Long-term dynamics of CA1 hippocampal place codes', *Nature Neuroscience*, 16(3), pp. 264–266. Available at: https://doi.org/10.1038/nn.3329.